Rate and processes of river network rearrangement during incipient faulting: The case of the Cahabon River, Guatemala

Gilles Brocard, Jane Willenbring, Barbara Suski, Philippe Audra, Christine Authemayou, Beatriz Cosenza-Muralles, Sergio Moran-Ical, François Demory, Pierre Rochette, Torsten Vennemann, et al.

▶ **To cite this version:**

Gilles Brocard, Jane Willenbring, Barbara Suski, Philippe Audra, Christine Authemayou, et al.. Rate and processes of river network rearrangement during incipient faulting: The case of the Cahabon River, Guatemala. American journal of science, 2012, 312 (5), pp.449-507. 10.2475/05.2012.01 . hal-04671543

HAL Id: hal-04671543
https://hal.science/hal-04671543v1

Submitted on 13 Oct 2024

HAL is a multi-disciplinary open access archive for the deposit and dissemination of scientific research documents, whether they are published or not. The documents may come from teaching and research institutions in France or abroad, or from public or private research centers.

L'archive ouverte pluridisciplinaire **HAL**, est destinée au dépôt et à la diffusion de documents scientifiques de niveau recherche, publiés ou non, émanant des établissements d'enseignement et de recherche français ou étrangers, des laboratoires publics ou privés.

Published in the American Journal of Science, Vol. 312, May, 2012, P. 449–507,
DOI 10.2475/05.2012.01

RATE AND PROCESSES OF RIVER NETWORK REARRANGEMENT DURING INCIPIENT FAULTING: THE CASE OF THE CAHABO N RIVER, GUATEMALA

Gilles Brocard (1,2)
Jane Willenbring (2)
Barbara Suski (3)
Philippe Audra (4)
Christine Authemayou (1,5)
Beatriz Cosenza-Muralles (6)
Sergio Morán-Ical (7)
François Demory (8)
Pierre Rochette (8)
Torsten Vennemann (9)
Klaus Holliger (3)
Christian Teyssier (1,10)

(1) Institute of Geology and Paleontology, University of Lausanne, Anthropole, CH-1015 Lausanne, Switzerland

(2) Department of Earth and Environmental Science, University of Pennsylvania, 240 South 33rd Street—254-b Hayden Hall, Philadelphia, Pennsylvania 19104-6316 USA

(3) Institute of Geophysics, University of Lausanne, Anthropole, CH-1015 Lausanne, Switzerland

(4) Polytech'Nice-Sophia, Universite´ de Nice–Sophia Antipolis, 1645, Route des Lucioles, 06410 Biot, France

(5) Laboratoire Domaines Océaniques, UMR 6538, Université de Brest, Place Copernic, Plouzané, France

(6) Physics Department, Faculty of Engineering, University of San Carlos de Guatemala, Guatemala City, Guatemala

(7)Department of Geology, University of San Carlos, Centro Universitario del Noreste, Cobán, Guatemala

(8)CEREGE, CNRS/Aix-Marseille University, BP80 13545, Aix en Provence, Cedex 4, France

(9) Institute of Mineralogy and Geochemistry, University of Lausanne, Anthropole, CH-1015 Lausanne, Switzerland

(10)Department of Geology and Geophysics, University of Minnesota–Twin Cities, 310 Pillsbury Drive SE, Minneapolis, Minnesota 55455, USA

ABSTRACT

Deeply incised river networks are generally regarded as robust features that are not easily modified by erosion or tectonics. Although the reorganization of deeply incised drainage systems has been documented, the corresponding importance with regard to the overall landscape evolution of mountain ranges and the factors that permit such reorganizations are poorly understood. To address this problem, we have explored the rapid drainage reorganization that affected the Cahabón River in Guatemala during the Quaternary. Sediment-provenance analysis, field mapping, and electrical resistivity tomography (ERT) imaging are used to reconstruct the geometry of the valley before the river was captured. Dating of the abandoned valley sediments by the ^{10}Be-^{26}Al burial method and geomagnetic polarity analysis allow us to determine the age of the capture events and then to quantify several processes, such as the rate of tectonic deformation of the paleovalley, the rate of propagation of post-capture drainage reversal, and the rate at which canyons that formed at the capture sites have propagated along the paleovalley. Transtensional faulting started 1 to 3 million years ago, produced ground tilting and ground faulting along the Cahabón River, and thus generated differential uplift rate of 0.3±0.1 up to 0.7 ±0.4 mm.y^{-1} along the river's course. The river responded to faulting by incising the areas of relative uplift and depositing a few tens of meters of sediment above the areas of relative subsidence. Then, the river experienced two captures and one avulsion between 700 ky and 100 ky. The captures breached high-standing ridges that separate the Cahabón River from its captors. Captures occurred at specific points where ridges are made permeable by fault damage zones and/or soluble rocks. Groundwater flow from the Cahabón River down to its captors likely increased the erosive power of the captors thus promoting focused erosion of the ridges. Valley-fill formation and capture occurred in close temporal succession, suggesting a genetic link between the two. We suggest that the aquifers accumulated within the valley-fills, increased the head along the subterraneous system connecting the Cahabón River to its captors, and promoted their development. Upon capture, the breached valley experienced widespread drainage reversal toward the capture sites. We attribute the generalized reversal to combined effects of groundwater sapping in the valley-fill, axial drainage obstruction by lateral fans, and tectonic tilting. Drainage reversal increased the size of the captured areas by a factor of 4 to 6. At the capture sites, 500 m deep canyons have been incised into the bedrock and are propagating upstream at a rate of 3 to 11 mm.y^{-1} while deepening at a rate of 0.7 to 1.5 mm.y^{-1}. At this rate, 1 to 2 million years will be necessary for headward erosion to completely erase the topographic expression of the paleovalley. It is concluded that the rapid reorganization of this drainage system was made possible by the way the river adjusted to the new tectonic strain field, which involved transient sedimentation along the river's course. If the river had escaped its early reorganization and had been given the time necessary to reach a new dynamic equilibrium, then the transient conditions that promoted capture would have vanished and its vulnerability to capture would have been strongly reduced.
Key words: Drainage reorganization, river capture, drainage reversal, knickpoint propagation, tectonic defeat, electrical resistivity, tomography, ^{26}Al-^{10}Be burial dating, groundwater sapping, paleovalley

Introduction

Deeply incised river networks are commonly regarded as very stable landforms in plan view. The lateral migration of rivers, or their propensity to capture surrounding streams, is indeed limited by the amount of rock that has to be removed for breaching inter-stream divides. In many mountain belts the geometry of river networks is therefore thought to be inherited from earlier stages of mountain growth (for example Seeber and Gornitz, 1983; Hovius, 1996; Talling and others, 1997; Hovius and others, 1998; Castelltort and Simpson, 2006). Further changes in drainage plan form would then result from diffuse (Brookfield, 1998; Hallet and Molnar, 2001; Ramsey and others, 2004) or localized (for example Replumaz and others, 2001) tectonic deformation, and are used to quantify horizontal finite tectonic strain. However, some mountain ranges display a combination of passively advecting and dynamically rearranging drainages (Schlunneger and others, 1998; Craw and others, 1999). The regularly spaced drainage typical of many linear mountain ranges is sometimes regarded as an inheritance from the early stages of mountain growth (Hovius, 1996; Talling and others, 1997), or as the most achieved manifestation of drainage adjustment to temporal changes in orogen width (Leeder and Jackson, 1993; Harbor, 1997; Ellis and others, 1999; Horton and DeCelles, 2001; Densmore and others, 2005; Frankel and Pazzaglia, 2006; Bonnet, 2009). The shape of the individual catchments is modified either by progressive lateral migration of drainage divides or incrementally by episodic diversion of the river of one catchment into another catchment. In deeply incised drainages the phenomenon of river diversion should be one of the most efficient processes of network modification because it only requires the localized erosion of an interfluve (the water divide between two adjacent catchments). In addition, river diversion does not extensively modify the network of flow lines. In the present paper, the term river diversion is used regardless of the processes that drive the diversion and only means that a river segment is disconnected from the next downstream reach and connected to the course of another river.

The processes that drive diversions have been grouped into top-down and bottom-up processes (Bishop, 1995). In humid, non-arid landscapes without glacier cover, the most common case of top-down process is river avulsion, while the most common case of bottom-up process is river capture. Avulsion refers to an episode of river aggradation that result in the filling of a valley to such a height that the river eventually spills over a drainage divide and is rerouted into a conterminous catchment. This process is arguably very efficient in low relief landscapes where valleys are shallow and can be easily filled up to the height of the intervening divides (for example Hoorn and others, 1995; Jackson and others, 1996; Burbank and others, 1996; Keller and others, 1999; Humphrey and Konrad, 2000; van der Beek and others, 2002). Avulsion is expected to be less common along deeply incised valleys. In such deep valleys capture should be favored. Headward erosion, stemming from a river at lower elevation (captor), propagates upslope up to the drainage divide, breaches the divide down to a higher standing river (captive) and triggers its rerouting into the lower lying river (for example Lugeon, 1901; Mather, 2000; Brocard and van der Beek, 2006; Brocard and others, 2011). It has been pointed out that the exact mechanism of interfluve breaching is difficult to explain if headward erosion is controlled by surface processes, because surface runoff and slope creep at the divide do not favor rapid lateral divide migration and deep breaching (for example Strahler, 1945; Bishop, 1995). Underground capture is less sensitive to the depth of drainage entrenchment than surface capture. This phenomenon has been documented in soluble rocks, such as carbonates (Höltz, 1996; Losson and Quinif, 2001; Hill and others, 2008), as well as in permeable rocks, such as sandstones (Dunne, 1990; Pederson, 2001). Connection between the river to be captured and its captor is first established underground. The interfluve is breached either by collapse of subterraneous conduits or because groundwater circulation increases the erosive power of the captor thus allowing headward erosion at the head of the captor to propagate up to the divide and beyond. The divide breaching is then only a late-stage surface manifestation of an already established capture.

Here, we document a case of rapid drainage reorganization along a river already well incised into the flanks of an elongated mountain range. This river belongs to a series of range-

transverse rivers that experienced a first pulse of drainage rearrangement during the Late Miocene (Brocard and others, 2011). The river studied here experienced a pulse of reorganization in the Quaternary. We show that reorganization was driven by the same processes, namely river capture and drainage reversal. Reorganization is a direct response to the recent rise of fault-bounded blocks in a transtensional regime, which is, in a way, quite similar to the response of the Late Miocene rivers to the rise of a transpressional range. In the present case, however, the sediments that were deposited along the valley are widely preserved because rearrangement is very young. This chronology allows us to put more precise temporal benchmarks on landscape evolution, and thus quantify the rates of tectonic deformation, drainage rearrangement (capture and drainage reversal), and post-capture canyon development. We show that the rearrangement spans the last million years and has been taking place within a few millions of years after fault activation. We use the well preserved morphology of the abandoned valleys and capture sites to gain insights on the capture process. Groundwater-driven erosion appears to have played a major role not only in the breaching of the interfluves, but also in drainage reversal along the abandoned valleys. We suggest that without groundwater contribution, the reorganization of the drainage would have proceeded much more slowly. The time required for the rearrangement would have been much longer than the timescale of tectonic deformation, such that the drainage would have appeared as a passive marker of deformation. We show that groundwater-driven capture and reversal were favored by sediment deposition along the captured river. Sediment deposition was likely a transient adaptation to the new pattern of deformation that the river was facing. The theory predicts that upon return to dynamic equilibrium, the sediments would have been dispersed and the conditions that had catalyzed the ground-water driven captures would have vanished. Drainage stability or vulnerability would therefore be strongly time-dependent and related to the degree of equilibrium achieved by the river network. Such a higher vulnerability of drainages to reorganization has already been proposed during the transient adjustment of river profiles to accelerated faulting (Whittaker and others, 2008).

The first section of this paper introduces the geomorphology of the field area. The second section then reviews the methods that have been used for reconstructing and dating the paleovalley, for which we used a combination of sediment provenance analysis (gravel assemblage and sediment matrix elemental analysis), isotopic tracing of water sources, valley-fill mapping using outcrops and the imaging of the subsurface by electrical resistivity tomography (ERT), and eventually dating of the valley-fill using the differential decay of ^{10}Be and ^{26}Al coupled with the geomagnetic polarity in buried river sediments. The results of these methods are presented in the third section. The sediment provenance analysis is used to formally demonstrate the initial continuity of the paleovalley. The analysis of the valley-fill architecture shows that sediment deposition was controlled by transtensional faults, and that the river was defeated by tectonics. The dating reveals the piecemeal abandonment of the paleovalley over the last million years. In the fourth section, we use these results to quantify the rate of bedrock deformation, the rate of drainage reversal along the abandoned valleys, and the growth of canyons that have initiated at the sites of capture and we discuss which processes allowed for these rapid changes in the morphology from divide breaching to drainage reversal and canyon development.

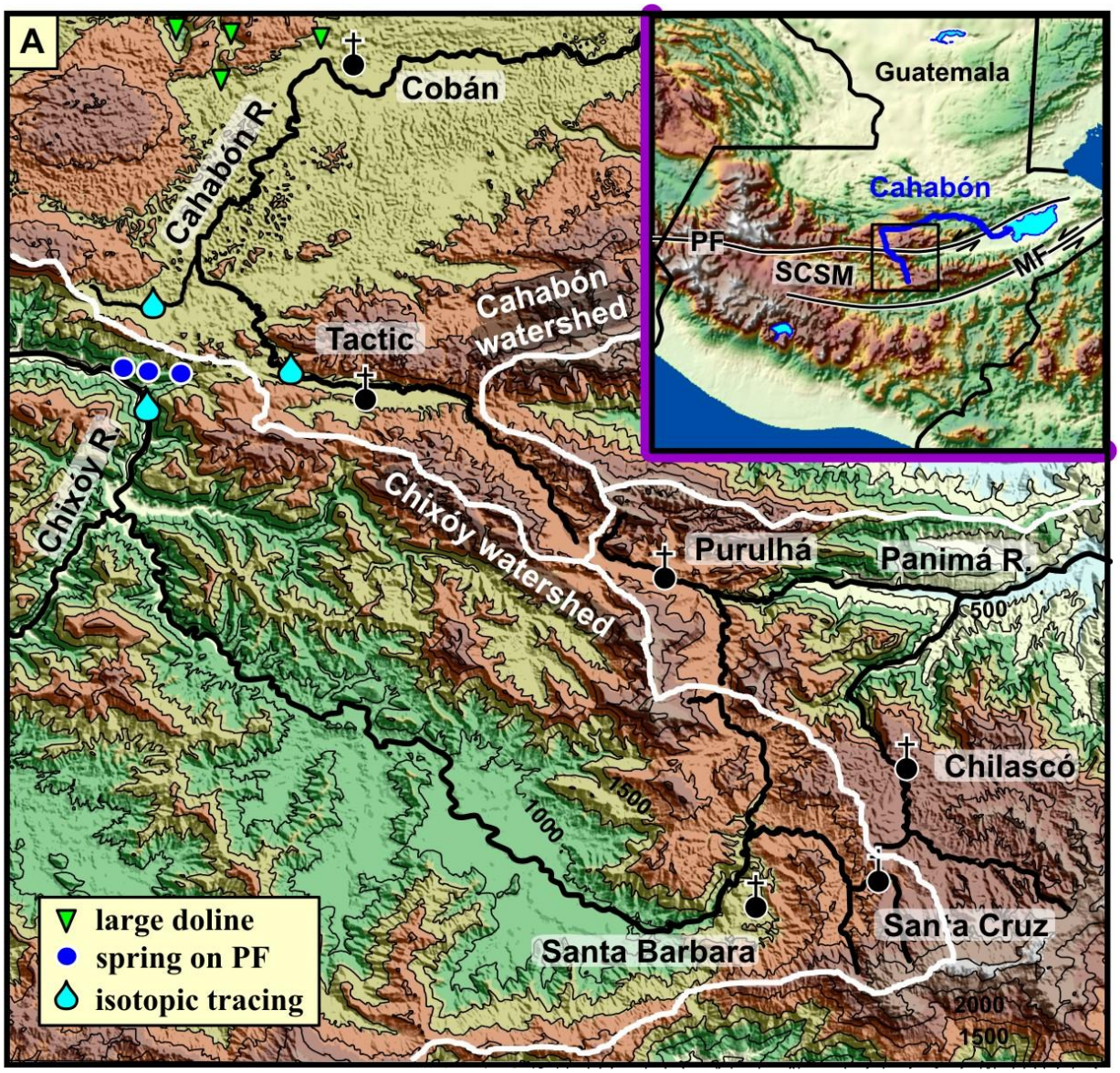

Fig. 1. Map of the Cahabón River paleovalley.

(A): Topography of the Cahabón River paleovalley. Contour spacing is 250 m. Inset for location in Guatemala: PF: Polochic Fault, MF: Motagua Fault, SCSM: Sierra de Chuacús–Sierra de las Minas.

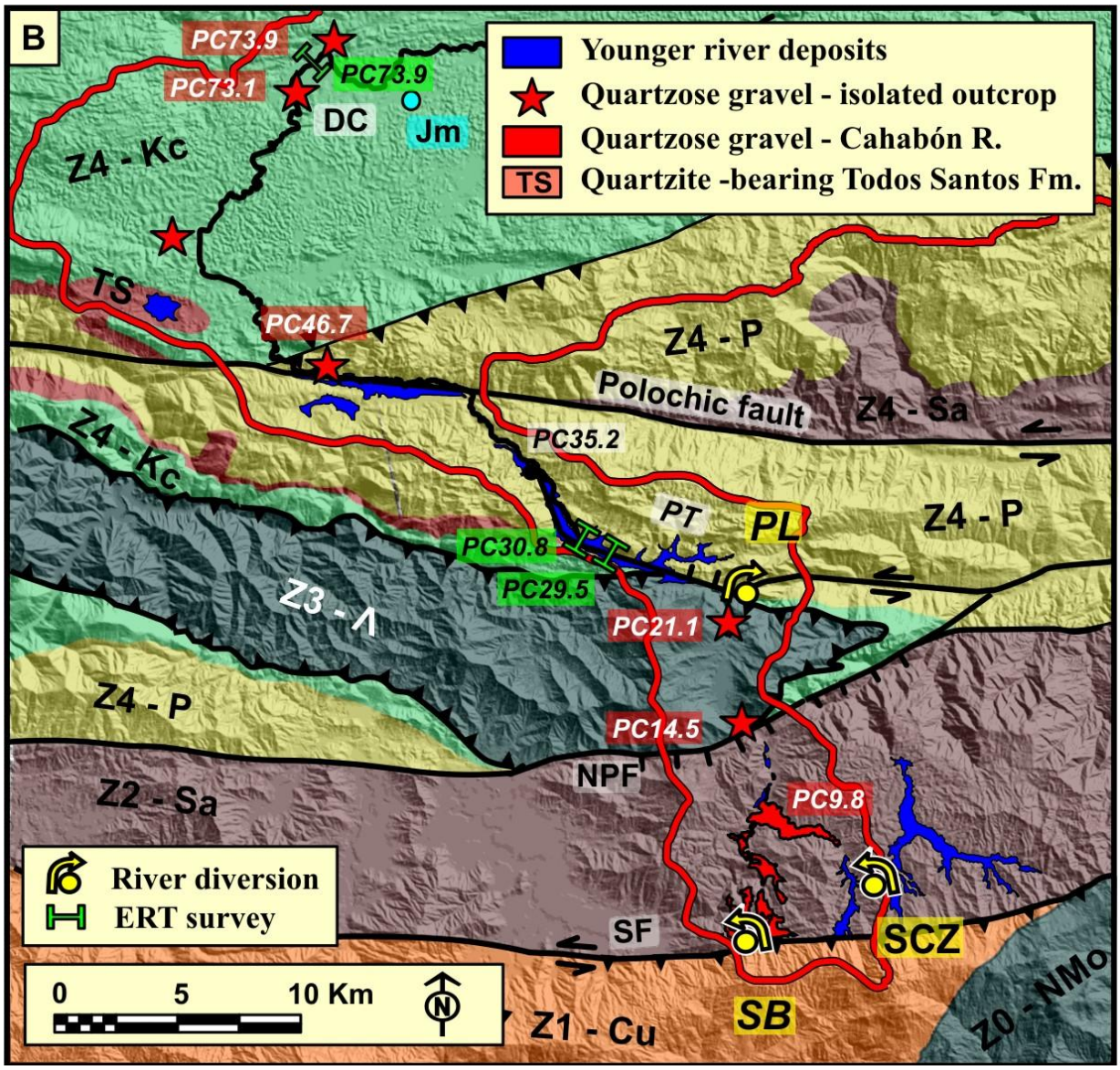

Fig. 1. Map of the Cahabón River paleovalley.

(B): Basement geology along the paleovalley (after McBirney, 1963, modified). Zone 0, NMo: North Motagua Ophiolite; Zone 1, Cu: Chuacús gneisses and micaschists; Zone 2, Sa: Salamá Formation low-grade metamorphic (phyllites and intrusives); Zone 3, _: Baja Verapaz ophiolite; Zone 4, P: Permian carbonates (Chochal Fm.), shales (Tactic Fm.) and conglomerates (Sacapulas Fm.), TD: Jurassic red beds (Todos Santos Fm.), Kc: Cretaceous carbonates (Cobán and Campur Fms.), Jm: Pleistocene Jolomná Fm. lacustrine beds. DC: Depression of Cobán, PF: Polochic Fault, PT: Purulhátrough, NPF: NiñoPerdido fault, SF: Salamá Fault.

Study area: the Cahabón river valley

The 180 km-long Cahabón River is one of the main rivers of Guatemala (inset, fig. 1). It drains the narrow elongated range known as Sierra de las Minas–Sierra de Chuacús (SMSC), which has formed along the plate boundary between North America and the Caribbean domain. The range is the product of transpressional and transtensional deformations that characterize this plate boundary since the Late Cretaceous (McBirney, 1963; Donnelly and others, 1990). Its present topography is attributable to renewed uplift starting in the Middle Miocene (Brocard and others, 2011; Authemayou and others, 2011). The 2 $cm.y^{-1}$ left-lateral displacement of the plate boundary (DeMets and others, 2000) is mostly accommodated along the southern side of the SMSC by the Motagua Fault (Lyon-Caen and others, 2006). Another important strike-slip fault parallels the Motagua fault 50 km further north, across the northern side of the SMSC. Between these two faults, the core of the range experiences left-lateral transtensional shearing since the Pliocene (Authemayou and others, 2011). Deformation is distributed over numerous smaller faults that disrupt the topography. The Cahabón River headwaters are located within this array of secondary faults, half-way between the main drainage divide and the Polochic fault (fig. 1A). From its source, the river flows first northwards, down to the city of Cobán. Along this first stretch the river traverses the Polochic fault, across which the river displays a left-lateral offset. Past the city of Cobán, the river turns east and ultimately debouches into Lake Izabal. The present study focuses on the evolution of the first 45 km of the river, from the range main drainage divide down to the city of Cobán.

A topographically well-defined valley extends from the current river head up tothe range drainage divide (fig. 1A and Appendix 1). This dramatic paleovalley wasonce occupied by the Cahabón River, when the river initiated at the range drainage divide. In the following, the location of the described features is given according totheir distance to the range drainage divide, using notation PCx with x denoting thedistance in kilometers. The coordinates of the line along which distance is determined are given in Appendix 2. The paleovalley is breached at two sites, near Santa Barbara (SB, PC6), and near Purulhá (PL, PC22). The Cahabón River has been diverted through these breaches toward the Chixóy and Panimá Rivers, respectively. Extensive drainage reversal has subsequently modified the residual drainage of the paleovalley. Drainage is reverted over 11.5 km north of SB and over 6 km north of PL. The diverted waters experience a tremendous drop in base level as they flow into the breaches, with the water cascading through the SB breaches 500 m down to the ChixóyRiver and 1000 m down to the Panimá River through the PL breach. Water cascading into the breaches has carved dramatic canyons (see pictures, Appendix 1). A smaller diversion occurred near Santa Cruz (SCZ). It affected a divide between the Cahabón River and the Chilascó River. We use the breach of Santa Cruz as an analog of the early state of evolution of the SB breach. The eastern branch of the Chilascó River is regarded as a modern analog of the Cahabón River, as it appeared before the drainage rearrangement.

The valley of the Cahabón River incises a relict upland surface. This upland surface started to be dissected in the Middle-Upper Miocene (Brocard and others, 2011). The depth of incision of the Cahabón River valley into the upland surface varies along stream and is controlled by a series of tectonic blocks that disrupt the upland surface. The main features limiting these blocks are the Salamá Fault (SF, McBirney, 1963) at PC2, an unnamed fault that we propose to call the NiñoPerdido Fault (NPF) at PC14, a fault bordering to the south the tectonic trough of Purulhá(TP-SF) at PC22, the Polochic fault in the trough of Tactic from PC40 to PC50, and an array of recent faults generating diffuse subsidence in the depression of Cobán (DC) between PC70 and PC80.

The paleovalley contains river sediments deposited by the Cahabón River before the reorganization (fig. 1B). They have been extensively dissected after the breaching of the paleovalley, except in the tectonic troughs of Purulhá and Tactic. These old river sediments crop out along the paleovalley but also in fill-terraces along the modern residual Cahabón River. The

two largest and thickest occurrences of ancient gravels are found between PC2 to PC10, and in the depression of Cobán (PC70-80). Smaller outcrops are common all along the valley. River sediment accumulation has also occurred along the east and west branches of the Chilascó River, the next range-transverse river to the east. The west branch of the Chilascó River has been beheaded in Santa Cruz (SCZ) and its valley-fill is now exposed in a short canyon post-dating the breaching. The eastern branch of the river is still an actively aggrading river.

Methods

Sediment Provenance: Clast Assemblage and Matrix Elemental Analysis

The Cahabón paleovalley retains most of its original morphology and is therefore easily identifiable in the topography. However, a geological demonstration of the initial extension of the Cahabón River is desirable, considering that this paleovalley is described here for the first time. Its initial extent is demonstrated by the provenance of the deposits that predate the river's diversions. Sediment provenance is often the most compelling evidence of former sediment pathways (for example Pissard and others, 1997; Bridgland and Gibbard, 1997; Maher and others, 2007). We also test the ability of the sediment provenance to provide constraints on the relative chronology of captures PL and SB.

The Cahabón River is perfectly suited for a provenance study because the river crosscuts a series of rock belts composed of very distinctive rock types (fig. 1B). Petrographic assemblage determinations were carried out on one hundred clasts larger than 2 cm at 20 sites along the river deposits in combination with grain-size analysis (Appendix 3). Rocks such as serpentinite and shales are prone to rapid mechanical attrition and disappear from the gravel-cobble fraction within a few kilometers of their injection along the river. We therefore also conducted a bulk chemical analysis of the sandy-silty matrix at all sites to ensure comprehensive detection of all upstream rock types. The elemental composition of the matrix has proven useful in tracking sediment sources (for example Jaffey and Robertson, 2005). A subset of the sieved _1mmsediment fraction was powdered using an agate crusher and fused with lithium tetraborate in platinum crucibles. Major and trace elements composition was then measured by X-ray fluorescence spectrometry using a Rhodium anode at the Centre for Mineralogical Analysis of the University of Lausanne, Switzerland. The detection limit is 0.01 weight percent for major elements.

Water Provenance: Isotopic Study

The stable hydrogen and oxygen isotope compositions of meteoric and surface water are related to temperature-controlled processes of evaporation at the origin of the air mass transporting the water vapor, the amount of precipitation, the temperature and humidity during which the condensation is formed (for example, Rozanski and others, 1993). As such, the isotopic composition of surface waters may vary from one drainage basin to another depending on the average altitude, and thus temperature of condensation, and topography of the catchment. Measurements of the isotopic composition of river and source waters may thus help to determine the provenance of the waters and potential mixing processes of waters of different catchments.

The oxygen and hydrogen isotope composition of waters was analyzed using a Picarro L1102i Wavelength-Scanned Cavity Ring Down Spectroscopy (WS-CRDS) system. Each sample was injected eight times and an average of the last five measurements was taken to calculate the raw value. Each sequence was calibrated using three different internal standards, which are periodically calibrated against the international VSMOW and SLAP standards of the IAEA. Isotopic ratios measured are reported in the common delta units (permil deviation of the isotope ratio of the sample relative to that of the international standard VSMOW). The standard deviation of repeated measurements of the standards and samples was ±0.07 permil for oxygen and ±0.4 permil for hydrogen.

Valley-Fill Structure Imaged by Electrical Resistivity Tomography

The paleovalley was surveyed extensively to identify all the outcrops of ancient river deposits. The outcrops were then correlated vertically using repeated measurements of their relative elevations by high precision altimeters and long-distance laser rangefinders with a vertical precision of ±1 m. A series of longitudinal and transverse sections of the paleovalley fill was then constructed. These sections highlight changes in sediment thickness and in valley floor elevation that are due to tectonic displacement on faults or to tectonic tilting.

In the tectonic troughs of Tactic and Purulhá, sedimentation is still taking place over much of the valley floor so that its inner structure cannot be investigated from outcrops. In such circumstances, we used 2D Electrical Resistivity Tomography (ERT) to image the architecture of the valley fill. Because of its sensitivity to porosity, salinity, and saturation as well as to the presence of clays, ERT is an efficient tool to image the shallow subsurface in general (for example Binley and Kemna, 2005) and for addressing neotectonic problems in particular (for example Caputo and others, 2003; Rizzo and others, 2004; Nguyen and others, 2005; Diaferia and others, 2006; Vanneste and others, 2008; Suski and others, 2010). Its relative simplicity, efficiency, and the robustness of the data acquisition make it particularly amenable to the difficult logistic conditions in remote regions, such as the one studied here. The measurements were undertaken in February 2008, 3 to 4 months after the end of the rainy season. The geoelectrical data were acquired using a Syscal multi-channel resistivity system and a dipole-dipole array of 48 steel electrodes. The spacing between the electrodes was 10m spacing, which provided a maximum exploration depth of ~80 m. The measured data were then tomographically inverted to obtain the spatial distribution of the electrical resistivity in the probed subsurface. The imaging procedure uses smoothness constrained least-squares inversion implemented by quasi-Newton optimization (Loke and Barker, 1996). The starting model for the inversion is a homogenous electrical resistivity distribution equivalent to the average apparent electrical resistivity values of each corresponding section. The tomographic inversion procedure then iteratively adjusts the 2D electrical resistivity distribution to reduce the difference between the calculated and measured apparent electrical resistivity values. The root-mean-square (RMS) error measures this difference. For the three profiles imaged in this study, convergence was achieved after 3 to 5 iterations with RMS errors stabilizing in the 2 to 5 percent range.

^{26}Al-^{10}Be Burial Dating of the Valley Fill

Dating of the valley fill was undertaken to determine the age of the river captures. The targeted sediment is the quartzose-bearing gravel deposited by the ancestral Cahabón River. It invariably appears as an alternation of quartzose-rich gravelly channel belts and clayey-silty floodplain deposits. Its high quartz content and substantial thickness make this deposit suited for a dating approach using the differential decay of cosmogenic ^{26}Al and ^{10}Be produced in the quartz gravel after its burial into the valley fill.

Terrestrial cosmogenic ^{26}Al and ^{10}Be are produced by cosmic particles interacting with soil and rock within the first few meters below the Earth's surface. The clasts sampled along the Cahabón valley have been exposed to cosmic rays upstream in the river catchment, mostly during their final exhumation as they travelled through the last few meters of soil before reaching the surface. Subsequent cosmogenic accumulation during river transport down to the site of deposition is regarded as minimal compared to the accumulation during previous exposure. Samples are composed of sand and individual gravel clasts that were extracted at the base of 1 to 3 m deep channels to minimize the amount of post-deposition exposure at the beginning of the burial period. Post-deposition exposure decreases as more sediment is deposited above the samples. Then, as burial becomes deep enough to ensure complete shielding from cosmic rays, the concentration of ^{26}Al and ^{10}Be will decrease according to their decay half-lives of 0.71 My and 1.4 My, respectively (Samworth and others, 1972; Chmelleff and

others, 2010; Korschinek and others, 2010). Provided that the $^{26}Al/^{10}Be$ production ratio is known, the current $^{26}Al/^{10}Be$ concentration ratio of the buried samples can be used to retrieve their burial age (Lal, 1991; Granger and Muzikar, 2001). The method can be applied to burials ranging in age from a few 10^5 y to ~4.10^6 y. The $^{26}Al/^{10}Be$ production ratio in quartz is 6.1 at the Earth's surface (Nishiizumi and others, 1989; Bierman and Caffee, 2002).

In a plot of $[^{26}Al]/[^{10}Be]$ versus $[^{10}Be]$, two curves delimit an "erosion island" defining the range of initial values that can be observed at the Earth's surface. The upper curve represents the range of values that are expected on non-eroding surfaces of various ages, while the lower curve represents the range of values expected on surfaces of infinite age but various erosion rates. The surfaces that have experienced a simple exposure/erosion history are expected to occupy the value domain bracketed by these curves delimiting the "erosion island." Along most rivers, transportation and sediment storage is generally of short duration compared to the duration of exhumation of rocks through the cosmogenic production zone. Therefore, it does not affect the initial ratio significantly (Schaller and others, 2001). Upon settlement and burial, the $^{26}Al/^{10}Be$ ratio of the sediment drifts below the "erosion island" and the distance below the erosion island is proportional to the burial duration. More complex exhumation and burial will affect the final ratio and make age determination not unique. Therefore, initial ratios are either assumed to conform to theory or are approximated by the ratio measured in modern sediments used as proxies for the buried sediment. The proxy is generally the modern bedload of the same dispersal system that conveyed the buried sediment in the past, if this system still exists (for example Granger and others, 1997; Stock and others, 2004; Haeuselmann and others, 2007). Here, because the Cahabón drainage has been modified, we have chosen to use the $^{26}Al/^{10}Be$ ratio of river sediments along the streams that now drain various sub-catchments of the original catchments from which the samples were derived and from the east branch of the Chilascó River because of its environmental similarities to the ancestral Cahabón River.

^{10}Be and ^{26}Al were extracted from quartz grains according to routinely applied procedures. Samples were prepared at the University of Minnesota Cosmogenic Isotope Lab. Analysis was performed on single clasts of the gravel fraction, on amalgamated grains of the sand fraction, and on amalgamated gravel clasts at site PC73.9L due to the small clast size of less than 2 cm along the long axis. Sample crushing, quartz grains isolation and dissolution, ^{9}Be and ^{27}Al spike addition, and ion exchange of Be and Al were performed following an adaptation of the technique of Kohl and Nishiizumi (1992). The measurements of the ^{10}Be and ^{26}Al concentration were performed at the PRIME Lab Accelerator Mass Spectrometry (AMS) facility at Purdue University. The 10Be and 27Al analyses were calibrated against the revised ICN Standard (after September 2007). Results are given in table 1. For age calculation we used a high-latitude sea level production rate of 5.1 $atoms.g^{-1}.y^{-1}$ (Balco and others, 2008). The largest uncertainties on ratios and ages arise for ^{26}Al measurements and hence the few samples for which these uncertainties are very large are excluded from age calculations.

Geomagnetic Polarity of the Valley-Fill

The ages determined by the differential decay of ^{10}Be and ^{26}Al carry significant uncertainties. To reduce these uncertainties, we undertook the measurement of the geomagnetic polarity of floodplain sediments taken on the outcrops used for cosmogenic dating. The cosmogenic ages are expected to be consistent with the geomagnetic polarity of the Earth at the time of sediment deposition. The samples should have a normal (modern) polarity if they were deposited after 780 ky (Bruhnes chron) or between 1.06 My and 0.9 My (Jaramillo chron). They should exhibit a reverse polarity if deposited between 0.78 and 0.9 ky or before 1.06 My. The age uncertainty is reduced to the part of the uncertainty that remains within the chron consistent with the sample age. The measured sediment is composed of silty floodplain and silty channel deposits taken at seven sites along the Cahabón River (PC 2.5, PC 6.1, PC 9.8, PC 73.1, PC 73.9R and PC 73.9 L) and at one site along the West branch of the Chilascó River (CLW 6.2). Natural remanent magnetization was measured and subjected to stepwise alternating field demagnetization on 35 oriented samples. All remanent magnetizations were measured using the

Sampling site	Sample #	Clast type	Easting (°)	Northing (°)	Altitude (m)	*[^{10}Be] 10^4 at.g^{-1}*	*[^{26}Al] 10^4 at.g^{-1}*	^{26}Al/^{10}Be	Burial age (kyrs)	Initial *[^{10}Be] 10^4 at.g^{-1}*	P_o C: *at.g^{-1}.yr^{-1}*	ε_0 *mm.yr^{-1}*
PC 6.1	14	SC [B]	-90.1834	15.0954	1490	6.85 ± 0.41	31.95 ± 5.64	4.66 ± 0.24	580 ± 250	8.79	9.6	0.07
	15	SC [B]	-90.1834	15.0954	1490	5.00 ± 0.30	23.19 ± 3.96	4.64 ± 0.23	590 240	6.44	9.6	0.10
	18	*S [B]*	*-90.1834*	*15.0954*	*1490*	*5.86 ± 0.33*	*21.39 ± 10.58*	*3.65 ± 0.55*	*1 100 ± 950*	*9.40*	*9.6*	*0.06*
PC 4.7	1	S [M]	-90.1820	15.0792	1450	27.56 ± 1.12	156.71 ± 16.61	5.69 ± 0.15	-	-	10.2	0.02
PC 9.8	1	SC [B]	- 90.1687	15.1116	1510	4.23 ± 0.29	20.64 ± 3.20	4.88 ± 0.22	480 ± 190	5.20	10.7	0.14
	3	SC [B]	- 90.1687	15.1116	1510	4.37± 0.27	20.98 ± 3.59	4.80 ± 0.23	520 ± 240	5.45	10.7	0.13
	4	*SC [B]*	*- 90.1687*	*15.1116*	*1510*	*10.35 ± 0.53*	*46.49 ± 27.70*	*4.49 ± 0.65*	*660 ± 1200*	*13.7*	10.7	*0.05*
	7	S [B]	- 90.1687	15.1116	1510	3.99 ± 0.20	17.24 ± 4.32	4.32 ± 0.30	740 ± 430	5.49	10.7	0.13
	8	SC[M]	- 90.1687	15.1116	1510	87.23 ± 2.72	531.60 ± 21.30	6.09 ± 0.07	-	87.2	11.4	0.01
	9	*SC[M]*	*- 90.1687*	*15.1116*	*1510*	*3.97 ± 0.78*	*27.59 ± 3.22*	*6.96 ± 0.31*	-	*4.0*	*11.4*	*0.22*
	13	S [M]	- 90.1687	15.1116	1510	21.46 ± 0.90	128.41 ± 11.66	5.98 ± 0.13	-	21.5	11.4	0.04
PC 73.9L	1	AC [B]	-90.4126	15.4753	1319	8.95 ± 0.59	38.5 ± 11.7	4.3 ± 0.37	750 ± 520	12.4	10.3	0.05
CLE 9.5	2	SC [M]	-90.1015	15.1041	1830	38.00 ± 0.19	230 ± 33.0	6.05 ± 0.19	-	38.0	12.8	0.02
CLW 6.2	1	SC [B]	-90.0949	15.0949	1823	65.00 ± 0.26	390 ± 42.2	6.01 ± 0.15	33 ± 150	65.9	12.6	0.01

Table 1, ^{10}Be - ^{26}Al concentrations, inferred ages and initial erosion rates

Analytical uncertainties are based on counting statistics (1σ), and conservative assumptions of 5% variability in accelerator response based on a 15 yrs. ^{10}Be/^{9}BeNIST=2.68.10^{-11}; ^{9}Be carrier: 300 µl of 10^{-3} g.l^{-1} . Clast types— SC: single clast, S: sand, AC: amalgamated clasts, [B]: buried, [M]: modern. In italic: samples discarded from calculations for their large uncertainty. Burial age: calculated considering an initial ^{26}Al/^{10}Be ratio of 6.1, and half-lives of 720 ky (^{26}Al) and 1390 ka (^{10}Be, Chmeleff *et al*., 2008); P_oC — production rate in reconstructed catchment, from modern elevations, calculated using polar sea-level ^{10}Be production rate of 5.1 at.g^{-1}.y^{-1} (Balco, 2008), and, for each cell in the 30' SRTM DEM, scaling factor for latitude and elevation following Dunai, (2001), shielding factor following Heidbreder *et al.* (1971) for topography, and Plug *et al.* (2007) for forest cover. Forest cover from data on Fig.13b, ε0 — average erosion rate in reconstructed catchment.

Site	Sample	Statistics	Range (mT)	n	Declination (°)	Inclination (°)	α95(°)	k	Quality	Polarity
CLW6.2	8	Kir	005-050	9	325.9	54.9	4.3		High	Normal
	9		005-050	9	25.7	29.7	4.3			
	10		015-050	7	3.8	32.6	3.9			
PC73.9R	7	Kir	010-050	8	24.3	31.1	11		High	Normal
	8		010-050	7	18.9	16.4	4.8			
	9		010-050	8	6.8	25.7	4.6			
	6		020-050	7	10.4	38.8	7.8			
PC73.9L	2	Kir	020-050	5	256.8	39.8	23.4		High	Undetermined
	3		010-050	8	266.4	15.5	18.3			
	4		010-050	8	209.7	32.6	14			
	5		010-050	8	192.5	31	29.2			
PC73.4	3		010-050	7	252.9	31.1	31.2		Low	
PC2.5	1	Fish	005-100	14	21.9	-51.5	8.4	23.6	Low	Undetermined
	2		000-120	13	116.3	-6.5	11.2	14.7		Reverse
	2		025-120	10	128.1	-17.8	12.8	15.2		Reverse
PC6.1	21	Fish	005-100	14	179.4	-75.4	3	27.9	Low	Reverse
	22	Kir	015-030	4	196	-23.6	33.4		Medium	
PC9.8	19	Kir	010-050	8	358.7	26	7.1		High	Normal
	21		010-050	6	213.5	7.3	6.5			Undetermined

Table 2, Geomagnetic results

From left to right: samples and sites identification, type of statistics: Kir (Kirschvink, 1980) or Fish (Fisher, 1953), range of demagnetization alternating field and number of data used for statistical calculation. Declination and inclination of the characteristic remanent magnetization: statistical parameters (alpha 95 and k), quality of the demagnetization pattern and interpretation in terms of geomagnetic polarity. All calculations and statistics have been produced using PaleoMac software (Cogné, 2003).

superconducting rock magnetometer 2G760R (2G enterprises) of the CEREGE (Aix-en-Provence, France). Five samples presented bad quality demagnetization patterns and 10 samples presented high coercivity magnetic signal impeding efficient alternating field demagnetization. Geomagnetic polarity determinations were therefore possible for the 20 remaining samples (table 2).

Results

Initial Continuity of the Paleovalley Demonstrated by Sediment Provenance

Sediment provenance analysis was used to demonstrate the initial continuity of the Cahabón River paleovalley from the range drainage divide down to the present river head. For the needs of the provenance analysis, rock sources were grouped into five regions (fig. 1B). From south to north, the region is composed of the high-grade metamorphic ophiolitic belt of the Motagua suture zone (Z0), the high-grade metamorphic Chuacús parautochthon (Z1), the low-grade metamorphic Salamá series s.l. (Z2), the Baja Verapaz ophiolite (Z3), and a "Laramian" fold-and-thrust belt comprised of Permian to Cretaceous siliciclastic and carbonate platform sediments (Z4). The range drainage divide is currently located within Z1. Petrographically, Z1 is essentially a monotonous alternation of micaschists and gneisses (McBirney, 1963). Z2 includes Cambrian to Carboniferous phyllites crosscut by granodioritic-granitic intrusives (McBirney, 1963). Z3 is composed of highly serpentinized peridotites and Z4 is composed of non-metamorphic rocks, such as Permian detrital sedimentary rocks (Sacapulas conglomerate, Tactic shales), Permian carbonates (La Esperanza and Chochal Formations), Jurassic continental red beds (Todos Santos Formation), Cretaceous evaporites and carbonates (Cobán and Campur Formations), and Upper Cretaceous turbidites (Sepur Formation).

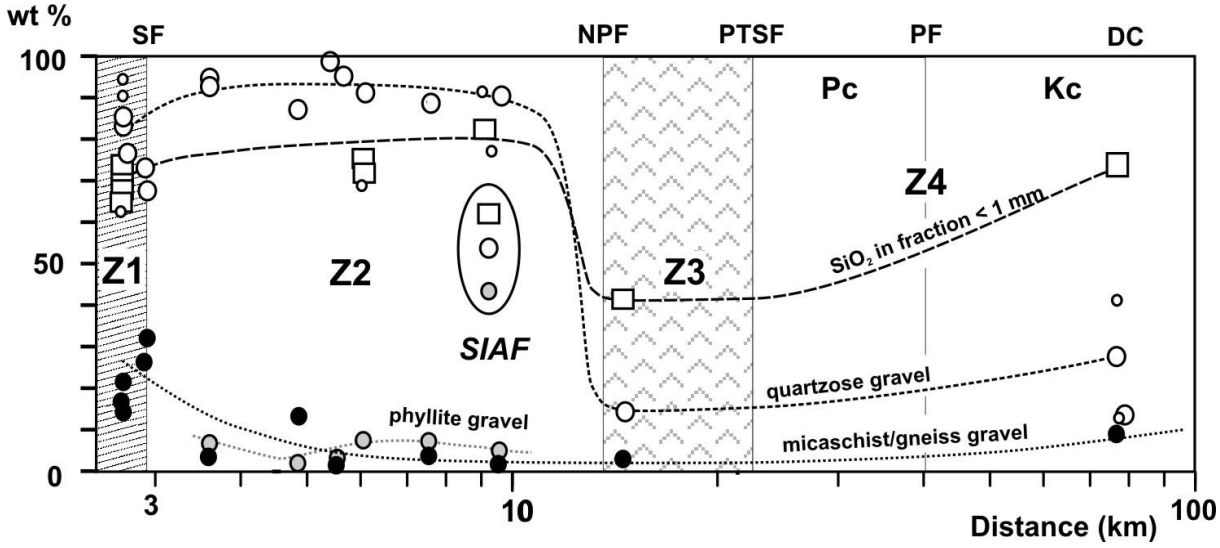

Figure 2. ***Downstream compositional changes in the deposits of the ancestral Cahabón River****. Bedrock composition divided in belts Z1: gneisses and micaschists, Z2: shales and phyllites, Z3: serpentinite, Z4-Pc: Permian limestones, Z4-Kc: Cretaceous limestones. Clast composition: solid circles: high grade micaschists, gray circles: low grade phyllites, large open circles: quartzose in clast fraction 2 cm; small open circles: quartz in the sand fraction, open squares: total SiO2 in fraction _1 mm. Features encountered along the Cahabón River: SF: Salamá Fault, SAIF: San Isidro alluvial fan, NPF: Niño Perdido Fault, PTSF: Purulhá trough south fault, PF: Polochic fault, DC: depression of Cobán.*

The modern Cahabón River only drains Z4, but its paleovalley drained zones Z0 to Z4 (fig. 1B). The composition of modern and ancient sediments along the Cahabón River reflects these temporal changes. The modern river bedload is composed almost exclusively of carbonates and is notably devoid of quartz. Conversely, the ancestral Cahabón River carried a lot of quartz. The only source of quartz in Z4 is quartzite gravel in the Jurassic red beds of the Todos Santos Formation (fig. 1B). Judging from the trace abundance of quartzite in the streams that currently drain Z4, it is likely that the Jurassic red beds have never been a major source of quartz for the Cahabón River. In addition, the quartz observed in the ancestral river deposits is composed of coarser grained, more translucent quartz (quartzose) than the one produced by the Jurassic red beds. The quartzose is derived from pervasive veins crosscutting Z1–Z2 rocks, in which the veins only occupy 5 percent or less of the host rock volume. Over Z1–Z2, the gravel-cobble fraction of the ancestral river deposits contains 60 to 95 percent quartzose (fig. 2). Their over-representation in the river sediment results from the combined effects of differential chemical weathering during rock exhumation and differential attrition during river transport. The ancestral gravel locally contains more abundant granite and schist elements (such as in SIAF, fig. 2), but the quartzose gravel rapidly concentrates again downstream due to its greater resistance to attrition (for example Attal and Lavé, 2005). The quartz fraction temporarily decreases over Z3 due to a large input of serpentinite before increasing again over Z4. For most of its length, the pre-capture Cahabón alluvium is thus typically a quartzose-rich gravel and the extent of the gravel demonstrates the initial continuity of the Cahabón River paleovalley from the drainage divide down to the city of Cobán (fig. 1).

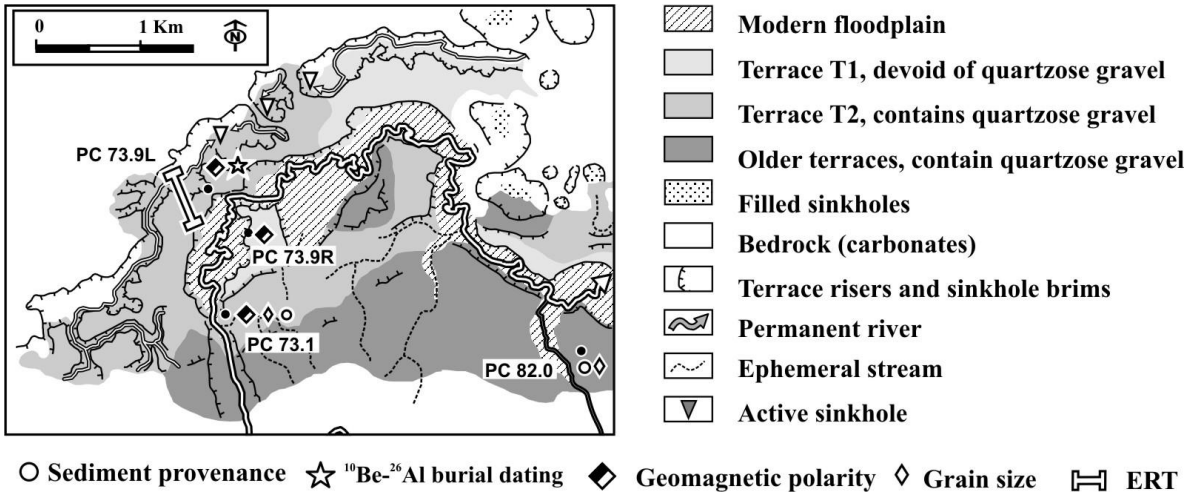

Figure 3. Sampling sites in the sediment fill of the Depression of Cobán.

The temporal shift from the quartz-dominated to the carbonate-dominated Cahabón is recorded over Z4 in a staircase of fill-terraces in the Depression of Cobán (DC, fig. 3). It reflects the occurrence of captures SB and PL upstream, along the Cahabón River. The main change in sediment composition occurs between terrace T2 (~+ 25 m) and T1 (~+ 10 m), in the form of a complete disappearance of the quartzose gravel. Quartzose shortage can be a consequence of capture PL, because capture PL cut-off quartzose feeding from Z1–Z2. It does not record the SB capture because this latter only partially captured the quartz feeding region. However, after the SB capture, the part of the feeding zone that escaped the initial diversion was progressively rerouted toward the capture site by drainage reversal along the Cahabón valley, to such an extent that today the entire former quartz-feeding zone is rerouted toward SB. As a result, quartzose shortage in Cobán either benchmarks the completion of this rerouting, in which case capture PL later affected an upstream area already devoid of quartz or capture PL cut-off access to an area still draining the quartz-feeding zone to an unknown extent, in which case no relative chronology between the two captures can be proposed. A petrographic tracer specific to the area located between capture PL and the reversed drainage is necessary to solve this

indetermination. By chance this reach of the Cahabón River only drains serpentinites (Z3). If the disappearance of quartz is a consequence of drainage reversal toward SB, then the serpentinite will still feed the Cahabón River in Cobán after reversal completion until the occurrence of capture PL. If the disappearance of quartz results from capture PL, then the serpentinite and the quartzose should disappear at the same time. Serpentinite gravel is comminuted down to sand and silt within a few kilometers from its source area. In the Depression of Cobán, the serpentinite must therefore be searched for within the sandy-clayey matrix of the terraces. To achieve this, we use the elemental concentration of Cr measured by XR fluorescence as a tracer of serpentinite. The method is validated by looking at the downstream evolution of the Cr concentration along the ancestral river course. The quartzose gravel is poor in Cr over Z1 and Z2 (14-70 ppm). The gravel then becomes strongly enriched in Cr after its passage over Z3, and its concentration is still high in terrace T2 in Cobán (120-300 ppm). Conversely, the concentration of Cr in terrace T1 (53 ppm) is indistinguishable from that of the upper reaches thus indicating that the river was no longer flowing over Z3 when T1 was deposited. The coeval cut-off of quartz and serpentinite suggest that quartz disappearance is due to the PL capture. The test is, however, not entirely conclusive as an intermediate stage of quartz-devoid but Cr-rich alluvium could have existed and not be preserved. At this stage, the provenance study demonstrates the initial continuity of the valley but the relative chronology of the captures cannot be established based on the sediment composition.

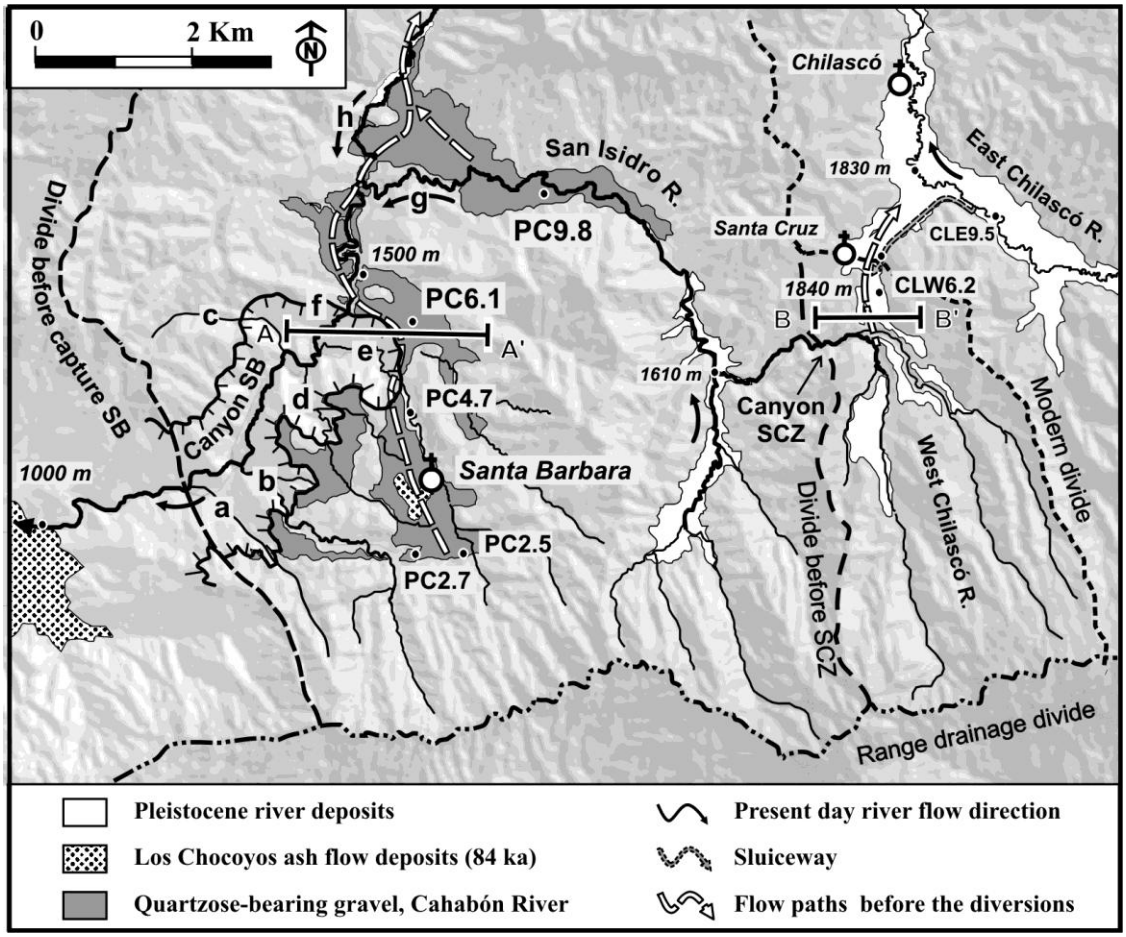

Figure 4. Map of the Santa Barbara (SB) and Santa Cruz river (SCZ) diversion sites.
This map shows the extent of the river deposits exposed near the sites of diversion, some sampling sites mentioned in the text (PCx), and the piecemeal eastward migration of the Chixóy River watershed as a result of these diversions. A-A´ and B-B': cross-sections of figure 5. Streams (a) to (g) feed the Santa Barbara Canyon.

Control of Faulting on Valley-Fill Formation

The geometry and extent of the paleovalley fill is used to reconstruct the tectonic pattern that the Cahabón River drainage was facing before it was reorganized. We correlate all the outcrops of quartzose-bearing gravel along the paleovalley. Where the valley-fill is not incised, we used the ERT to image the subsurface. The final reconstruction shows that the valley was partially filled with river sediment accumulating into separate depocenters delimited by tectonic faults. There is a link between valley filling and tectonic activity, and between the inception of tectonic activity and the initiation of the valley-filling period. This is illustrated here by the architecture of three depocenters.

Sedimentation between the Salamá Fault and the NiñoPerdido Fault.

Sedimentation has occurred between the Salamá and Niño Perdido faults along four streams: the Cahabón River, the San Isidro River, the West Chilascó River, and the East Chilascó River (fig. 4). The deposits look alike from valley to valley, invariably composed of gravelly channel belts alternating with sandy-silty floodplain sediments. Quartzose is always the dominant lithology in the gravel fraction. Cross-sections of the Cahabón and West Chilascó valleys (fig. 5) show that the fills are underlain by wide straths cut across vertically foliated phyllites. The straths are blanketed by boulder-sized lag deposits with a thickness of a few meters overlain by the main fill unit, which is a 40 m thick alternation of 1.5 to 3.5 m thick gravely channel belts and 0.5 to 1.0 m thick sandy-silty floodplain deposits. The whole sequence of river-borne sediments is sealed by a veneer of 1 to 2 m of greenish clays covered by colluvium and air-borne volcanic ash. The whole succession shows a systematic decay of the erosive power of valley axial drainage: an initial period of valley incision, coeval strath formation and sediment bypass is followed by the accumulation of substantial amounts of sediment. This aggradational stage is still underway along the East Chilascó River, which makes the East Chilascó River a modern analogue of the rivers that flowed in the three other valleys during the deposition of their fills.

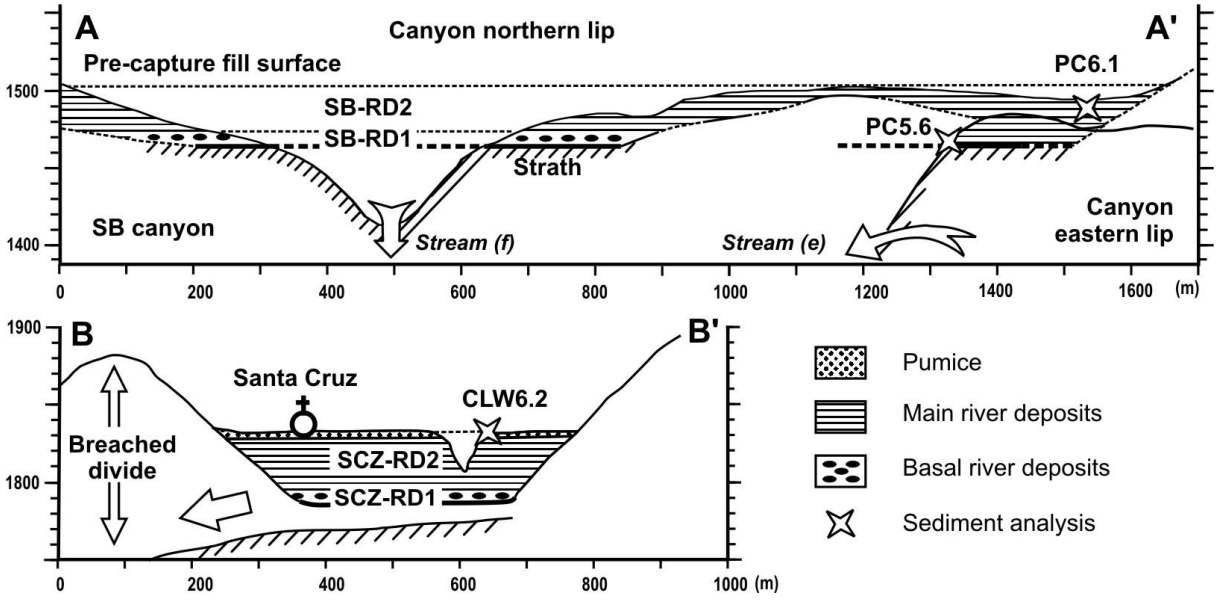

Figure 5. Cross sections of the paleovalleys of the Cahabón River. *(A) and West Chilascó River (B) near the capture site of Santa Barbara (SB, A-A' on fig. 4), and Santa Cruz (SCZ, B-B' on fig. 4), showing the general geometry of the valley fills and the location of some sampling sites. More detailed stratigraphic descriptions of the valley-fill subunits SB-RD1-2 and SCZ-RD1-2 are available in Appendix 2.*

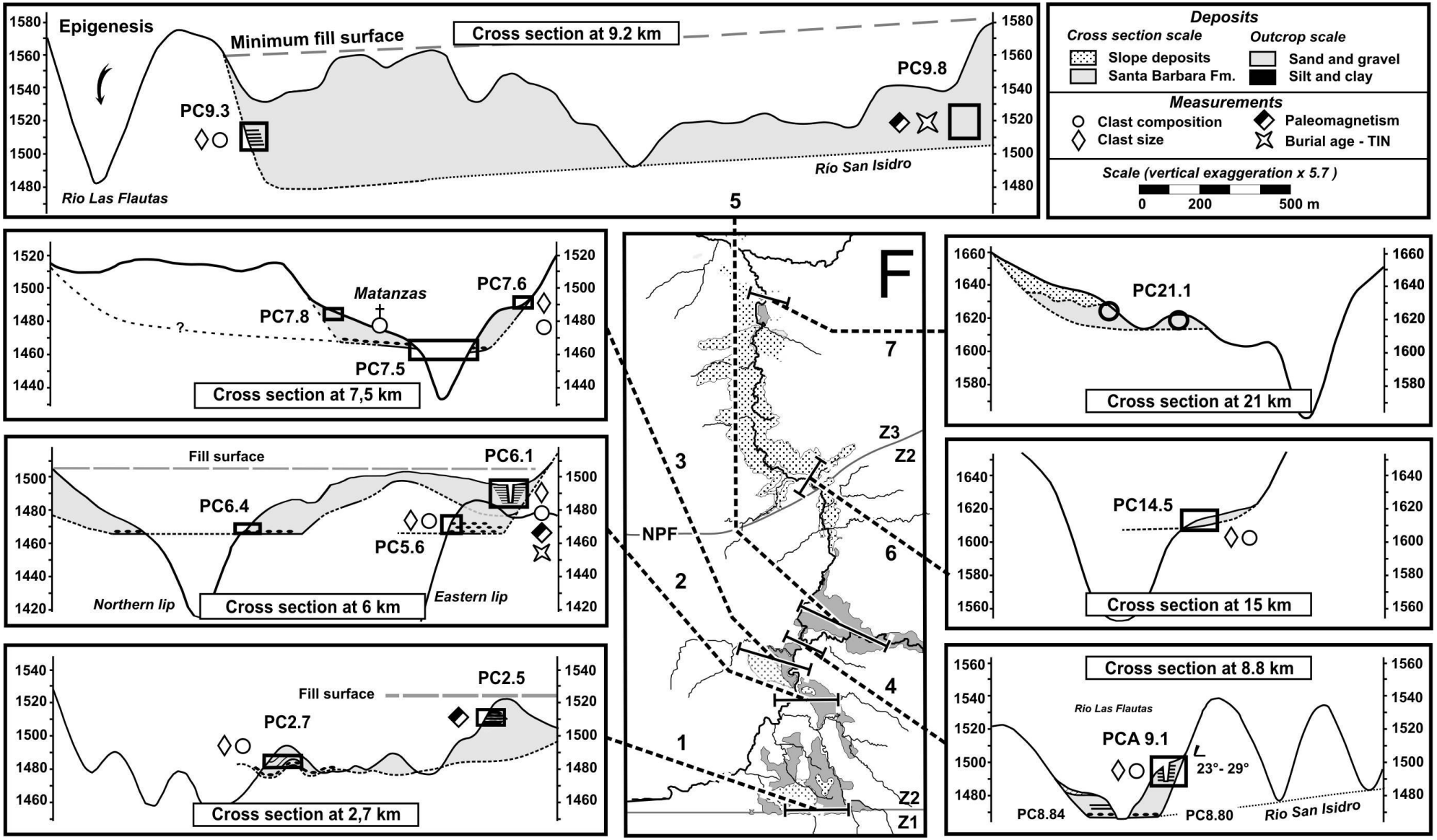

Figure 6. Seven cross-sections of the Cahabón River paleovalley between DC2 and DC21. The central map panel shows the location of each section. The section numbers corresponds to the section numbers on the longitudinal profile of the Cahabón paleovalley on figure 7.

The geometry of sediment deposition in plan-form and in cross-section shows the influence of tectonic deformation on the sedimentation pattern. In plan-form, the actively aggrading East Chilascó River possesses a strongly asymmetrical floodplain. The river tends to flow along the SW side of its plain, leaving 70 percent of the floodplain on the NE side (fig. 4). This allows for the development of large alluvial fans along the NE side, even if the tributaries feeding theses fans only drain 30 percent of the river catchment. Conversely, the larger SW tributaries have not built alluvial fans across the Chilascó River and alluviate along their own lower reaches well before joining the East Chilascó River. No difference in bedrock erodibility, climate, or catchment slope can account for this asymmetry. We therefore ascribe the asymmetry to tectonic tilting with a tilting vector striking between south and west. The valley fill of the West Chilascó River decreases in thickness from 40 m at Santa Cruz (SCZ), where it is entirely exposed, to zero north of the town of Chilascó (fig. 5). The combination of the tilting directions along the NW-SE East Chilascó valley and N-S West Chilascó valley suggests that the tilting vector strikes close to south.

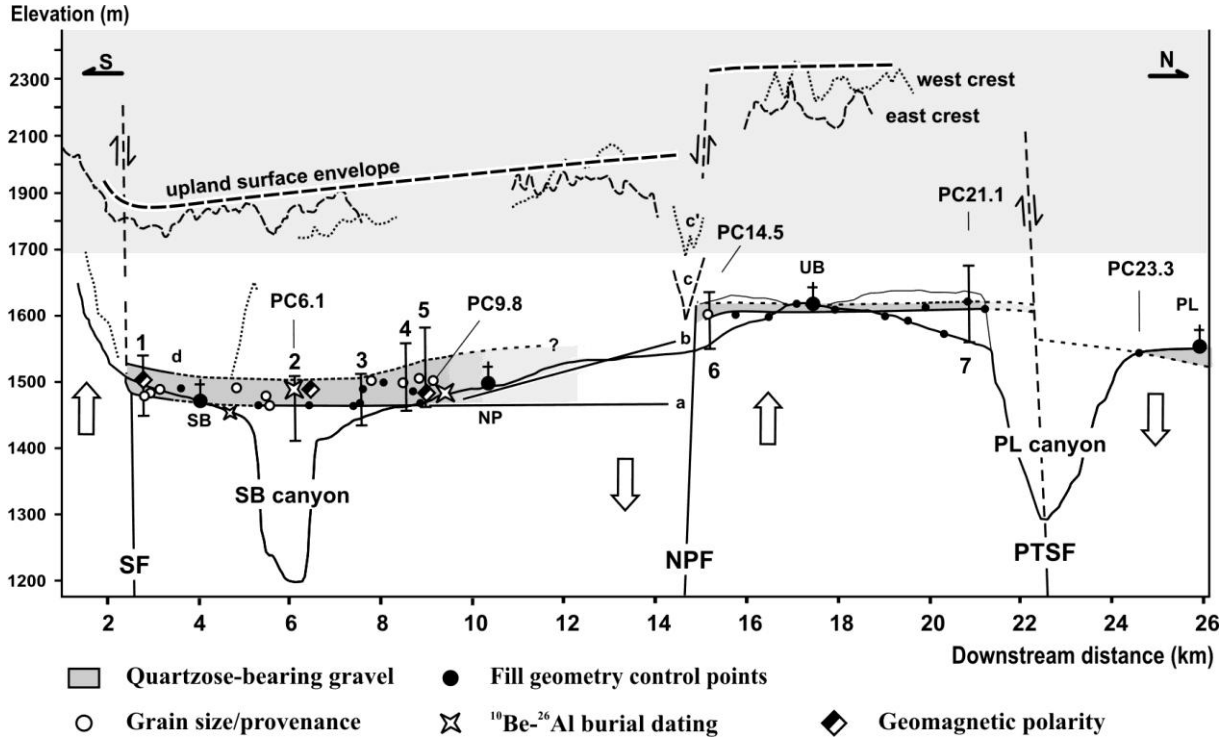

Figure 7. Long profile of the sediment fill in the Cahabón River paleovalley.
The features displayed on this profile have been projected on a valley axis defined in Appendix 1. The section shows the vertical and longitudinal extent of the valley-fill together with the faults that disrupt the valley-fill continuity, the location of our sampling sites, the location of the outcrop sections displayed on figure 11, the topographic profiles of the crests bordering the valley on each side, as well as the projected envelope of the relict upland surface. Solid lines (a) and (b) represent end-member models for the northward continuation of the valley basal strath near the Niño Perdido Fault used for fault slip rate calculations; (c) and (c') are deep breaches in the eastern and western interfluves; (d) corresponds to the breach associated with capture SB. Towns: NP: Nin˜o Perdido, PL: Purulhá, SB: Santa Barbara, UP: La Unión Barrios. Faults: SF: Salamá, NPF: Niño Perdido, PTSF: Purulhá Trough South fault.

The pattern of decreasing thickness observed along the West Chilascó valley is also observed along the Cahabón valley (figs. 6 and 7). The depocenter is located a few kilometers north of the Salamá Fault, between PC2 and PC8. Folds and faults are observed in the valley fill in the vicinity of the Salamá Fault and indicate that the Salamá Fault has been reactivated with a

left-lateral component of displacement during the current episode of transtension (Authemayou and others, 2011). The valley fill thins progressively northwards, except where the deposit incorporates the lateral fan of the San Isidro stream, the largest tributary of the Cahabón River. Further north, the base of the fill is no longer exposed, making its thickness difficult to evaluate near the NiñoPerdido fault (NPF). North of the fault the base of the fill is well exposed (PC15; PC21), but the original fill surface is nowhere preserved. However, because the preserved fill thickness nowhere exceeds 5 to 10 m in that area, it is likely that the original fill was not much thicker north of the NPF. The pattern of sedimentation along the valley thus indicates that the Salamá and NiñoPerdido Faults have delimited an area of relative, uneven subsidence between the two faults.

The role of these faults in controlling the pattern of subsidence is best evidenced along the NPF, because the NPF most clearly displaces the upland relict surface. The valley fill surface has experienced ~115 m of differential uplift from PC8 to PC15. Over the same stretch, the older base of the valley fill has experienced ~200 m of vertical displacement and the older upland surface was uplifted by 510 m. The increasing offset with time demonstrates that the fault has been active throughout the accumulation history of the valley fill and has continued since with one shallow earthquake recorded on the NPF between 1964 and 2005 A.D. (Lodolo and others, 2009). The deformation of the upland surface is a combination of distributed warping/tilting south of the NPF and discrete offset across the NPF. It is unclear whether tilting and faulting of the relict surface are coeval or have occurred in succession, and if, therefore, the basal strath of the Cahabón valley is only offset or also tilted. Both possibilities have been considered (profiles "a" and "b" on fig. 7). In any case, the Cahabón River responded to the rise of the downstream reaches by accumulating 40 m of sediments upstream of the NPF fault, while still incising the bedrock downstream of the fault. The amount of incision achieved during upstream sedimentation is unknown but at most 400 m, which is the difference in valley incision into the upland relict surface across the NPF.

Sedimentation in the tectonic trough of Purulhá

From the capture site PL down to the Polochic fault, the Cahabón valley crosses two tectonic depressions: the trough of Purulhá (TP) and the trough of Tactic (fig. 1). These depressions are active areas of sedimentation occupied by extensive floodplains. The ancestral quartzose-bearing deposits crop out at the extremities of these depressions. They show that the gravel initially covered these areas continuously but has foundered in places as a result of tectonic subsidence. Considering the recent age of the gravel, we assume that the current pattern of subsidence is a continuation of the pattern that the ancestral Cahabón River was facing when the gravel was deposited. We analyzed the modern pattern of subsidence by looking at the architecture of the subsurface sediment fill in the trough of Purulhá (fig. 8). The floor of the depression displays a succession of marshes that alternate with large alluvial fans built by NE tributaries. The tributaries are separated by the triangular facets of a recent normal fault scarp that borders the trough to the NE. We refer to this fault as the Purulhá Trough–Northern Fault (PT-NF). The trough is bounded on the other side by a less conspicuous fault here referred to as the Purulhá Trough–Southern Fault (PT-SF). The PT-SF vertically offsets the Cahabón paleovalley at PC22, where the floor of the paleovalley hangs 50 m above the surface of the fill in the Purulhá Trough. In spite of its dramatic, youthful facets, the PT-NF does not disrupt the surface of the fans crossing its trace and sediment accumulation is abundant on its footwall. The morphological observation therefore suggests that subsidence is actually controlled by the PT-SF.

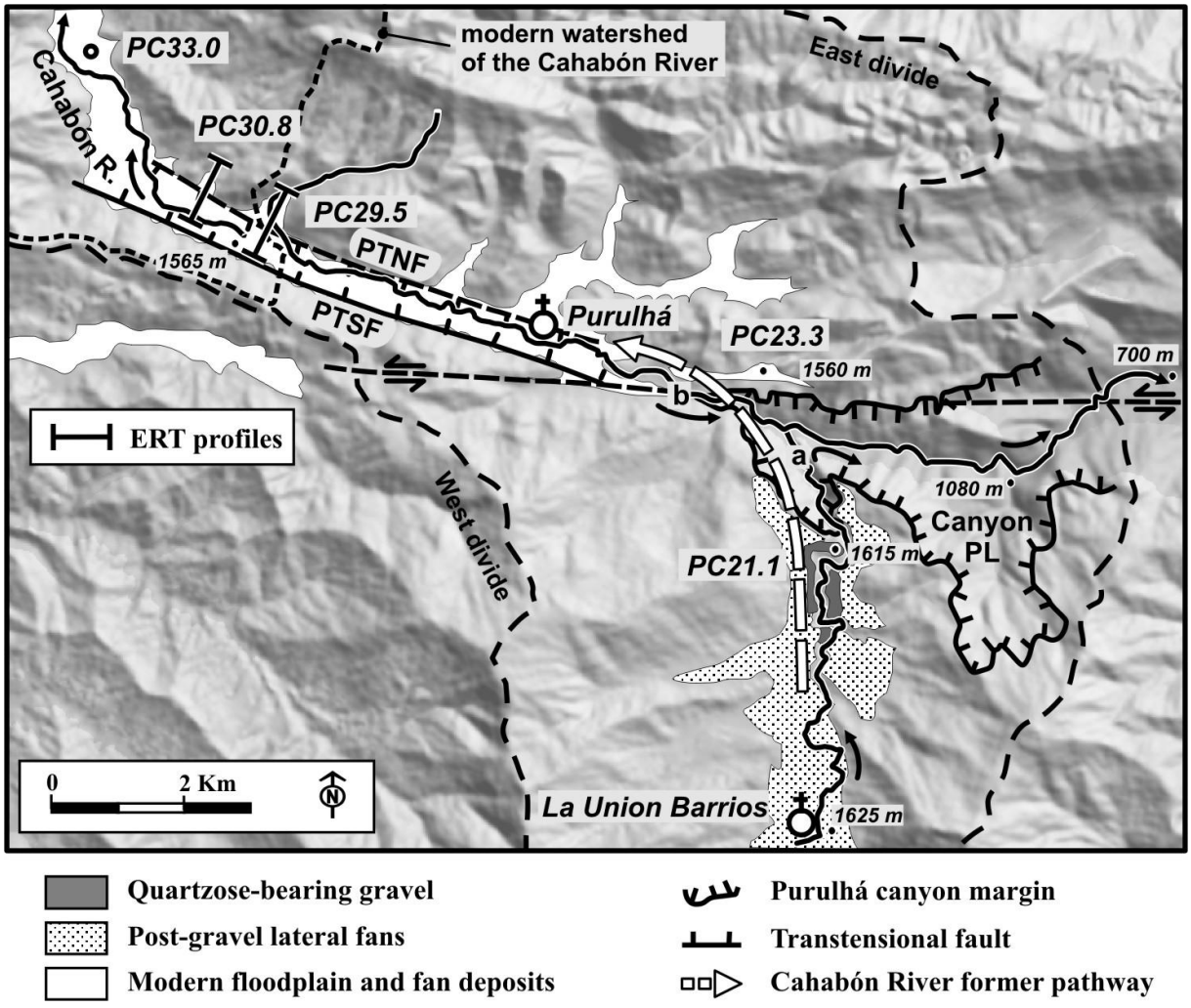

Figure 8. Topographic map of the Purulhá capture site and Purulhá trough.
PTNF: Purulhá trough northern fault, PTSF: Purulhá trough southern fault. Streams (a) and (b): upstream and downstream branches of the Purulhá canyon.

To confirm this inference, we used ERT to image the subsurface of the sediment fill. Two profiles were acquired along two alluvial fans. These profiles were located 1 km apart and straddled the entire width of the trough (fig. 8). The tomographic inversion of the observed apparent resistivity distributions shows that at both sites the valley fill is well layered (fig. 9). None of the tomographic images reached the bedrock, which in turn indicates that the valley fill is more than 80mthick. The fill is imaged as a regular alternation of thick units (8-40 m) of contrasting electrical resistivity (see Appendix 6 for details). Commercial boreholes drilled in another alluvial fan 2 km further downstream have encountered an alternation of silty clay and silty sand in a succession that matches the overall electrical layering of the upstream fans (PC33.0 on fig. 8, courtesy of Rodolfo Alvarado, Swissboring Overseas Inc., see Appendix 6). The deepest imaged unit (L4) was not penetrated by the boreholes. Because of its higher resistivity, we speculate that it corresponds to the quartzose alluvium. The electric profile at PC29.5 intersected the PT-NF. The fact that no offset is discernible in the layering down to a depth of 70 m confirms that the PT-NF is not active. Instead, a southward fanning of dips is discernible on both profiles, which we interpret as a rotational subsidence in the hanging wall of the PT-SF. This rotation/warping of the hanging wall seems to affect the Cahabón valley north of the trough far beyond the limits of the trough. It probably explains the extensive aggradation along the NE tributaries feeding the fans, up to 2 km north of the trough (fig. 8). The morphology of the

Cahabón valley itself, downstream of the trough, suggests that the entire domain between the TP-SF and the Polochic Fault undergoes a 7 km wide tilting/warping delimited by these faults. Where the Cahabón River exits the trough, its valley floor narrows down and contains highly degraded 20 to 50 m high strath terraces. Further north, in the absence of significant lithological change, the valley bottom keeps narrowing until it is reduced to the active river channel. The number of active landslides increases coevally in the downstream direction. These changes are compatible with an increase in incision rate in the downstream direction in response to block rotation/warping (fig. 10) with an axis of rotation located 4.4 km north of the PT-SF. The maximum measurable topographic throw of the PT-SF (380 m) would produce _5° of rigid rotation. The pattern of deformation faced by the Cahabón River observed in this area is similar to the pattern observed around the Niño Perdido Fault in that the valley is disrupted by transtensional faults and distributed warping or rigid tilting.

Sediment trapping in the Depression of Cobán

The last site of substantial sediment storage is the Depression of Cobán (DC, fig. 1), which is surrounded by carbonate highlands, in an area of lesser tectonic activity. The depression is delimited by fuzzy contorted boundaries that can be approximated by the drowning line of the regional cone karst within the sediments filling the depression (fig. 3). The sediment fill is a stack of imbricate fill-terraces or a staircase of fill-cut terraces incised into one single large body of quartzose gravel. The depression is bordered to the NW by a long trench along the contact of the carbonates with the sediment fill. The trench is separated from the Cahabón River by a tread of the terrace level T2 and results from the entrainment of the quartzose gravel into a series of sinkholes located 30 m below the level of the Cahabón River. The sinkholes collect the abundant leakage of the Cahabón River aquifer through terrace T2 and connect at depth with a cave network that feeds the Samcoc Spring, a resurgence located 7 km further north and 300 m below (Rykwalder, 2008). We conducted an ERT survey across the terrace T2 from the Cahabón River down to the NW trench (fig. 9). The imaged fill comprises an upper resistive sediment layer (300 Ohm.m, F1) overlying a more conductive formation F2 (25 Ohm.m). Water seepage and rock exposures along the free face of F2 show that these units correspond to the water-soaked river gravel. Below F2 a more resistive layer F3 corresponds at the surface to the carbonate country rock. From the ledge of the depression, the roof of F3 plunges down and disappears below the imaged section under the Cahabón River. The sediment fill is thus more than 95 m thick under terrace T2 and more than 70 m thick below the modern Cahabón River.

The depression of Cobán results from carbonate dissolution. Several similar large karstic depressions occur in the same area (fig. 1A). The floor of these depressions stands at the same elevation or at lower elevations than the bedrock floor of the depression of Cobán. These depressions drain into long underground pathways and feed large springs further north, hundreds of meters below. In the Depression of Cobán an extensive lacustrine and palustrine formation crops out along the southeast margin of the depression (Jolomná Formation, fig. 1B). The quartzose gravel of the Cahabón River is inset into the quartz-rich lacustrine deposits. The depression of Cobán thus resembles the other depressions in the area, but at some point in its history the Depression of Cobán became choked by the quartzose gravel brought by the Cahabón River. Tectonic subsidence may have also contributed to the formation of the Depression of Cobán, because the sediments of the Jolomná Formation are disrupted by NE-trending strike-slip faults (Authemayou and others, 2012) and its bedding sags gently towards the center of the depression.

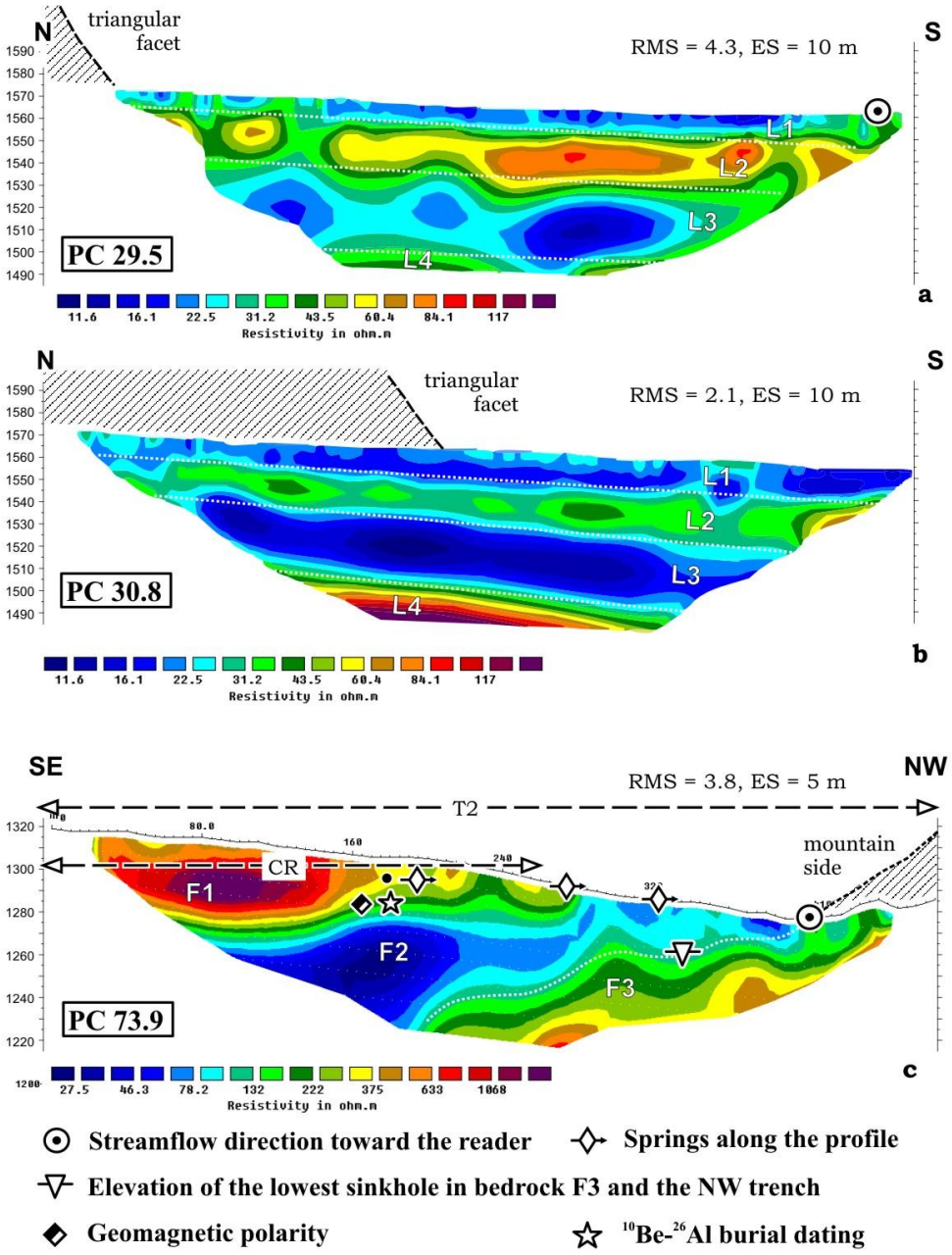

Figure 9. Electrical Resistivity surveys across the trough of Purulhá (at PC 29.5, PC 30.8) and across terrace T2 in the Depression of Cobán (at PC 73.9).

RMS: percent root mean square differences between observed and calculated data, ES: electrode spacing, CR: Cahabón River water line level, T2: terrace T2 surface level; L1 to L4 and F1 to F3 are electrical resistivity bodies described in the text and in Appendix 6.

Age of the Valley Fill

The sediment of the ancestral Cahabón River was dated by combining measurements of the *in-situ*-produced ^{10}Be-^{26}Al in quartz with the geomagnetic polarity of overbank deposits.

Sampling strategy

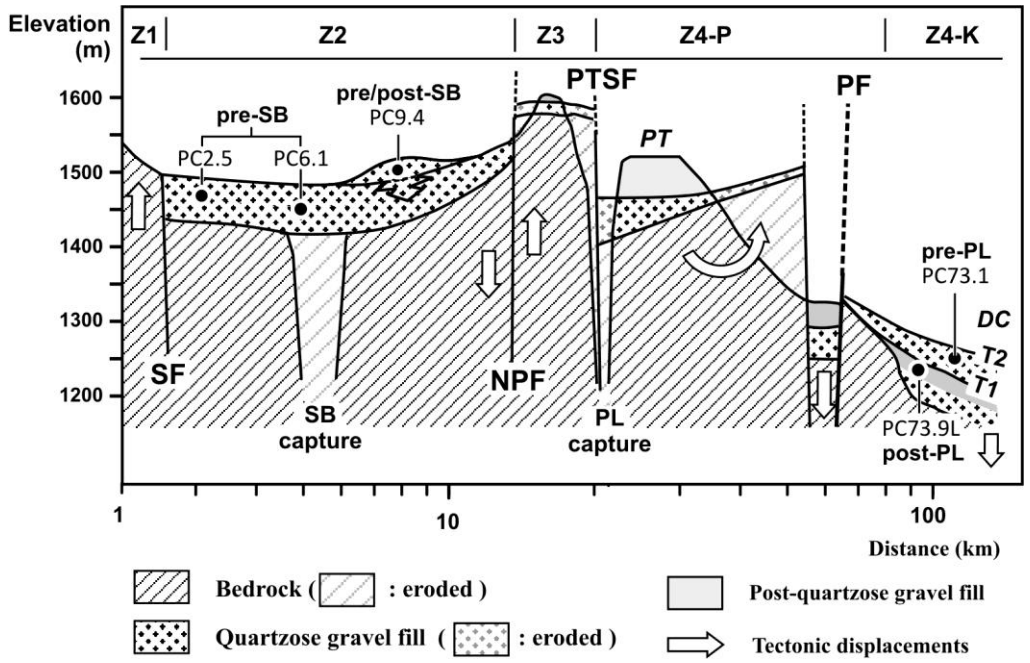

Figure 10. *Sketch longitudinal profile of the Cahabón River valley, showing the spatial relationship between the selected locations for sediment dating, the capture sites and the faults. Zones Z1 to Z4 correspond to the lithology groups used for the sediment provenance analysis (see the Sediment Provenance section in the methods section). SF: Salamá Fault, NPF: Niño Perdido Fault, PTSF: Purulhá trough South Fault, PF: Polochic Fault, DC: Depression of Cobán.*

The sampling sites provide temporal milestones to track the process of drainage rearrangement within the limitations imposed by material suitability and outcrop availability. Six sites were retained: CLE9.5, CLW6.2, PC2.5, PC6.1, PC9.8, and PC73 (figs. 1, 6, and 10). Sites PC 2.5 and PC 6.1 are located immediately upstream and downstream of capture site SB. They expose beds of the Cahabón valley fill 20 m below its upper surface, and 30 m and 20 m above its basal strath, respectively (fig. 6). They are aimed at dating the capture itself, because at the site of capture river aggradation likely ended just after the capture. Site PC 9.8 is located 3.5 km further downstream along the paleovalley and provides constraints on the propagation of the drainage reversal along the paleovalley. It is located within a large alluvial fan built by the San Isidro tributary at its junction with the Cahabón River. During its final growth the fan completely obstructed the valley and abuts the facing flank. Its growth was rendered possible by the inability of the beheaded Cahabón River to disperse downstream the alluvium delivered at the confluence by the San Isidro tributary. At the confluence, the Cahabón River lost three-quarters of its drainage area following capture SB and thus most of its transportation capacity. Fan inflation stopped and incision started when, during the drainage reversal, the San Isidro River was rerouted toward the south. Incorporation of the San Isidro tributary almost completely cut off the feeding of the Cahabón River in quartzose gravel, as it removed 67 percent of the largest source of quartzose gravel left in the Cahabón catchment after the river's beheading in SB. Sites PC-73.1R and PC-73.9L are located in the depression of Cobán within T2, the youngest of the quartzose-bearing terraces, whereas site PC-73.9R is located in the younger quartz-devoid

terrace T1. Disappearance of quartzose gravel from T2 to T1 is a consequence of capture PL or of the completion of drainage reversal toward SB. T1 and T2 therefore bracket in age one of these events or both.

Site CLW-6.2 is located near SCZ. It is aimed at confirming that the diversion of the West Chilascó River is very recent so that the 26Al/10Be ratio and the geomagnetic polarity at this site are expected to be indistinguishable from modern values.

^{26}Al-^{10}Be burial dating.

At the Earth's surface, *in-situ*-production of ^{10}Be and ^{26}Al is predominantly due to neutrons (98.5%) and to a much lesser extent to muons (1.5%, Braucher and others, 1998). In the subsurface, production by muons becomes dominant and amounts to ~1 percent of the surface production at a depth of 8 to 10 m. We therefore sampled the deepest and freshest outcrops currently available in order to minimize post-burial cosmogenic production. At all sites the samples have been unearthed in the last decade. In addition, the samples have been collected at the base of 1.5 to 2.0 m deep stream paleo-channels in order to maximize the depth of shielding at the beginning of the burial period. Site PC6.1 is a 10 m deep road trench (fig. 11). Gravel and sand were sampled at a depth of 9.5 m in the trench, some 20 m below the original upper surface of the valley fill. Site PC9.8 is a large gravel quarry (fig. 11). Gravel and sand were sampled 19.3 m to 20.6 m below the ground surface, 5 m above the base of the sediment fill, and 45 m below the top depositional surface of the San Isidro fan (fig. 11). Site PC73.9L is a scar of a large recent landslide triggered by water seepage through terrace T2. Gravel was collected 20 m below the surface of terrace T2. Site CLE6.2 is a scar in a 3-year-old landslide, located in the wall of a canyon incised into the sediments of the West Chilascó River. It was sampled 9 to 12 m below the surface of the valley fill. The measured values are reported in table 1 and figure 12.

We first verified that the ^{26}Al/^{10}Be ratios of modern sediments originating from the same catchments conform to the values expected for surfaces experiencing continuous erosion. We measured ^{10}Be and ^{26}Al in streams draining different parts of the ancestral catchment of the Cahabón River. Site PC4.7 is thus a proxy for the expected initial ^{26}Al/^{10}Be ratio at site PC6.1; and site PC9.8 is a proxy for the initial ratio at site PC9.8. At site CLE9.5 we sampled the East Chilascó River because this river, still in the depositional stage, is a modern analog of the ancestral Cahabón River. Almost all these initial ^{26}Al/^{10}Be ratios fall, as expected, within the given uncertainties, into the erosion island (fig. 12). One sample plots in the forbidden zone above the erosion island (PC9.8#9), but has a large measurement error. Such a high ratio sometimes results from aluminum loss during sample preparation (Ivy-Ochs, ms, 1996). We therefore believe that the observed drift of the ^{26}Al/^{10}Be ratio below the erosion island can be entirely attributed to post-burial decay.

At site PC6.1, three ^{26}Al/^{10}Be ratios give apparent burial ages between 580 _ 250 ky and 1100 ± 950 ky, with an average of 760 ± 340 ky. The one sand sample (PC6.1#18) is distinctly older and has a much larger uncertainty than the two single gravel clasts. Excluding this sample for its very large uncertainty yields a more restricted average of 590 ± 170 ky. At site PC 9.8, four 26Al/10Be ratios yield apparent burial ages ranging from 480 ± 190 ky to 740 ± 430 ky and an average of 600 ± 320 ky. One clast sample (PC9.8#4) carries a much larger uncertainty than the three others. Excluding this sample yields a more restricted apparent average of 580 ± 180 ky. All samples considered, site PC6.1 seems slightly older that PC9.8, though this is not significant within the given uncertainties. Excluding the samples with the largest uncertainties makes the two sites quasi identical in age.

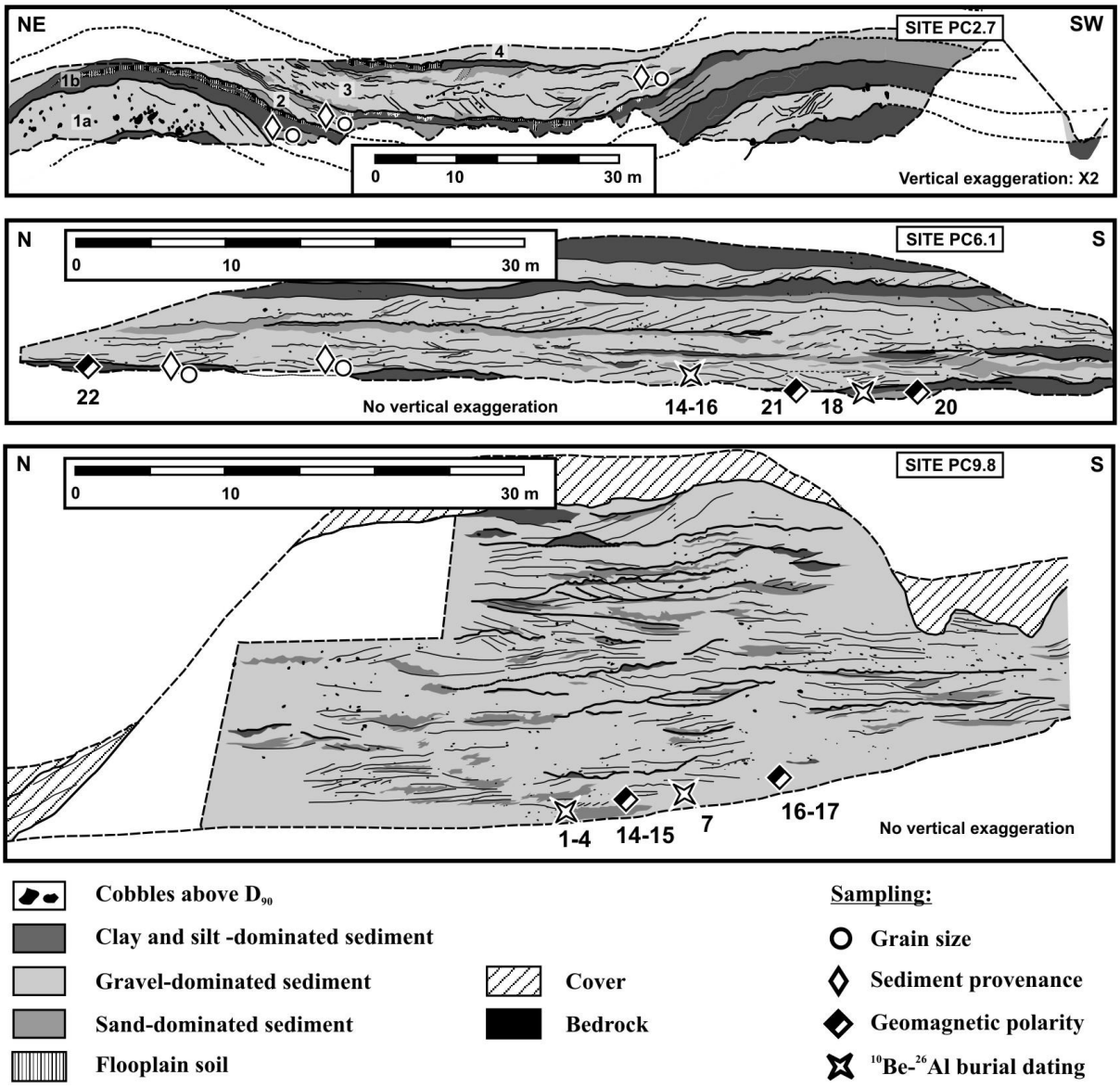

Figure 11. *Outcrop-scale sections illustrating the sediment architecture of the quartzose-gravel fill of the Cahabón paleovalley. Sample locations on outcrops are reported with number corresponding to sample numbers in tables 1 and 2. Results for geomagnetic polarity measurements: N: normal, R: reverse.*

At site PC 73.9, the amalgamated gravel sample yields an age of 750 ± 520 ky and predates the removal of the quartzose-feeding areas from the Cahabón catchment. Site CLW6.2 provides a maximum age for the diversion of the West Chilascó River in CSZ. As expected, the $^{26}Al/^{10}Be$ ratio is undistinguishable from the modern ratio with an apparent age of 30 ± 150 ky. A maximum age for the diversion is provided by a 84 ± 5 ky-old pumice ash layer which blankets the abandoned channel of the beheaded river (Los Chocoyos pumice, Drexler and others, 1980; Rose and others, 1986). The measured samples have been exposed to production by muons after their initial burial, during their descent and subsequent exhumation before we collected them at a final depth of 9 to 25 m. To evaluate the importance of this production and its possible distorting effects we ran numerical simulations of the maximal effect of post-burial production on the apparent ages (Appendix 4). Post-burial production tends to make apparent ages younger than the actual burial ages. We investigated the effect of the following variables: 1) catchment-wide initial erosion rate at the time of deposition (EC), 2) initial depth of burial (ID), and 3) long-term average sedimentation rate in the flood plain (SR). We ascribed reference values for each of

these parameters based on the local morphology and then varied successively the value of each parameter over more than an order-of-magnitude to test its influence. The age corrections for the reference values are only significant at site PC6.1 (5%) and remain within the AMS measurement uncertainties (≤15%). The correction is not sensitive to variations in EC, ID, and SR, except at site PC6.1, where the apparent age can be younger than the actual burial age by as much as 10 percent.

Geomagnetic polarity of the valley fill

The ^{26}Al-^{10}Be burial ages carry large uncertainties, which we seek to reduce by combining these ages with analyses of the paleogeomagnetic polarity of the sediments. The age uncertainty was thus reduced to the period over which the geomagnetic polarities overlap with the uncertainties of the ^{26}Al-^{10}Be ages (fig. 12). The samples are taken from silty floodplain and silty channel deposits at seven sites along the Cahabón River (PC-2.5, PC-6.1, PC-9.8, PC-73.1, PC-73.9R, and PC-73.9L) and at one site along the West Chilascó River (CLW-6.2). At several sites the measurements were inconclusive due to the migration and re-precipitation of iron oxides long after sediment deposition.

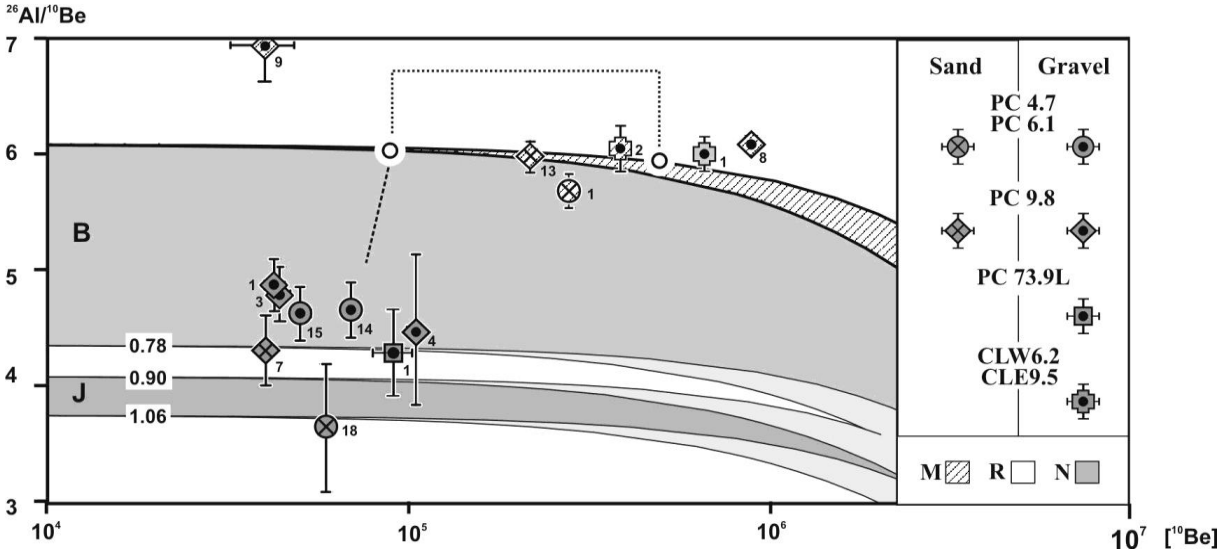

Figure 12. Plot of ^{26}Al/^{10}Be vs. [^{10}Be]. Geomagnetic chrons projected in the diagram: B—Bruhnes, J—Jaramillo.

Site CLW-6.2 was used to test the behavior of recent sediment. Avulsion SCZ is very recent and geomagnetic polarity was therefore expected to be normal. Samples taken 2 to 4 m below the top of the valley fill displayed a clear normal geomagnetic polarity (Appendix 5 and table 2). The samples collected near capture SB (PC2.5 and PC6.1, fig. 11B) display low- to moderate-quality reverse geomagnetic polarity. Reverse polarity is reconcilable with the large error bars of the sand sample at PC6.1, but it is inconsistent with the gravel ages as they fall within error into the normal Brunhes chron. The reverse polarity is thus in favor of the sand burial age despite its large error bars. Site PC9.8 has a similar cosmogenic age, but there one sample yielded a clear normal polarity (fig. 11C). These results seem contradictory, but we cannot rule out the possibility that the reverse polarity recorded at sites PC2.5 and PC6.1 may reflect a geomagnetic excursion, such as those documented during the Brunhes chron (Thouveny and others, 2008). In this case, the paleomagnetic results would agree with the gravel burial ages.

In the Depression of Cobán the samples are composed of massive to finely laminated silty clays collected between sandy bedforms in the quartzose-devoid terrace T1 (+10 m, PC73.5R), and of matrix lenses within the massive quartzose gravel of terrace T2 (+35 m, PC73.5L and 73.4, fig. 3). Terrace T2 did not yield any clear polarity, whereas terrace T1 clearly exhibits a

normal polarity. The polarity of terrace T1 is consistent with the cosmogenic age of terrace T2, which plots on the beginning of the current Brunhes normal chron (770 ± 530 ky).

From burial age to capture age

The ages obtained here correspond to the age of burial of specific sediment clasts at a certain depth in an aggrading floodplain. They provide a minimum age for the end of sedimentation, which, depending on the location, results either from a capture or from a drainage reversal event. A closer estimate of the age of the drainage reorganization can be proposed by assessing the time elapsed between sediment burial and the end of sedimentation. For this the time-averaged rate of sedimentation must be known at each site. This rate can be estimated at site PC6.1. During sedimentation, accommodation space was controlled by tilting downstream combined with offset on the Niño Perdido Fault (see the *Sediment Provenance: Clast Assemblage and Matrix Elemental Analysis* section under Methods). Once sedimentation ceased, tilting and faulting resulted in 115 m of differential uplift. Considering that PC 6.1 is located 20 m below the fill surface, a minimum of 135 m of differential uplift has accumulated at an average rate of 0.24 ± 0.07 $mm.y^{-1}$ since its deposition at 620 ± 180 ky. Considering that floodplain aggradation was keeping up with differential uplift prior to valley abandonment, this value corresponds to rate of sedimentation in the floodplain, assuming no significant change in fault velocity since valley abandonment. The proposed rate of sedimentation is consistent with the requirements of mass balance between erosion and sedimentation in the Cahabón catchment. The calculated initial 10Be concentration of the river sediments at sites PC6.1 and PC9.8 implies that the Cahabón River catchment was eroding at rates of 0.08 $mm.y^{-1}$ and 0.14 $mm.y^{-1}$ upstream of PC6.1 and PC9.8, respectively (table 1). The ancestral 90 km2 quartzose-feeding area shed onto a ~25 km^2 floodplain. The sedimentation rate (SR) cannot be more than 3.8 times larger than the erosion rate (EC), or SR/EC ≤ 3.8, for enough sediment to fill the accommodation space. In that respect, the fault-controlled sedimentation rate (0.24 ± 0.07 $mm.y^{-1}$) and the 26Al-10Be derived paleo-erosion rate (0.06-0.14 $mm.y^{-1}$) fulfill this requirement with SR/EC =1.6 ± 1.2. Applying the proposed sedimentation rate to the sediment column over PC6.1 then leads to an end of the sedimentation at 530 ± 210 ky. Capture SB occurred in the immediate vicinity and likely stopped the aggradation process at PC 6.1. This age is used in subsequent calculations as the age of capture SB, and is about 10 percent younger than the burial age.

In the absence of similar constraints at other sites, we use the sedimentation rate obtained at site PC6.1 to estimate the age at which sedimentation ends at the other sites. Applying PC6.1 rate at CLW6.2 is probably correct, considering that these sites share similar catchment sizes, erosion rates, bedrock types, and location within the same subsiding area. The inferred age of -10 ± 160 ky for the river diversion in CSZ is 40 ky younger than the burial age, but it is still consistent within uncertainties with the geological constraints (older than 84 ± 5 ka). It is more difficult to assess whether this rate overestimates or underestimates the age of cessation of sedimentation at PC9.8 (San Isidro fan) and at PC73.9 (Depression of Cobán). Our estimation of 400 ± 230 ky in the San Isidro fan is 30 percent younger than the burial age and is interpreted as the initiation of incision as a result of drainage reversal toward capture SB. The inferred age of 690 ± 550 ky for the abandonment age of terrace T2 in Cobán represents the maximum possible age of capture PL and is only 8 percent younger than the burial age.

Discussion: factors and rates of drainage evolution

A River Defeated by Slow-Moving Normal Faults

On the brink of being reorganized, the Cahabón River flowed across a series of tilted and faulted blocks (fig. 10). The defeat of a river by rising tectonic structures is expected to be favored by high fault velocities and large amounts of deformation, especially if, like in the case of the Cahabón River, the depth of the river valley impedes its lateral escape and forces it to cope with the imposed pattern of uplift through geometric adjustments to its channel (for example Finnegan and others, 2005). Here we calculate slip rates for the faults successively crossed by the Cahabón River using the age of the valley-fill and the amount of displacement accumulated across these faults (table 3).

		NPF	PC2-PC15	PTSF	PTSF –PF
Post paleosurface vertical offset (m)		220 (150-250)	520	300-350 (at PC31)	
Post fill vertical offset (m)		50[a]–115[b]	115	50 (at PC21)	
Post fill velocity below Cahabón R. (mm.y^{-1})		0.10 ± 0.03[a] 0.24 ± 0.07[b]	0.24 ± 0.07	0.07 ± 0.06[d] 0.13 ± 0.07[c]	
Maximum visible post fill velocity (mm.y^{-1})		0.12 ± 0.03[a] 0.27 ± 0.08[b]	0.27 ± 0.08	0.2 ± 0.2[d,e] 0.5 ± 0.3[c,f]	0.2 ± 0.2[d,e] 0.7 ± 0.4[c,f]
Velocity from ERT (mm.y^{-1})	interglacials MIS 2 and 5			0.6- 0.9	
	glacial MIS 2 to 4			0.4	
Inception of tectonic activity (Ma)		0.92 ± 0.27[b] 2.2 ± 0.6[a]		0.9 ± 0.5[cf] 3.5 ± 2.8[d,e]	
Pre-capture rock uplift below river (m)		170[a]-105[b]	400	500[f]-90[e]	400-500
Horizontal offset (m)		600		-	
Maximum horizontal velocity (mm.y^{-1})		1.0 ± 0.3[a]		-	

Table 3. Indicative tectonic slip rates along the faults successively crossed by the Cahabón River, *inferred from the valley-fill age. NPF: NiñoPerdido Fault; PC2–PC15: overall differential uplift from PC2 to PC15; PT-SF: Purulhá Trough–South Fault; PSTF-PF: rotated bloc between the PT-SF and the Polochic fault (PF). Upper script numbering refers to calculation following various tectonic and geomorphic models as explained in the text and Appendix 6.*

The finite throw of the Niño Perdido Fault represents _40 percent of the finite differential uplift between PC 2 and PC15 (see details in Appendix 6). If this apportionment has been constant throughout the deformation history (model "a", table 3), then the NPF has been moving at an average vertical velocity of 0.10 ± 0.03 mm _ y_1 since its activation. If differential uplift has been taken up increasingly by the NPF with time, then the fault vertical slip rate is on average 0.27 ± 0.08 mm.y^{-1} since the burial of PC6.1 (model "b", table 3). With such average slip rates the NPF would become active 2.2 ± 0.6 My ago according to model "a", and 0.9 ± 3 My ago according to model "b". The quartzose-gravel-covered valley floor of the Cahabón River has been uplifted by some 50 m in the footwall of the southern fault of the Purulhátrough (PT-SF, fig. 8). The gravel-covered valley floor of the ancestral Cahabón River became perched following either capture SB or capture PL (see Appendix 6). The age of the offset is thus bracketed by the minimum age of capture SB and the maximum age of capture PL (models "d" and "c" in table 3). The inferred vertical velocity (0.07-0.13 mm.y^{-1}) is comparable to that of the NPF.

The vertical throw of these faults changes rapidly along strike: it increases eastwards along the NPF and westwards along the PT-SF. The maximum throw on the PT-SF is observed at PC30, near the sites chosen for the ERT surveys. By combining our end-member models "c" and "d" for the age of the displaced paleovalley with end-members models of footwall rebound ("e"

and “f” in table 3), we obtain the range of maximum slip rates at PC 30 (0.2 ± 0.2 to 0.5 ± 0.3 $mm.y^{-1}$) and ages of inception for the PT-SF (0.9 My-3.5 My). If the sediment layering imaged by ERT in the hanging wall of the fault is due to the last glacial-interglacial oscillations, then the subsidence rate necessary to accommodate sediment deposition at PC 30 imposes a slip rate of 0.6 to 0.9 $mm.y^{-1}$ on the PT-SF over the past 200 ky (see Appendix 6). This value is consistent with the independent estimate obtained using the offset of the quartzose gravel.
From Purulhá to the Polochic Fault, the Cahabón River traverses a tectonic block delimited to the south by the PT-SF and to the north by the Polochic fault. Ground subsidence diminishes down to PC35 (fig. 1), where it reverts to uplift, which then increases down to the Polochic fault. Assuming rigid block rotation with an E-W horizontal axis passing by PC35, and the previously calculated vertical subsidence along the PT-SF, the downstream increase in uplift is found to peak at 0.2 to 0.7 $mm.y^{-1}$ near the Polochic fault.

Altogether these estimates show that the Cahabón River has been confronted since the Late Pliocene–Early Pleistocene to the activation of a series of faults. Despite its entrenchment into a ~400 to 500 m deep valley, the river was defeated by these faults after only ~1 to 2 My of tectonic activity. Yet, these faults have been moving at slow to moderate velocities of the order of 0.1 $mm.y^{-1}$ and, with only 100 to 200 m of offset across the NPF and 100 to 500 m of offset across the PT-SF, had accumulated only a limited vertical displacement by the time the captures occurred. We suspect that some agent of change has greatly facilitated the rearrangement of the river and its tectonic defeat. This aspect is explored in the *Role of Groundwater in Interfluve Breaching* section.

Growth Rate of the Canyons of Capture

Dramatic canyons have developed at the sites of capture. Their incision has been initiated by the drop in base-level that the streams have experienced upon capture. Base-level drop amounts to 250 m in Santa Cruz (SCZ), 500 m in Santa Barbara (SB), and 1000 m in Purulhá (PL). Vertical incision was accompanied by headward erosion that propagated first upstream, along the initially captured catchments, and then also downstream, along these segments of the Cahabón paleovalley that have experienced drainage reversal. Incision propagated swiftly across the valley fill but did not proceed into the bedrock except near the capture sites, where very deep and short bedrock canyons have formed.

Some characteristics of the canyons suggest a possible role of mass-wasting, such as the semicircular heads of the canyons and the steepness of the canyon lips. At site SB, headward erosion has carved a 6 km long and 500 m deep canyon into vertically bedded low-grade phyllites (fig. 13A). The canyon head is 250 m tall and semicircular. The streams cascade sharply into the canyon forming waterfalls as high as 35 m (El Chupadero, see Appendix 1). At site PL, headward erosion has carved a 3.5 km long canyon that follows the trace of the PT-SF. The fault zone puts Permian carbonates and shales into contact with Cretaceous carbonates and serpentinites (fig. 13B). Streams cascade into the canyon with waterfalls as high as 40 m, such as, for example, the Ram Tzúl and Peña del Angel waterfalls. In the PL and SB canyons, the volume of eroded bedrock is much larger than the volume of the valley fill that covered the bedrock (table 4). Canyon SCZ is hardly incised into the bedrock and still mostly confined to the valley fill (fig. 13C). The smaller canyon SCZ is a younger version of canyon SB: it incises the same rock formation but its drainage area is twice as small as the initial drainage area of canyon SB.

Overall, there is good agreement between canyon age and canyon volume. Our geochronologic data indicate that canyon SB started to grow ~0.55 My ago, that canyon PL is younger than 780 ky, and that canyon SCZ is slightly older than 84 ± 5 ky. The volume of the canyons (table 4) was obtained by restoring the pre-capture topography. We used a digital elevation map with a precision of 20 m obtained by digitalization of 1:50 000 topographic maps produced by Instituto Geografico Nacional de Guatemala as a starting point to restore the continuity of the valley fill surface and of the bedrock flanks over the canyons. The canyon volume was obtained by

subtracting the modern topography from the reconstructed topography (fig. 13). Canyon SB is the largest canyon. It also possesses the largest catchment, because extensive drainage reversal has progressively augmented its area. Canyon CSZ is 25 to 50 times smaller but only 6 times younger. This apparent increase in canyon growth velocity over time is possibly attributable to the effect of drainage reversal, considering that the drainage area of canyon SB was initially twice as large as that of canyon SB and that it was multiplied by 9 under the effects of drainage reversal. Canyon PL is 2.8 times smaller than canyon SB and its current drainage area 2.5 times smaller. We do not know the age of canyon PL, but its size suggests that it is younger than canyon SB. However, the relationship between canyon volume and age is obscured by a variety of factors: first, canyon PL grows over rocks of unknown relative erodibility with respect to the rocks over which the SB develops and it follows a faulted contact. Second, the breaching of the valley in PL has allowed the engulfment of Caribbean moisture into the Cahabón River paleovalley, which is evidenced in capture PL by a sharp and localized change in vegetation and soils. As a result, precipitations are higher in PL than in SCZ and SB.

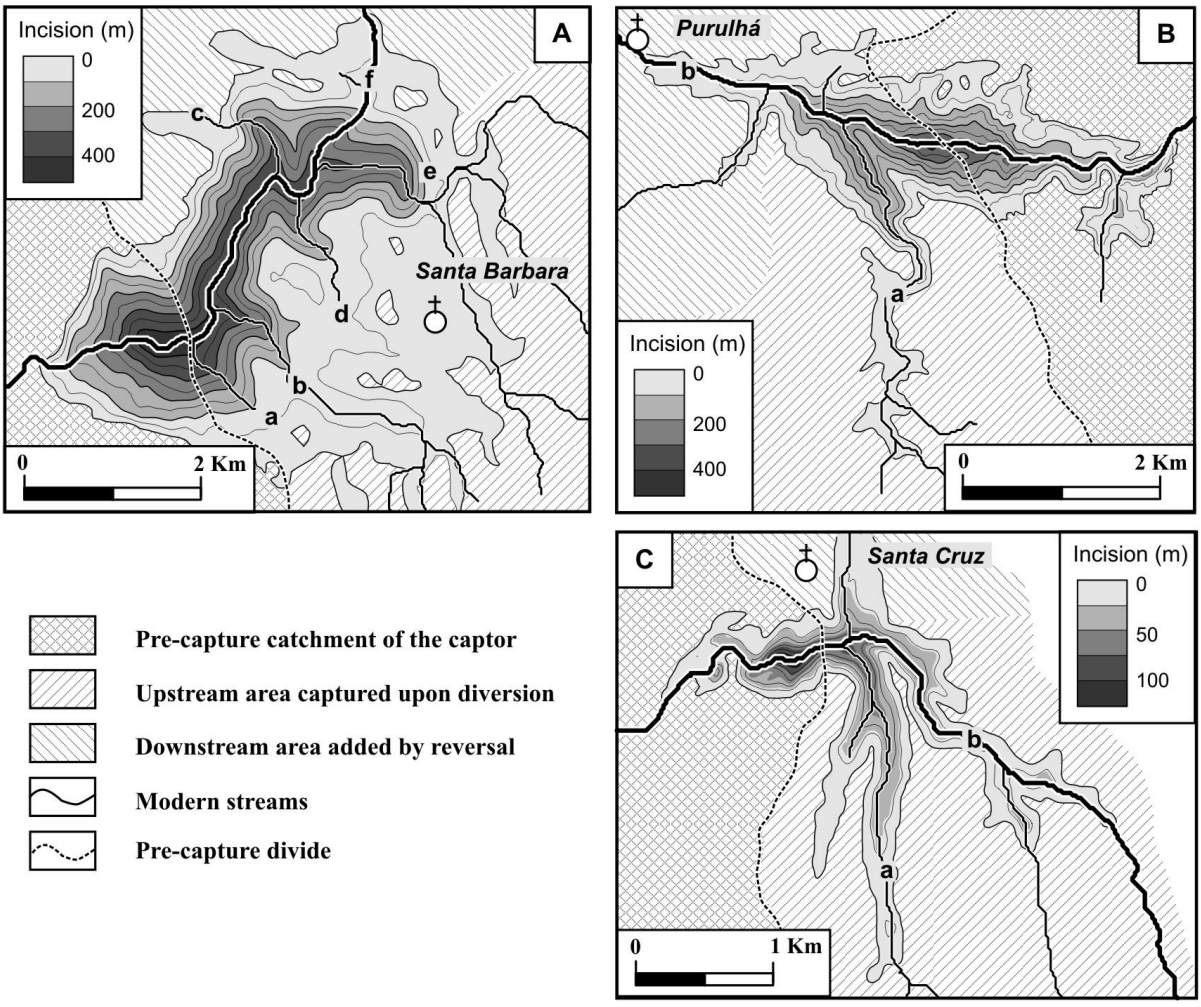

Figure 13. Incision along the canyons that formed near Santa Barbara (A), Purulhá(B) and Santa Cruz (C).

The largest difference, however, is probably attributable to the time-dependent changes in catchment size. At site SB, reversal first added 75 km^2 to the initially captured catchment (30 km^2). The affected area jumped to 155 km^2 when the West Chilascó River was rerouted into the San Isidro tributary of the Cahabón River (diversion SCZ), because at that time the San Isidro tributary was already belonging to the reverted drainage. The reverted area is currently 4 times larger than the initially captured area. It is even expected to increase in the future, because

drainage reversal is still underway along the West Chilascó River (see the next section titled *Mechanisms of Drainage Reversal*). The resulting increases in drainage area in SCZ mechanically increase the drainage area of canyon SB. We anticipate that drainage reversal at SCZ is going to affect all the West Chilascó River and will eventually lead to the capture the East Chilascó River (see the next section titled *Mechanisms of Drainage Reversal*). For canyon SB this will bring up the ratio of reverted to initial area to 6:1.

	Santa Barbara	Purulhá	Santa Cruz
Drainage area upstream (km^2)	30	25 (180)	18
Drainage area downstream (km^2)	145*	45 *	1*
Infill thickness (m)	40	? (10-80+)	40
Age (Ma)	**0.55**	**< 0.75**	**>0.1*** **
Volume (km^3)	1.5 (1.7**)	0.6 (0.7**)	0.028 (0.063**)

Table 4, General characteristics of post-capture canyons
*: still increasing. — **: including sediment fill. — ***: inferred from geology

Table 4 . Some general characteristics of the post-capture canyons
* Still increasing. ** Including sediment fill. *** Inferred from geology.

In spite of these complexities, we tested the ability of a simple model of canyon propagation to reproduce the observed canyon growth and we then use this model to evaluate the age of the canyons against our estimates previously based on our geochronologic data. In this model, knickpoint propagation is governed by fluvial erosion (for example Seginer, 1966; Crosby and Whipple, 2006). If knickpoint propagation is dominated by other processes, such as mass wasting, then this relation is not observed (Weissel and Seidl, 1998). Stream incision is expected to scale with stream power or basal shear stress (for example Tucker and Whipple, 2002; Bishop and others, 2005; Crosby and Whipple, 2006). We assume here that incision is proportional to unit stream power so that propagation velocity only depends on drainage area (Tucker and Whipple, 2002):

$C = \phi A^b$

where C is the canyon propagation velocity (m. y^{-1}), A the drainage area (m2), ϕ the efficiency of retreat ($m^{1-2b}.y^{-1}$), and b a non-dimensional constant. In this model, velocity is independent from the river gradient at the canyon lip, which is convenient considering that we do not have field constraint on this parameter over time. Field calibrations show that velocity is usually more sensitive to drainage area than river gradient (Bishop and others, 2005).

The model was calibrated on canyon SB because its age is better determined. We tested if the canyon shape fits a simple model of canyon propagation and tested the sensitivity of canyon growth to drainage reversal. The canyon was divided into 6 different branches (fig. 13A). We followed two separate approaches to calibrate the relationship. We first set the value of exponent "*b*" to its theoretical value of 0.5, and calibrated along branch "*a*" of canyon SB. The stream in branch "*a*" (fig. 13A) joins the trunk stream "*f* " of canyon SB at the site where the capture has taken place. Headward erosion along stream "*a*" became disconnected from headward erosion along stream "*f* " immediately after capture so that the upstream changes in drainage area that affect stream "*f* " due to drainage reversal have not affected stream "*a*". A value of $\sim 2.10^6$ $m^{1-2b}.y^{-1}$ is obtained along stream "*a*" in the range of values encountered elsewhere (for example Whittaker and others, 2008).

In a second approach, we determined the appropriateness of the theoretical value b _ 0.5 by running combinations of b and values over the entire network (*a*-*f*) considering three scenarios of temporal changes in the drainage area of stream "*f* ". In the minimum area case (SBA_{min}), stream "*f* " drains the Cahabón valley up to the vicinity of the San Isidro tributary without incorporating it during the entire growth of the canyon. The canyon contributing area only reaches its present size instantaneously at the end of the run. In the maximum area case

(SBA_{max}), the drainage area of "*f*" reaches its present-day size immediately after the capture. In the intermediate case (SBA_{int}), we introduce a piecemeal drainage growth assuming that the San Isidro tributary is integrated at _400 ky and the West Chilascó River at ~100 ky (see the *From burial age to capture age* section). In all cases, we perform a forward modeling of headward erosion starting at the capture site and propagating up the canyon branches for many combinations of *b* and ϕ (see Appendix 7). The best combinations (table 5) have the lowest RMS misfit between today and the time at which the knickpoints arrive to their current location along all canyon branches according to the model. These best fits have lower misfits than those obtained using *b* = 0.5 and the value of _ calibrated along stream "*a*". Best-fitting values of *b* are in the range of 0.31 to 0.42 and are compensated by higher retreat efficiency values.

Model	b_{SB}	ψ_{SB} 10^{-6} m^{1-2b} y^{-1}	RMS_{SB} 10^6 y	**Age CSZ** *ka*	**Age PL** *ka*
SB_{Amin}	*0.50*	*1.9*	*1.24*	*80-110*	*190-270*
	0.42	6.3	1.12	90-125	240-330
SB_{Aint}	*0.50*	*1.9*	*1.61*	*80-110*	*190-270*
	0.34	20	1.14	90-135	320 -380
SB_{Amax}	*0.50*	*1.9*	*1.23*	*80-110*	*190-270*
	0.31	30	1.09	115-155	360 -450

Table 5 ***Best-fit values for b and ϕ in equation (1), and inferred age for canyons SCZ and PL.*** Models of drainage reversal: SBA_{min}: no drainage reversal until the present; SBA_{max}: full drainage reversal at the time of capture; SBA_{int}: progressive drainage reversal. Columns: b_{SB} and SB: best-fit values of parameters b and ϕ in equation (1) for calibration in canyon SB; RMS_{SB}: root mean square deviation in arrival time of knickpoints at their present location between calculated time and real, present time. Age CSZ and age PL: ages of the river diversions of Santa Cruz and Purulhá, calculated using b_{SB} and ϕ_{SB}. Range in age represents the span in age calculated using various canyon branches. Best-fit value extraction is detailed in Appendix 7.

The values of *b* and ϕ are only moderately affected by the uncertainties on the drainage reversal chronology. As a result, the end-member models of drainage reversal only introduce a twofold change in canyon growth celerity, in spite of much larger uncertainties on the catchment size. The residual misfit observed for the best combination of *b* and ϕ is attributable to celerity variations between tributaries. This misfit is presented on figure 14 in the form of a graphical mismatch between the time at which headward erosion is expected to sweep the successive junctions of trunk stream "*f*" according the forward modeling along stream "*f*" (solid line), and the time at which headward erosion is supposed to sweep these same junctions calculated by retro-eroding the canyon branches from their modern tips using the same combination of *b* and _ as for stream "*f*" (white circles). This residual misfit results from minor temporal changes in the drainage area of the various canyon branches and from the effect of bedrock anisotropy. Bedrock foliation is oriented roughly N70–80 and explains for example the difference in propagation between streams "*e*" and "*f*" (fig. 13). However, the effect of anisotropy varies with foliation dip. As a result, the introduction of a homogenous E-W anisotropy into the model does not significantly improve the fit (see Appendix 7).

The values of *b* and ϕ calibrated on canyon SB are used to assess the age of canyons CSZ and PL (fig. 14). The uncertainties in the upstream drainage evolution of canyon SB translate into a twofold change in the ages of canyons CSZ and PL (table 5). The modeled age of canyon CSZ is 80 to 155 ky, perfectly consistent with our other estimates: field data indicate that the canyon is older than a blanket of 84 ± 5 ky-old pumice; geomagnetic data indicate that it has formed during the current normal geomagnetic chron; the canyon ^{26}Al-^{10}Be corrected age is -10 ± 160 ky, and ground tilting calculations in the next *Mechanisms of Drainage Reversal* section suggest an age of 170 to 220 ky. The age of canyon PL (240-450 ky) is only indicative because retreat efficiency ϕ varies with bedrock erodibility and climate. Bedrock erodibility along canyon

PL is probably higher than along canyon SB, because canyon PL follows a tectonic contact along which the bedrock is damaged. The greater amount of precipitation may result in more surface runoff and more mass wasting. As a result of both effects, canyon PL may develop more rapidly and its modeled age could be therefore an upper estimate. The modeled age of canyon PL is consistent with the age of terrace T2 in the Depression of Cobán (690 ± 550 ky). The relative ages of captures PL and capture SB have not been resolved, neither by the study of sediment provenance nor by the cosmogenic dating of the valley-fill. Our model of canyon development suggests that capture PL is younger than capture SB, which is consistent with the coeval disappearance of quartzose-bearing gravel and chromium in terrace T2 (see the *Sediment Provenance: Clast Assemblage and Matrix Elemental Analysis* section). The development of the canyons of capture closely follows a simple law of knickpoint retreat, in spite of the presence of waterfalls and steep canyons heads, the propagation of which could be governed by mass wasting and not by fluvial processes.

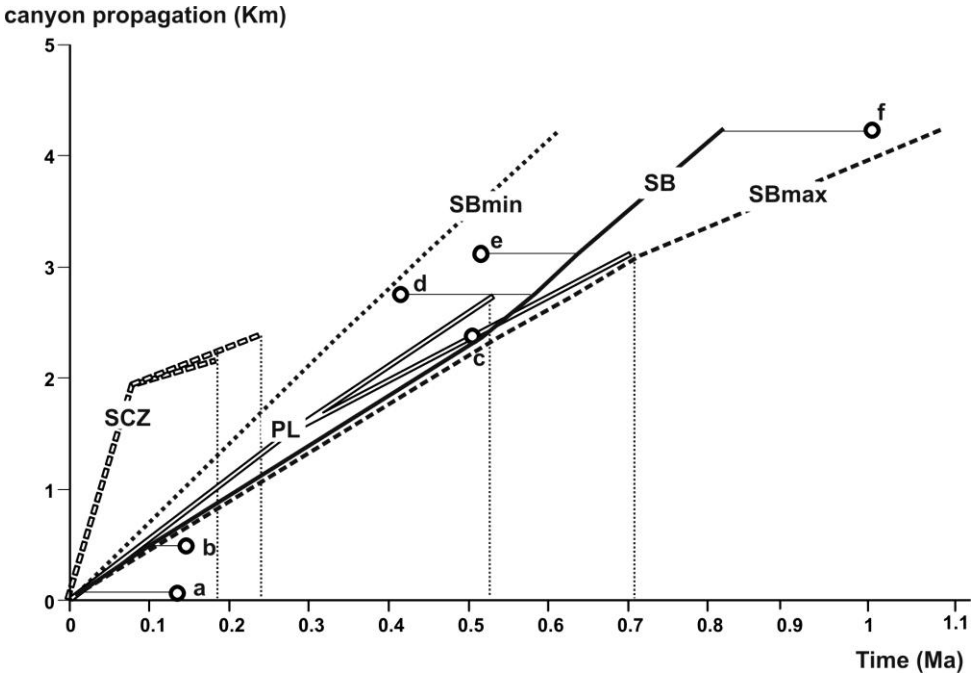

Figure 14. Determination of the ages of the Santa Cruz (SCZ) and Purulhá (PL) canyons using the canyon growth model calibrated on the Santa Barbara (SB) canyon. The curves illustrate the best-fitting _ and *b* values of model ASBint. Open circles correspond to the passage of the SB canyon lip at the successive junctions between main stem "*f*" and lettered tributaries ("*a*-*e*", figs. 3 and 15), calculated using the drainage area (A) and incised length (L) of the tributaries. The black lines depict the same propagation, but calculated using the drainage area of the stem stream "*f*", for various models of changes in "*f*" drainage area: A_{SBmin} (dotted line), A_{SBint} (solid line) and A_{SBmax} (dashed line). Thin horizontal lines represent the mismatch between the two methods. The curves illustrating the growth of canyons PL (open line) and SCZ (open dashed line) are calculated using the same ϕ- and *b*-values. The inferred canyon ages are showed as vertical dotted lines, and reported in table 5.

The modeling calibrated on canyon SB predicts ages for canyons CSZ and PL that are consistent with all the other available data, and the modeling further suggests that capture PL occurred after capture SB. Because of limited upstream drainage areas of a few 10s of km^2, canyon lips have only propagated upstream at a velocity of 0.3 to 1.1 $cm.y^{-1}$ over the last few hundreds of thousands of years, but with vertical bedrock incision rate on the order of 0.7 to 1.5 $mm.y^{-1}$ in canyon SB and 1 to 2 $mm.y^{-1}$ or more in canyon PL, forming deep, short canyons. Canyon SB will not deepen further, because it has reached the base-level of its captor, whereas PL can deepen an additional 500 m before it gets graded to its captor. Drainage reversal can still

double the drainage area of canyon PL and increase by 30 percent the drainage area of canyon SB. This should promote canyon growth, but even with such an increase the canyons are unlikely to propagate over the entire length of the Cahabón River paleovalley in less than 1 to 2 millions of years. Until then, the paleovalley will be identifiable in the landscape and some perched river deposits could be preserved. Afterwards, all direct evidence will be effaced and the only subsisting trace of the paleovalley will be the presence of barbed tributaries in the stream network.

Mechanisms of Drainage Reversal

After its capture, the drainage of the Cahabón River was affected by extensive reversal. Here, we use the dating of the Cahabón paleovalley together with field observations to estimate the duration of the reversal process and evaluate the contribution of several possible driving mechanisms, namely tectonic back-tilting, impediment by lateral fans, and dissection of the valley fill by ground sapping.

Drainage reversal is often regarded as the result of the tectonic tilting of a fluvial valley in a direction opposite to the initial direction of flow of its axial drainage. The way the reversal is achieved in detail is, however, rarely addressed. It requires somehow the accumulation or evacuation of the flow within the former headwaters with the formation of lakes or/and areas of sedimentation, the water being ultimately evacuated either by evaporation, infiltration, lake overspill, or river avulsion (see for example Süzen and others, 2006; Attal and others, 2008; Clendenon, 2009). In the present case, drainage reversal was greatly promoted by the captures in two ways. First, by beheading the axial drainage, the captures considerably reduced the erosive and dispersal power of the axial drainage that they beheaded, thereby impairing their ability to cope with tectonic tilting. Second, the captures were offering low-elevation pathways for the evacuation of the reversed flow through the lateral breaches that they had created. The areal extent of the reversal is compatible with the model of tectonically driven reversal: the streams of the rearranged drainage currently flow from the most uplifted areas towards the less uplifted areas. This is true along all branches of the SB catchment (fig. 7). At capture site PL, reversal has proceeded half way along the subsiding floor of the Purulhá tectonic trough (fig. 8). If driven by tectonics, then reversal at site PL should propagate further downstream along the Cahabón valley down the next area of bedrock uplift, which is located downstream of PC35. At site SCZ, drainage reversal is incipient and the beheaded West Chilascó River is being back-tilted (see the *Control of Faulting on Valley-Fill Formation* section). Considering the extent of tilting there, tectonics is expected to drive reversal as far north as the town of Chilascó (fig. 4).

A closer look at the reversal underway in SCZ reveals that its development is more complex (fig. 15). Following interfluve breaching, the valley fill upstream of SCZ has been incised down to the bedrock. This has induced a complete drawdown of the aquifer from the dissected sediment fill. Downstream of SCZ, the sediment fill remains unscathed, but its aquifer leaks upstream through a free face at SCZ. Retro-flow and seepage at SCZ generates groundwater sapping, mass wasting, and the formation of a 500 m long canyon that propagates into this valley fill. The canyon is thus a manifestation of drainage reversal driven by groundwater sapping. The valley fill surface is blanketed by an 84 ± 5 ky-old pumice ashfall (H member of the Los Chocoyos eruption, Rose and others, 1986), which has been removed from the bed of the residual streams draining the floodplain. The canyon crosscuts some of these young channels, which indicates that the canyon keeps growing. Its catchment is currently about one square kilometer at the surface, but it probably taps underground a much larger area of the 40 m thick sediment fill, possibly as far north as the junction with the East Chilascó River. The East Chilascó River offers unlimited recharge to West Chilascó aquifer and to the canyon, as the river stands 35mhigher than the canyon floor. Such a configuration suggests that the underground capture of the East Chilascó River may have started. If so, one can expect the groundwater sapping process to continue until the canyon propagates down to the junction with the East Chilascó River, resulting in a surface capture of the river. Mankind has somehow anticipated this event by

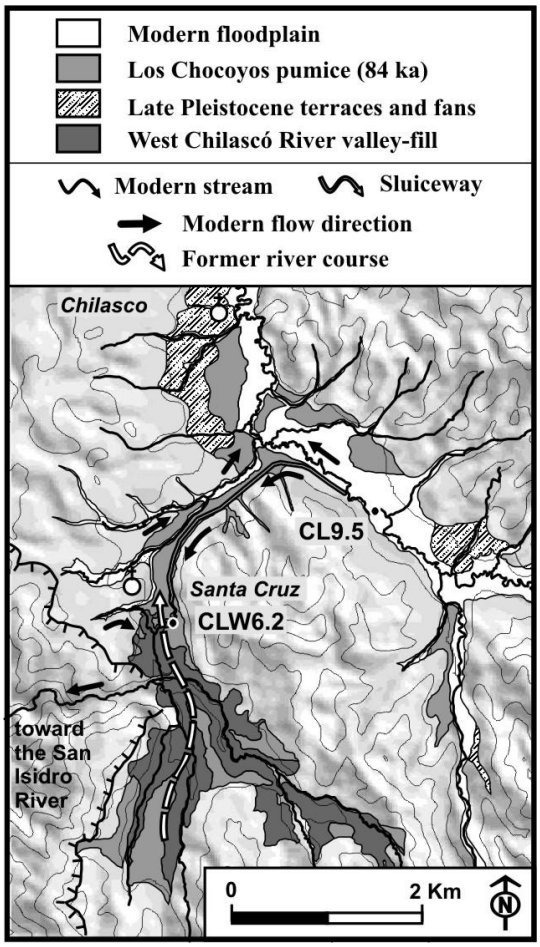

digging a sluiceway that conveys water in a direction opposite to the natural surface drainage, from the East Chilascó River to the canyon in SCZ, where the elevation drop is used to fuel a power plant. Upon surface capture, the East Chilascó River valley fill would be dissected and in a later stage retro-flow could proceed further north in what is left of the sediment fill as far north as the town of Chilascó where the valley fill eventually thins out.

Figure 15. Topographic map of site of the Santa Cruz (SCZ). *The map shows the extensive dissection of the West Chilascó River upstream of Santa Cruz, where the river has been diverted into the San Isidro River. It also shows the incipient propagation of a canyon across the residual drainage of the West Chilascó River, as well as an artificial diversion of the East Chilascó River that prefigures its natural capture.*

Reversal driven by groundwater sapping may also be ongoing at site PL, if the reversed drainage taps the sediment fill of the Purulhá trough (fig. 8). For now the incision of the fill is limited, but it can potentially propagate by groundwater sapping over the entire extent of the fill. At site SB, reversal has expanded over the entire extent of the sediment fill and even beyond. Because at both sites the areas potentially affected by groundwater sapping tend to coincide with the areas affected by tectonics, the areal extent of the reversal is not diagnostic of the reversal mechanism. In addition, both mechanisms can occur simultaneously or relay one another over time. Reversal by groundwater sapping should be dominant before tectonic rotations become large enough to reverse the dipping direction of the floodplain. At site SCZ the fill surface currently still slants in the initial downstream direction. To estimate the time necessary for the fill surface to dip upstream we use our dating of the Cahabón River valley fill and the tectonic pattern that we have identified. Along the Cahabón River, since capture SB, the valley fill has been tilting southwards at a maximum angular velocity of 0.023–0.048‰.ky^{-1} (this is a maximum value obtained by assuming that uplift is partitioned between fault slip on the NPF and distributed tilting; see *A River Defeated by Slow-Moving Normal Faults* section). The tilting affects the Cahabón, West Chilascó and East Chilascó Rivers (see the *Control of Faulting on Valley-Fill Formation* section). The NE-striking West Chilascó valley fill has currently a surface gradient of 4 ‰. At the angular velocity calculated along the Cahabón valley, the fill surface dipping direction will flip to the south in 120 to 260 ky. The initial gradient of the fill surface was likely similar to the modern 7.6 to 9.8 ‰ depositional slope of the East Chilascó River considering the similarity in sediment grain size distribution and drainage area of the two rivers. Retro-tilting the West Chilascó River to its initial slope necessitates 170 to 220 ky at the angular velocity used in the previous calculation. This estimate for the SCZ avulsion is slightly higher than our estimate based on the ^{10}Be-^{26}Al burial dating and compatible with the minimum age of avulsion provided by the pumice layer (84 ± 5 ky). In this estimate, the time necessary for the topographic reversal to occur along the West Chilascó River is 290 to 480 ky. Along the N-striking Cahabón River, the same calculations suggest that 190 to 430 ky were necessary for the floodplain to slant southwards after capture SB. This estimate is consistent with the time separating capture SB (530±210 ky, PC6.1) from the propagation of incision up to the San Isidro

River fan (400 ± 210 ky, PC9.8). Before this event, groundwater sapping had been likely the dominant process of reversal and had completed an unknown amount of this reversal.

In this respect, the San Isidro alluvial fan is a key element for identifying the respective contributions of tectonics, groundwater sapping, and sedimentation to the drainage reversal. First, the fan illustrates a case of valley obstruction by the growth of a lateral fan. The fan surface stands 60 m above the axial infill surface (fig. 7) and less than 10 m of this difference can be ascribed to ground tilting. Beheading of the Cahabón River in SB made the residual Cahabón River 2.3 times smaller than the San Isidro stream. The relative importance of the San Isidro stream kept increasing as reversal propagated along the valley. The San Isidro tributary could still both flow northwards and feed in the meantime the southern valley fill aquifer, if this aquifer was already draining toward SB. The fan is now incised and cross-cut by a superimposed drainage: the San Isidro stream flows along the southern border of the fan and is incised into the bedrock of the filled valley flank (stream "*g*", fig. 4); likewise, the axial drainage of the Cahabón valley is now incised within the eastern flank of the valley across from the fan (stream "*h*", fig. 4, and cross section at 9.2 km, fig. 6). The modern network records the position of the rivers just before they started to incise. Their positions suggest that the rivers had been pushed aside along the margins of the valley fill due to the inflation of the San Isidro fan. The fact that the San Isidro tributary had been rejected along the southern ledge of its fan and that a reversed axial drainage already existed across from the fan both suggest that tectonic tilting had set the location of these streams before incision started. Importantly, instead of following the deepest parts of the valley fill, incision tracked the surface drainage along the sides of the valley fill, where groundwater sapping has no influence. This shows that groundwater sapping was not the cause of the drainage reversal at this locality. Other epigenic incisions at the margin of the sediment fill are observed here and there along the Cahabón paleovalley (for example near NiñoPerdido and to the west of Santa Barbara, fig. 4). They show that neither tectonic tilting nor groundwater sapping are the sole agent of reversal.

Overall, the observations outlined in this section show that drainage reversal resulted from the combined effects of tectonic deformation, sediment accumulation, and groundwater sapping. The respective contribution of each of these three processes is difficult to unravel, as all three processes have played a role that depends on their distance to the capture sites and on the time that has elapsed since the captures. The reversal observed near SCZ illustrates a case where groundwater sapping predominates. Such a phenomenon is generally unrecognized, yet it can significantly contribute to drainage reversal. In particular, it provides an explanation for the coincidence of drainage heads astride drainage divides, where one network is developing at the expense of another and reuses its flow lines. The coincidence of valley heads has been attributed to tectonic advection of the topography across a divide in the case of growing folds (Miller and Slingerland, 2006). In more quiet settings (for example Vogt, 1991), the reoccupation of the network heads could be driven by groundwater flow reversal in the valley fill provided that the valleys of the shrinking network host substantial sediment accumulations.

Role of Groundwater in Interfluve Breaching

Before being captured, the Cahabón River was adapting to spatial variations in rock uplift rate. To maintain its course, the river deposited_40mof sediment between the Salamá and Niño Perdido faults and more than 80 m of sediment over the hanging wall of the PT-SF. At the same time, the river kept eroding the intervening rising blocks. The river stands at an elevation of 1400 to 1600 m asl., far above its base level in Lake Izabal (1 m asl). The equilibrium profile of the Cahabón River is expected to be that of an incising river adjusting its gradient, width, and depth to the spatial variations in rock uplift rate so that incision everywhere counterbalances rock uplift (for example Harbor, 1998; Lavé and Avouac, 2001; Finnegan and others, 2005; Brocard and van der Beek, 2006; Cowie and others, 2008). Dynamic equilibrium is attained through a transient phase of adjustment, the duration of which is controlled by the time required for the tectonic perturbations to be propagated along the trunk of the river and its tributaries (for example Tucker and Whipple, 2002; Attal and others, 2008; Cowie and others,

2008). Such a transient phase commonly combines incision within rising structures and aggradation upstream (for example van der Beek and others, 2002; Attal and others, 2008). With its succession of aggrading and incising reaches, the Cahabón River seems to have been in such a transient phase before being captured. It is the river's response to the propagation of transtensional faulting to the tectonic sliver delimited by the Motagua and the Polochic fault during the Pliocene and the Quaternary (Authemayou and others, 2011).

River networks are susceptible to reorganization during such transient phases. Rivers can rearrange upstream of rising structures by avulsion (for example van der Beek and others, 2002; Attal and others, 2008) or by captures promoted by the enhanced differences in incision rate between adjacent catchments (Cowie and others, 2006). Here, we also see a causal link between the initiation of faulting, sediment deposition, and the capture of the river. The mechanism of capture is identifiable using the geomorphic and geologic information at hand. Three river diversions have occurred in the drainage of the Cahabón River, near Purulhá (PL), Santa Barbara (SB), and Santa Cruz (SCZ). Each of these diversions is located near a sediment depocenter. River aggradation upstream of the rising structures and river capture occur along the least uplifted reaches of the river and can therefore be viewed as genetically independent but spatially coincident manifestations of the tectonic defeat of a river. Both of these phenomena can also be viewed as genetically related. In SCZ, deposition of ~40 m of river sediment elevated the floodplain of the West Chilascó River 10 to 40mbelow the lowest saddles in the divide that separates this river from the San Isidro River valley. The diversion of the West Chilascó River is thus very likely the result of a simple avulsion of the West Chilascó River over the divide.

Avulsion cannot account for the diversions in SB and PL because there the divides stand hundreds of meters above the valley floor and the Cahabón River only deposited a few tens of meters of sediment. If the Cahabón valley had been rapidly dammed, a lake could have formed without leaving much sediment. Its catastrophic overflow could, in principle, produce the observed breaches. This would, however, require the damming of the valley by a landslide of considerable volume and height. The paleovalley retains most of its original morphology and deposits. These include only a few landslides of small size unable to dam the valley to any noticeable extent. We therefore consider that interfluve breaching was not a top-down process, but a bottom-up process of river capture (Bishop, 1995), whereby the erosion that achieved the breaching was initiated in the catchments surrounding the Cahabón valley and propagated toward the valley. River diversion is thus the final consequence of the interfluve breaching rather than its cause. The interfluves that have been breached have subdued long profiles that stand generally within ~100 m of the elevation of the relict upland surface envelope (fig. 7). From the range divide down to PL, the interfluves are only interrupted by four deep breaches. Two breaches are associated to captures SB and PL and two other breaches are located above the trace of the Niño Perdido Fault (c and c' in fig. 7). From the crest of the interfluves down to the valley fill surface, the breaches are 300 m deep in SB and 350 to 600 m deep in PL (fig. 7). Following capture, erosion in these breaches has proceeded further down so that these breaches are now 800 m and 1200 to 1500 deep, respectively. The breaches above the Niño Perdido fault are not associated with surface captures. The deeper eastern breach is 400 m deep and its bottom stands only 75 m above the floor of the Cahabón valley. They may have formed in the same way as the other breaches but have not deepened enough for the Cahabón River to be captured.

Regardless of the mechanism of capture, it is clearly the difference in elevation between the Cahabón River and its neighbors that is the primary reason for the rearrangement. Along the first 50 km of its course, the Cahabón River stands 500 m to 1000 m above the conterminous drainages of the Panimá and Chixóy Rivers (fig. 1B). Headward erosion is expected to have initiated in these catchments and propagated toward the Cahabón River. Steeper slopes in these catchments could drive this erosion, given the similar lithology. Upstream of the Niño Perdido Fault, the Cahabón catchment slopes are gentler than the slopes of the adjacent catchments (fig. 14B). Further downstream, however, the slopes are not so significantly different across the divides, especially near the PL capture and along the block delimited by the NPF and the PT-SF. There, slopes are steep and may have reached a critical angle above which erosion becomes

independent from slope steepness (Burbank and others, 1996). Therefore, the absence of slope dissymmetry does not mean that there is no difference in erosion rate. Headward erosion can also be driven by a difference in precipitation between catchments. There is a strong decrease in precipitation from east to west (fig. 16A) with high rainfall in the Panimá catchment, moderate rainfall in the Cahabón catchment, and a dry climate in the Chixóy basin. The higher erosion rates of the Panimá catchment could translate into higher erosion rates and would satisfactorily predict the formation of the PL breach, but fail to explain the breaching of the valley toward the drier Chixóy catchment in SB.

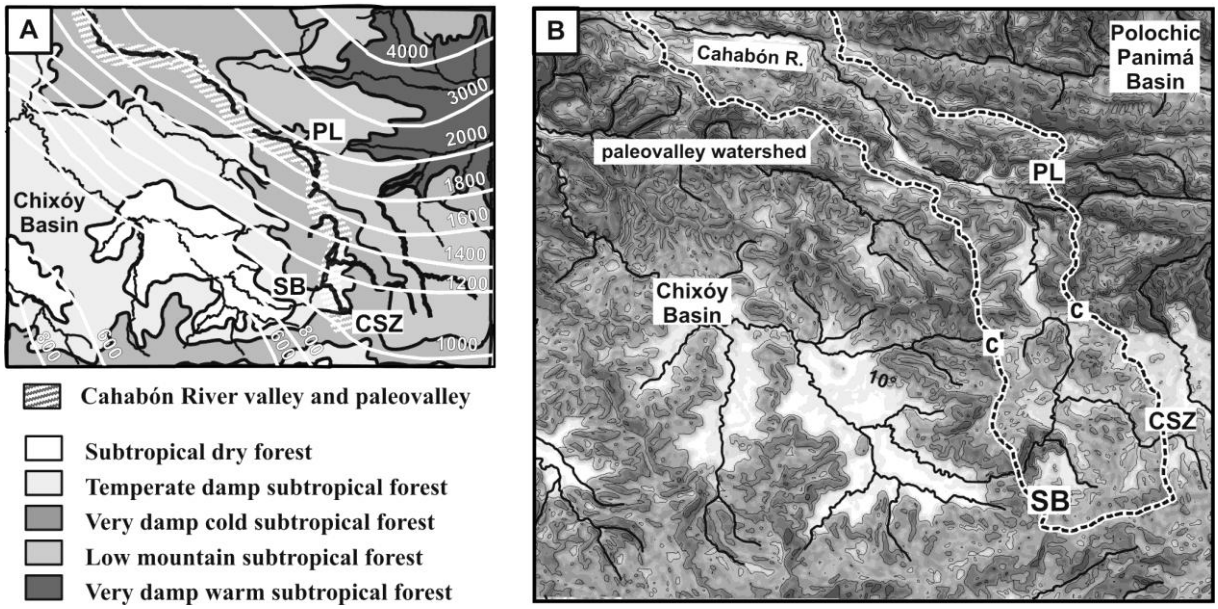

Figure 16. Climatic gradient (A) and topographic slope (B) in the study area. (*A): map of precipitations and of the vegetation cover: the Cahabón River valley is located between the very humid Panimá River catchment and the very dry basin ChixóyRiver catchment. White contours are mean annual rainfall isohyets (in mm.y^{-1}). Precipitation and forest types date from MAGA (Guatemalan agriculture, livestock and food administration). (B): map of slopes calculated using the SRTM 3 arcsec DEM slope, averaged over 250 m large cells, and contoured every 10°. Note the extensive remnants of the upland relict surface near Santa Cruz (SCZ), the flat floor of the Cahabón paleovalley around Santa Barbara (SB) and wide pedimented floors in the ChixóyRiver basin.*

Some striking spatial and temporal coincidences point to a major role of groundwater in the breaching of the interfluves. First, the breaches all coincide with active faults: breaching in SB has occurred above the Salamá Fault, two other breaches are located above the NiñoPerdido Fault, and the breach in PL is located above the PT-SF. In addition, according to geologic maps, three of these breaches have occurred over carbonate rocks (namely PL, and along the NPF, though in this latter case no carbonates are known from outcrops where the breaches are located). At all sites breaching has taken place over rocks that possess a high permeability: solution permeability in the case of the carbonates and fracture permeability in the case of the fault zones with a potential for subsequent rock dislocation due to fault activity. Naturally, the higher intrinsic erodibility of the material making up these zones could account on its own for their preferential erosion under the effect of surface runoff. However, several authors have pointed out the fact that surface runoff is null at the watershed itself and that mass wasting and soil creep slow down rapidly as the interfluve is lowered down to the river level and, as a result, could not on their own deepen the breaches down to the river level (Strahler, 1945; Bishop, 1995; Douglas and Smeeckle, 2007). The permeability of the belts, on the other hand, allows for water to leak from the Cahabón River through the bedrock and circulate across the interfluve down to lower standing rivers. This considerably enhances the erosive power required to

propagate the head of a captor across an interfluve (Gabbard and others, 1997; Pederson, 2001). In addition, the penetration of the captor head into the interfluve will induce a positive feedback enhancing groundwater flow toward the captor head (Dunne, 1990; Baker and others, 1990).

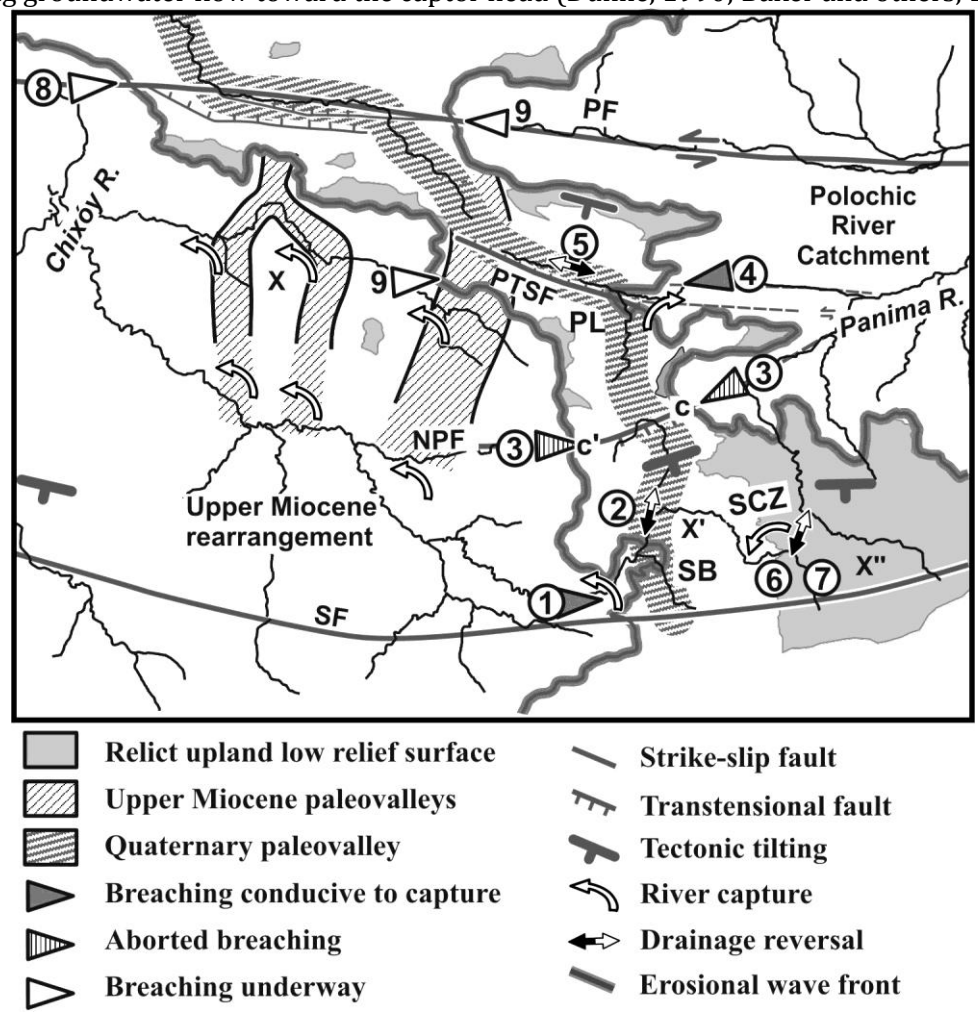

Figure 17. **Drainage rearrangement: succession of events.** *Chronology of the rearrangement after the activation of the transtensional faults: 1—breaching of the interfluve along the Salamá Fault and capture of Santa Barbara (SB), 2—drainage reversal toward SB, 3—interfluve breaching aborts above the Niño Perdido Fault (notches c and c') due to the incision of the valley-fill, 4—interfluve breaching along the Purulhá Trough South fault (PTSF) and capture of Purulhá(PL), 5—initiation of drainage reversal in the Purulhá trough, 6—avulsion of the West Chilascó over an interfluve in Santa Cruz (CSZ), 7—incipient reversal, 8—ongoing groundwater capture of the Cahabón River by the Chixóy River, 9—other potential future groundwater connections and captures. Note the similarity in the drainage pattern in plan view resulting from the reorganization in X and X', suggesting a similar origin for the pattern visible in X.*

The temporal succession of events also supports the assumption that breaching is groundwater-driven. West of the Cahabón valley, the Chixóy River basin is a large catchment that expanded by widespread interfluve breaching during the Upper Miocene (Brocard and others, 2011). Catchment growth stalled during the Pliocene, falling short of capturing the Cahabón River and leaving a strong topographic gradient between the Chixóy River and the Cahabón River (fig. 1). The Chixóy catchment became a dry area due to its topographic isolation (Brocard and others, 2011) and large pediments developed along valley floors (fig. 16). The Chixóy catchment expansion resumed during the Quaternary with the capture of the Cahabón River and the avulsion of the Chilascó River (fig. 17). Temporally, the most noticeable event that can account for the resumption of its expansion is the initiation of transtensional faulting in Plio-

Quaternary time. Fault activation may have created or increased the permeability of the fault zones or favored the dislocation of already weakened rocks. More importantly, the accumulation of sediment along the Cahabón River allowed for the formation of high-standing aquifers stagnating above the fault zones. These aquifers increased the head pressure in the groundwater systems located below the valley floor, in particular above the fault zones. We believe that they have helped to initiate or to increase water transit from the Cahabón River down to the Chixóy and Panimá catchments, thus promoting headward erosion and interfluve breaching. In this respect the breaches observed along the Niño Perdido Fault (fig. 17) could then be explained as follows: these breaches were forming concurrently with the breaches in SB and PL. However, river capture was completed first in SB and PL. The Cahabón valley fill was then incised and its aquifer was drained away above the Niño Perdido Fault. This reduced the pressure head needed for powering the breaching process and the breaches stopped deepening.

Groundwater-powered captures are probably underway at several other sites along the remaining course of the Cahabón River. This is better exemplified near Tactic, where the Cahabón River is on the verge of being captured by the Chixóy River (fig. 17). The capture may be catalyzed by groundwater seepage along the Polochic fault. Several large springs along the trace of the Polochic fault between the Cahabón River and the Chixóy River provide evidence for extensive water circulation in the fault zone (fig. 1A). The mountain flank above the springs is too small to sustain the discharge of these springs. The closest external source of water is Laguna Chicho´ j, a lake located north of the springs. The Cahabón River is another possible source of water. It is located at a greater distance but its water can flow along the Polochic fault. To determine the origin of the water, exploratory fingerprinting was attempted using measurements of the water stable isotope composition. The $\delta^{18}O$ and δD values of the spring waters were compared to those of the Cahabón River and of the lake. The waters were sampled at the start of the rainy season in July 2010 (Appendix 8). The $\delta^{18}O$ values of the springs (7.1 ± 0.08‰, n = 3) are unlike those of the lake (5.8 ± 0.12‰, n = 6) but similar to those of the Cahabón River at _7.2 ± 0.12‰. The same affinities are found for the δD values (springs: 44.9 ± 0.6‰; Cahabón: 42.6 ± 0.2‰; lake: 37.7 ± 0.9‰). The isotope-based tracing suggests that the Cahabón River, rather than Lake Chichój, is the main source of water of the springs and points to a circulation of water along the Polochic fault from the Cahabón River to the Chixóy River. This connection may precede a phase of headward erosion along the Polochic fault that will eventually trigger another capture of the Cahabón River. Further downstream, in the Depression of Cobán, a clear underground water connection of karstic origin is already well established. The water table of the Cahabón River leaks through the quartzose gravel and enters the subterraneous karstic system of the Samcoc cave (see the *Control of Faulting on Valley-Fill Formation* section). Continued development of this groundwater pathway could eventually lead to the intermittent or permanent disappearance of the Cahabón River at the surface. All these observations add to growing evidence that groundwater flow through topographic watersheds is a powerful initiator of river capture (for example Dunne, 1990; Höltz, 1996; Losson and Quinif, 2001; Pederson, 2001; Hill, 2008, among many others).

We therefore view the rearrangement of the Cahabón River as a tectonic defeat made possible by groundwater capture during the transient phase of river adjustment to a new tectonic strain field (fig. 18). Our model establishes a causal link between fault activation, valley-fill formation, and groundwater-assisted river capture. During an initial phase (t1), two adjacent incised catchments are in dynamic equilibrium. River gradients and slopes are such that erosion everywhere counterbalances rock uplift so that there is no net change in elevation (Hack, 1960). For simplicity rock uplift is held uniform during this initial phase (U1). During phase t2, a fault-bounded structure rises at a faster rock uplift rate (U2). Dynamic equilibrium is reestablished by an increase in the erosive power of the rivers across the rising structure. This is achieved by changes in various channel parameters, including river gradient (for example Harbor, 1998; Whipple and Tucker, 2002). The increase in river gradient necessitates a transitory reduction of the incision rate upstream of the rising structure until the new equilibrium gradient is attained through the rising structure. Because the required change in gradient is larger for smaller

streams, smaller streams experience more surface uplift than larger streams (phase 2 on fig. 18B). For rivers with high erosive diffusivity such as transport-limited rivers, the change in river gradient is rapidly propagated along stream (Whipple and Tucker, 2002; Tucker and Whipple, 2002). Along rivers of low erosive diffusivity such as detachment-limited rivers, knickpoints develop and migrate upstream (fig. 18). Incision is then strongly decoupled from uplift rates, and the amount of surface uplift upstream of the rising structure will depend on the rapidity of propagation of the knickpoints upstream. If the decoupling is high, a transient accumulation of sediment can occur upstream of the rising structure (for example Garcia-Castellanos and others, 2003). Due to decreased incision rates and increasing topographic gradient, the highest rivers will be susceptible to avulsion and capture during this period, if the process of avulsion or capture proceeds at a faster pace than the processes of long-profile adjustment (Cowie and others, 2006; Su¨zen and others, 2006; Attal and others, 2008). This is set for example by the time required for headward knickpoints generated by fault activation or fault acceleration to be propagated along the network (Cowie and others, 2006; Whittaker and others, 2007; Douglass and Schmeekle, 2007). In the case of the Cahabón River, we show that the drainage will be made more vulnerable to reorganization due to the presence of permeable interfluves and sediment accumulation along the valley. This process is largely ignored, yet could explain the defeat of other river networks, such as, for example, the drainage of the Peloponnese along the southern margin of the Gulf of Corinth in Greece (Rohais and others, 2007). There, several rivers were reverted by tectonic tilting on the hanging wall of large active normal faults. The reversal was aided by the possibility for the rivers to discharge through carbonates so that they currently flow into closed depressions where sediments accumulate while water is evacuated through large karstic systems (Clendenon, 2009).

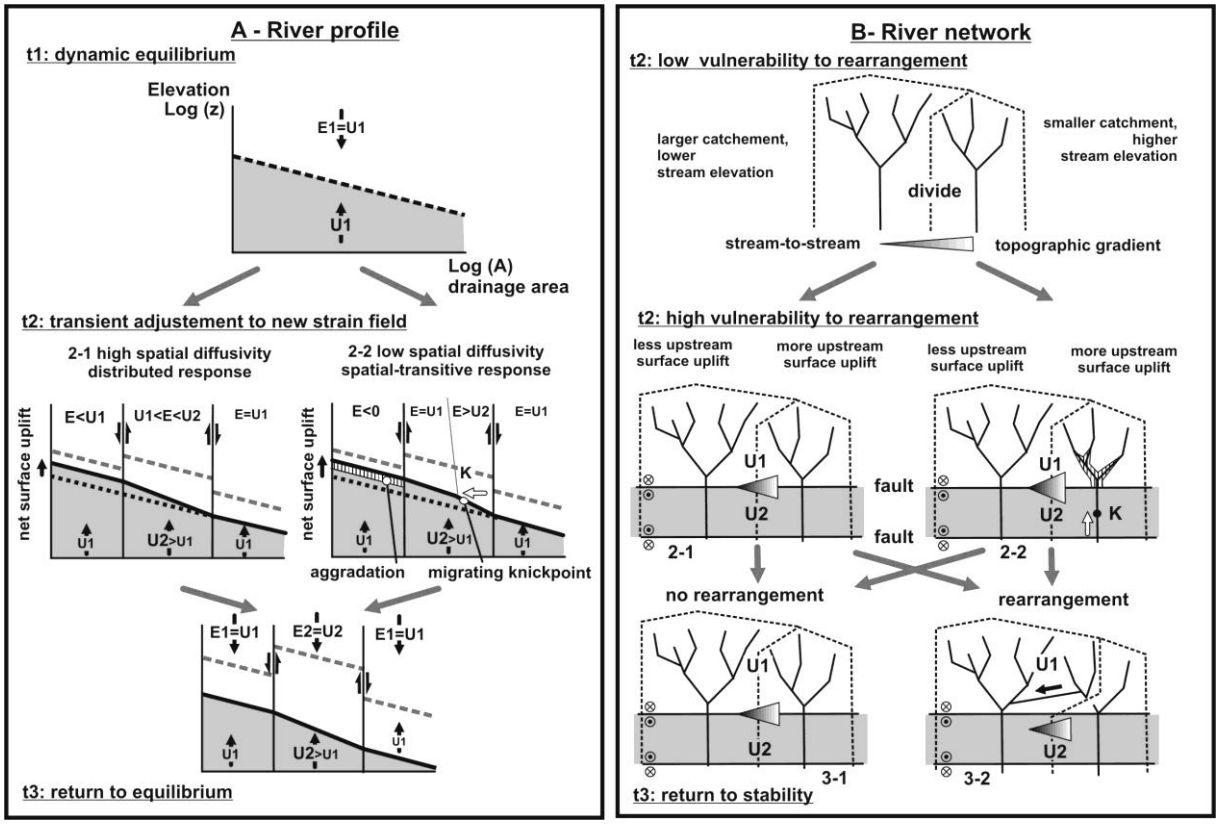

Figure 18. **Drainage reorganization in response to a change in the vertical tectonic rock uplift**. **Conceptual model showing the effect of a rising structure on the flow path of two adjacent rivers, in an incised landscape**: a*t time (t1) the landscape is in dynamic equilibrium between rock uplift (U1) and river incision, so that there is no topographic change. A gradient already exists between the rivers but is not sufficient to initiate rapid reorganization of the drainage network. At time (t2) a new structure starts to rise at rate U2 across the course of the*

streams. Rivers return to equilibrium by reducing their channel width and increasing their gradient above the rising structure, in order to attain a new equilibrium profile along which incision (E) equals uplift everywhere (t3). During the transitional phase, the reaches located upstream of the rising structure experience net surface uplift, and the topographic gradient between adjacent catchments increases. This difference in surface uplift will be less pronounced for a stream with a highly diffusive propagation of base-level changes along stream (for example transport-limited rivers), but will be exacerbated along streams with low-diffusivity (for example detachment-limited rivers, Whipple and Tucker, 2002), where headward migrating knickpoints can form (for example Whittaker and others, 2007), as well as areas of sediment accumulation (for example Su¨zen and others, 2006). Drainage is particularly susceptible to rearrangement during this transient phase, by river capture (for example Whittaker and others, 2008) or avulsion (for example van der Beek and others, 2002).

With the subsequent return to dynamic equilibrium (phase t3), the valley fills are dispersed and bedrock incision resumes (Attal and others, 2008), eliminating the high-standing fluvial aquifers. With the resulting drop in head pressure, the capture process will cease or slow down. This does not mean that captures cannot happen eventually, but the process of rearrangement could slow down to a pace so slow that the network will seem to be essentially passively deformed under the effect of tectonics. At the scale of the considered mountain range, the defeat of the Cahabón River marks the final demise of a range-transverse drainage that existed in Middle Miocene time. Drainage spacing scaled with the width of the orogen, then bracketed by the Motagua and Polochic faults (Brocard and others, 2011). Tectonic accretion north of the Polochic fault considerably widened the orogen in Late Miocene time. The transverse drainage was defeated by rising structures and its reorganization created wider catchments scaled to the larger width of the orogen. The evolution of the Sierra de Chuacús–Sierra de las Minas drainage is a good field-based illustration of the ability of drainages to scale with orogen width (Ellis and others, 1999; Horton and DeCelles, 2001; Densmore and others, 2005; Frankel and Pazzaglia, 2006; Bonnet, 2009). The Cahabón River survived this first pulse of rearrangement and its headwaters persisted as a long, narrow catchment hanging above the surrounding catchments, from which it was protected by high standing interfluves. The Plio-Quaternary tectonic disruption of this upper catchment precipitated the reorganization of this metastable drainage and its rapid integration into its surrounding catchments.

Conclusions

During Quaternary time, three dramatic river diversions modified the drainage network of the Cahabón River. The geomorphic traits left by these diversions are breached interfluves, deep, headward propagating canyons, and barbed tributaries. The initial extent of the drainage is demonstrated geologically by the presence of quartzose in the gravel fraction and chromium in the fine fraction, which both stem from rock sources located in the former headwaters of the river. Combined measurements of *in-situ*-produced cosmogenic 10Be and 26Al and of the geomagnetic characteristics of the ancestral river deposits show that these diversions occurred during the last 600 ky with the following succession of events: 1) capture of the Cahabón River near Santa Barbara at ~500 ky; 2) capture of the Cahabón River near Purulhá sometime latter (240-450 ky ago); and 3) avulsion of the West Chilascó River between 84 ± 5 ky and 200 ky ago.

The morphology of the Cahabón paleovalley and the architecture of its sediment fill were investigated using field mapping and ERT. The sediment fill was deposited by the Cahabón River and controlled by tectonic faults that remained active after the captures. The general pattern of deformation and sedimentation shows that the Cahabón River was facing the reactivation of pre-existing faults in a transtensional regime that started in Late Pliocene or Early Quaternary times.

Headward erosion nucleated at the capture sites, propagating along the upstream reaches, but also downstream the beheaded river, as a result of drainage reversal. Deep, short canyons started to form at the capture sites. The timing of canyon development was investigated using a simple mechanistic model. Canyon development is found to obey a simple dependence

on drainage area and bedrock erodibility, with a few departures from the theoretical unit stream power that can be explained by the very steep canyon margins, where other mechanisms that stream erosion alone contribute to canyon propagation. The model was calibrated on canyon SB and used to evaluate the age of the two other canyons. The modeled ages are consistent with geology, geochronology, and geomorphic inferences.

Surprisingly the most important amount of reorganization is not due to the captures themselves but the drainage reversal that ensued. Drainage reversal toward the capture sites has been so extensive that the drainage area of the canyons is now several times larger than what it was at the time of capture. Reversal was sparked by the river captures, because the captures weakened the main stream and prevented it from coping with tectonic uplift. They also offered new evacuation routes in the headwaters. Field observations show that reversal was controlled by three mechanisms that may have acted concurrently or in relay: the first one is the growth of lateral alluvial fans across the paleovalley following the drop in dispersal power of the axial valley drainage; the second one is flow reversal in the aquifer hosted by the sediment fill, which generates groundwater sapping of the sediment fill starting at the capture sites.

Tectonic back-tilting is the most commonly cited agent of reversal. However, along the studied drainage, tectonic tilting starts to contribute to the reversal only 200 to 500 ky after the captures, leaving ample time for the other mechanisms to achieve a substantial part of the reversal over this initial period.

The main reason for the reorganization of the drainage in the study area is the existence of strong topographic gradients with the Cahabón River being perched high above the surrounding rivers. Headward erosion toward the Cahabón River triggered the deep, localized breaching of the intervening ridges. Steeper slopes and higher precipitations observed here and there locally represent acceptable explanations for the breaching but are not satisfactory everywhere. The more systematic spatial coincidence of the breaches and permeable rocks, notably carbonates and fault damage zones, indicates that groundwater flow has been instrumental in breaching the interfluves. We propose that the connection between the Cahabón and its future captors was first established underground across the interfluves. A corresponding modern connection is evidenced by isotopic fingerprinting of the water flowing along the Polochic fault between the Cahabón River and the Chixóy River. Through these subterraneous connections, the Cahabón River supplied water to the headwaters of its captors. We propose that these connections intensify headward erosion at the head of the captors, promote the sapping of interfluves, and eventual lead to their breaching.

The topographic gradients between the Cahabón River and its captors existed before Quaternary times. Interfluve breaching followed the activation of transtensional faulting by only a few million years at most, suggesting that faulting catalyzed the rearrangement process. In this respect the captures mark the tectonic defeat of the Cahabón River and its rearrangement into a surface network that flows according to the current tectonic gradients. It is a tectonic defeat, classic in its result, but not in its mechanisms, because diversion was promoted by subterraneous water flow. Groundwater flow was promoted by increased fracture porosity/permeability in the fault damage zones, but also, and more importantly, by the formation of high-standing aquifers above the fault zones within the sediment that had accumulated along the Cahabón valley in response to the initiation of faulting.

Sediment accumulation was a transient feature of adaptation of the Cahabón River to the new tectonic regime and would have ceased, had the river been given the time necessary to attain a new dynamic equilibrium. The captures did, however, dismantle the river before such equilibrium was reached. Removal of the sediment fill would have lowered the head pressure in the subterraneous systems, thus closing this temporary vulnerability window during which rapid capture was promoted by groundwater flow.

At the scale of the mountain range, the defeat of the Cahabón River marks the final demise of a range-transverse drainage that had existed in Middle Miocene time. The Cahabón River survived a first pulse of rearrangement and persisted as a long, narrow, metastable catchment, hanging above the surroundings and protected from them by high-standing

interfluves. Its tectonic disruption in Quaternary time precipitated its reorganization and rapid integration into the new regional river network.

Acknowledgments

This work was supported in part by Swiss National Science Foundation grants 200021-112175/1 and 200020-120117/1 attributed to Christian Teyssier and 200020- 125108/1 attributed to Klaus Holliger. We thank Hans-Rudolf Pfeifer and Jean Claude Lavanchy from the Centre of Mineral analysis from the Institute of Mineralogy at the University of Lausanne for their assistance in geochemical analyses of sedimentary rocks. We also thank our colleagues from San Carlos University–Guatemala (USAC) who provided invaluable help during fieldwork. We thank Kyle Nichols, Kurt Frankel and Frank Pazzaglia for their thorough reviews and insightful suggestions that greatly improved the manuscript.

References

Allen, P. A., and Densmore, A. L., 2000, Sediment flux from an uplifting fault block: Basin Research, 12, n. 3–4, p. 367–380

Attal, M., and Lavé, J., 2005, Changes of bedload characteristics along the Marsyandi River (Central Nepal): implications for understanding hillslope sediment supply, sediment load evolution along fluvial networks and denudation in active orogenic belts, *in* Willett, S. D., Hovius, N., Brandon, M. T., and Fisher, D. M. editors, Tectonics, Climate, and Landscape Evolution: Geological Society of America Special Paper, v. 398, p. 143–171

Attal, M., Tucker G.,E., Whittaker A.C., Cowie P.A., Roberts G.P., 2008, Modeling fluvial incision and transient landscape evolution: Influence of dynamic channel adjustment: Journal of Geophysical Research, 113, F03013

Authemayou, C., Brocard, G., Teyssier, C., Simon-Labric, T., Chiquín, E.N., Guttierrez, A., and Morán, S., 2011, The Caribbean–North America–Cocos Triple Junction and the dynamics of the Polochic-Motagua fault system: Pull-up and a zipper model: Tectonics, 30, TC3010

Balco, G., Stone, J. O., Lifton, N. A., and Dunai, T. J., 2008, A complete and easily accessible means of calculating surface exposure ages or erosion rates from ^{10}Be and ^{26}Al measurements: Quaternary Geochronology, v. 3, n. 3, p. 174–195

Baker, V. R., Kochel, R. C., Laity, J. E., and Howard, A. D., 1990, Spring sapping and valley network development, with case studies, *in* Higgins, C. G., and Coates, D. R., editors, Groundwater Geomorphology: The Role of Subsurface Water in Earth-Processes and Landforms: Geological Society of America Special Paper, v. 252, p. 235–265.

Bierman, P. R., and Caffee, M., 2001, Slow rates of rock surface erosion and sediment production across the Namib Desert and Escarpment, Southern Africa: American Journal of Science, 301, n. 4–5, p. 326–358

Binley, A., and Kemna, A., 2005, DC resistivity and induced polarization methods, *in* Rubin, Y., and Hubbard, S. S., editors, Hydrogeophysics: Dordrecht, Springer, Water Science and Technology, v. 50, p. 129–156, http://dx.doi.org/10.1007/1-4020-3102-5_5

Bishop, P., 1995, Drainage rearrangement by river capture, beheading and diversion: Progress in physical geography, v. 19, n. 4, p. 449–473

Bishop, P., Hoey, T. B., Jansen, J. D., and Lexartza-Artza, I., 2005, Knickpoint recession rate and catchment area: the case of uplifted rivers in Eastern Scotland: Earth Surface Processes and Landforms, v. 30, n. 6, p. 767–778

Blott, S. J., and Pye, K., 2001, GRADISTAT: a grain size distribution and statistics package for the analysis of unconsolidated sediments: Earth Surface Processes and Landforms, v. 26, n. 11, p. 1237–1248

Bonnet, S., 2009, Shrinking and splitting of drainage basins in orogenic landscapes from the migration of the main drainage divide: Nature Geoscience, v. 2, p. 766–771

Braucher, R., Bourlès, D. L., Colin, F., Brown E. T. and Boulange, B., 1998, Brazilian laterite dynamics using in situ-produced ^{10}Be: Earth and Planetary Science Letters, v. 163, n. 1–4, p. 197–205

Bridgland, D. R., and Gibbard, P. L., 1997, Quaternary river diversions in the London Basin and the Eastern English Channel: Géographie physique et Quaternaire, v. 51, n. 3, p. 337–346

Brocard, G. Y., and van der Beek, P. A., 2006, Influence of incision rate, rock strength, and bedload supply on rate on bedrock river gradients and valley-flat widths: Field-based evidence and calibrations

from western Alpine rivers (southeast France), in Willett S. D., Hovius, N., Brandon, M. T., and Fisher, D. M., Tectonics, Climate, and Landscape Evolution: Geological Society of America Special Paper, v. 398, p. 101–125

Brocard, G., Teyssier, C., Dunlap, W. J., Authemayou, C., Simon-Labric, T., Cacao-Chiquín, E. N., Guttiérrez-Orrego, A., and Morán-Ical, S., 2011, Reorganization of a deeply incised drainage: role of deformation, sedimentation, and groundwater flow: Basin Research, v. 23, n. 6, p. 631–651

Brookfield, M. E., 1998, The evolution of the great river systems of southern Asia during the Cenozoic India-Asia collision: rivers draining southwards: Geomorphology, v. 22, n. 3–4, p. 285–312

Burbank, D. W., Leland, J., Fielding, E., Anderson, R. S., Brozovic, N., Reid, M. R., and Duncan C., 1996, Bedrock incision, rock uplift and threshold hillslopes in the northwestern Himalayas: Nature, v. 379, p. 505–510

Caputo, R., Piscitelli, S., Oliveto, A., Rizzo, E., and Lapenna, V., 2003, The use of electrical resistivity tomographies in active tectonic studies: Examples from the Tyrnavos Basin, Greece: Journal of Geodynamics, v. 36, n. 1–2, p. 19–35

Castelltort, S., and Simpson, G., 2006, River spacing and drainage network growth in widening mountain ranges: Basin Research, v. 18, n. 3, p. 267–276

Chmeleff, J., Horn, I., Steinhoefel, G., and Von Blanckenburg, F., 2008, In-situ determination of precise stable Si isotope ratios by UV-femtosecond laser ablation high-resolution multi-collector ICP-MS: Chemical Geology, v. 249, n. 1–2, p. 155–166

Chmeleff, J., von Blanckenburg, F., Kosser, K., and Jakob, D., 2010, Determination of the ^{10}Be half-life by multicollecter ICP-MS and liquid scintillation counting: Nuclear Instruments and Methods in Physics Research Section B: Beam Interactions with Materials and Atoms, v. 268, n. 2, p. 192–199

Clendenon, C., 2009, Karst hydrology in ancient myths from Arcadia and Argolis, Greece: Acta Carsologica, v. 38, n. 1, p. 145–154

Cogné, J. P., 2003, PaleoMac: A Macintosh™ application for treating paleomagnetic data and making plate reconstructions: Geochemistry Geophysics Geosystems, v. 4, 1, 1007, http://dx.doi.org/10.1029/2001GC000227

Cowie, P. A., Attal, M., Tucker, G. E., Whittaker, A. C., Naylor, M., Ganas, A., and Roberts G. P., 2006, Investigating the surface process response to fault interaction and linkage using a numerical modelling approach: Basin Research, v. 18, n. 3, p. 231–266

Cowie, P. A., Whittaker, A. C., Attal, M., Roberts, G., Tucker, G. E., and Ganas, A., 2008, New constraints on sediment-flux-dependent river incision: implications for extracting tectonic signals from river profiles: Geology, v. 36, n. 7, p. 535–538

Craw, D., Youngston, J. H., and Koons, P. O., 1999, Gold dispersal and placer formation in an active oblique collisional mountain belt, Southern Alps, New Zealand: Economic Geology, v. 94, n. 5, p. 605–614

Crosby, B., and Whipple, K. X., 2006, Knickpoint initiation and distribution within fluvial networks: 236 waterfalls in the Waipaoa River, North Island, New Zealand: Geomorphology, v. 82, n. 1–2, p. 16–38

DeMets, C., Jansma, P. E., Mattioli, G. S., Dixon, T. H., Farina, F., Bilham, R., Calais, E., and Mann, P., 2000, GPS geodetic constraints on Caribbean-North America plate motion: Geophysical Research Letters, v. 27, n. 3, p. 437–440

Densmore, A. L., Dawers, N. H., Gupta, S., and Guidon, R., 2005, What sets topographic relief in extensional footwall: Geology, v. 33, n. 6, p 453–456

Diaferia, I., Barchi, M., Loddo, M., Schiavone, D., and Siniscalchi, A., 2006, Detailed imaging of tectonic structures by multiscale Earth resistivity tomographies: The Colfiorito normal faults (central Italy): Geophysical Research Letters, v. 33, L09305

Donnelly, T. W., Horne, G. S., Finch, R. C., and López-Ramos, E., 1990, Northern Central America: The Maya and Chortis blocks, *in* Dengo, G. and Case, J. E., editors, The Caribbean region: Geological Society of America, Geology of North America, v. H. p. 37–76

Douglas, J., and Schmeeckle, M., 2007, Analogue modeling of transverse drainage mechanisms: Geomorphology, v. 84, n. 1–2, p. 22–43

Drexler, W. J., Rose, W. L., Sparks, R. S. J., and Ledbetter, M. T., 1980, The Los Chocoyos Ash, Guatemala: A major stratigraphic marker in Middle America and in three ocean basins: Quaternary research, v. 13, n. 3, p. 327–345

Dunai, T. J., 2001, Influence of secular variation of the geomagnetic field on production rates of in situ produced cosmogenic nuclides: Earth and Planetary Science Letters, v. 193, n. 1–2, p. 197–212

Dunne T., 1990, Hydrology, mechanics, and geomorphic implications of erosion by subsurface flow, *in* Higgins, C. G., and Coates, D. R., editors, Groundwater Geomorphology: Geological Society of America Special Paper, v. 252, p. 1–28

Ellis, M., Densmore, A. L., and Anderson, R. S, 1999, Development of mountainous topography in the Basin Ranges, USA: Basin Research, v. 11, n. 1, p. 21–41

Fisher, R., 1953, Dispersion on a sphere: Proceedings of the Royal Society of London, A 217, n. 1130, p. 295–305

Finnegan, N. J., Roe, G., Montgomery, D. R., and Hallet, B., 2005, Controls of the channel width of rivers: Implications for modeling fluvial incision of bedrock: Geology, v. 33, n. 3, p. 229–232

Frankel, K. L., and Pazzaglia, F. J., 2006, Mountain fronts, base-level fall, and landscape evolution: insights from the southern Rocky Mountains, *in* Willet, S. D., Hovius, N., Brandon, M. T., and Fisher, D. M., editors, Tectonics, climate and landscape evolution: Geological Society of America Special Paper, v. 398, p. 419–434

Gabbard, D. S., Huang, C., Norton, L. D., and Steinhardt, G. C., 1997, Landscape position, surface hydraulic gradients and erosion processes: Earth Surface Processes and Landforms, v. 23, n. 1, p. 83–93

Garcia-Castellanos, D., Vergès, J., Gaspar-Escribano, J., and Cloethingh, S., 2003, Interplay between tectonics, climate, and fluvial transport during the Cenozoic evolution of the Ebro Basin (NE Iberia): Journal of Geophysical Research, v. 108, 2347, n. B7, 2347

Granger, D. E., and Muzikar, P. F., 2001, Dating sediment burial with in situ-produced cosmogenic nuclides: theory, techniques and limitations: Earth and Planetary Science Letters, v. 188, n. 1–2, p. 269–281

Granger, D. E., Kirchner, J. W., and Finkel, R. C., 1997, Quaternary downcutting rate of the New River, Virginia, measured from differential decay of cosmogenic ^{26}Al and ^{10}Be in cave deposited alluvium: Geology, v. 25, n. 2, p. 107–110

Hack, J. T., 1960, Interpretation of erosional topography in humid temperate regions: American Journal of Science, v. 258-A, p. 80–97

Haeuselmann P., Granger, D. E., Jeannin, P.-Y., and Lauritzen, S.-E., 2007, Abrupt glacial valley incision at 0.8 Ma dated from cave deposits in Switzerland: Geology, v. 35, n. 2, p. 143–146

Hallet, B., and Molnar, P., 2001, Distorted drainage basins as markers of crustal strain east of the Himalaya. Journal of Geophysical Research, v. 106, B7, p. 13697–13709

Harbor, D. J., 1997, Landscape evolution at the margin of the Basin and Range: Geology, v. 25, n. 12, p. 1111–1114

Harbor, D. J. 1998, Dynamic equilibrium between an active uplift and the Sevier River, Utah: The Journal of Geology, v. 106, n. 2, p. 181–194

Heidbreder, E., Pinkau, K., Reppin, C., and Schöenfelder, V., 1971, Measurements of the distribution in energy and angle of high-energy neutrons in the lower atmosphere: Journal of Geophysical Research, v. 76, n. 13, p. 2905–2916

Hill, C. A., Eberz, N., and Buecher, R. H., 2008, A karst connection model for Grand Canyon, Arizona, USA: Geomorphology, v. 95, n. 3–4, p. 316–334

Hillesheim, M. B., Hodell, D. A., Leyden, B. W., Brenner, M., Curtis, J. H., Anselmetti, F. S., Ariztegui, D., Buck, D. G., Guilderson, T. P., Rosenmeier, M. F., and Schnurrenberger, D. W., 2005, Climate change in lowland Central America during the late deglacial and early Holocene: Journal of Quaternary Science, v. 20, n. 4, p. 363–376

Hoorn, C., Guerrero, J., Sarmiento, G. A., and Lorente, M. A., 1995, Andean tectonics as a cause for changing drainage pattern in Miocene northern South America: Geology, v. 23, n. 3, p. 237–240

Horton, B. K., and DeCelles, P. G., 2001, Modern and ancient fluvial megafans in the foreland basin system of the central Andes, southern Bolivia: Implications for drainage network evolution in fold-thrust belts: Basin Research, v. 13, n. 1, p. 43–63

Hötzl, H., 1996, Origin of the Danube-Aach system: Environmental Geology, v. 27, n. 2, p. 87–96

Hovius, N., 1996, Regular spacing of drainage outlets from linear mountain belts: Basin Research, v. 8, n. 1, p. 29–44

Hovius, N., Stark, C. P., Tutton, M. A., and Abbott, L. D., 1998, Landslide-driven drainage network evolution in a pre-steady-state mountain belt: Finisterre Mountains, Papua New Guinea: Geology, v. 26, n. 12, p. 1071–1074

Humphrey, N. F., and Konrad, S. K., 2000, River incision or diversion in response to bedrock uplift: Geology, v. 28, 1, p. 43–46

Ivy-Ochs, S., ms, 1996, The dating of rock surfaces using in situ produced ^{10}Be, ^{26}Al and ^{36}Cl, with example from Antarctica and the Swiss Alps: Zürich, Switzerland, Eidgenössische Technische Hochschule Zürich (ETHZ), Ph. D. thesis, Zurich, Diss. ETH 11763.

Jackson, J., and Leeder, M., 1994, Drainage systems and the development of normal faults: an example from Pleasant Valley, Nevada: Journal of Structural Geology, v. 16, n. 8, p. 1041–1059

Jackson, J. A., Norris, R., and Youngson, J., 1996, The structural evolution of active fault and fold systems in central Otago, New Zealand: evidence revealed by drainage patterns: Journal of Structural Geology, v. 18, n. 2–3, p. 217–234

Jaffey, N., and Robertson, A., 2005, Non-marine sedimentation associated with Oligocene-Recent exhumation and uplift of the Central Taurus Mountains, S. Turkey: Sedimentary Geology, v. 173, n. 1–4, p. 53–89

Keller, E. A., Gurrola, L., and Tierney, T. E., 1999, Geomorphic criteria to determine direction of lateral propagation of reverse faulting and folding: Geology, v. 27, n. 6, p. 515–518

Kirschvink, J. L., 1980, The least-squares line and plane and the analysis of paleomagnetic data : Geophysical Journal of the Royal Astronomical Society, v. 62, p. 699–718

Kohl, C. P., and Nishiizumi, K., 1992, Chemical isolation of quartz for measurement of *in situ*-produced cosmogenic nuclides: Geochemica et Cosmochimica Acta, v. 56, n. 9, p. 3583–3587

Korschinek, G., Bergmaier, A., Faestermann, T., Gerstmann, U. C., Knie, K., Rugel, G., Wallner, A., Dillmann, I., Dollinger, G., Lierse, von Gostomski, Ch., Kossert, K., Maite, M., Poutivtsev, M., and Remmert, A., 2010, A new value for the half-life of ^{10}Be by heavy-ion elastic recoil detection and liquid scintillation counting: Nuclear Instruments and Methods in Physics Research Section B: Beam Interactions with Materials and Atoms, v. 268, n. 2, p. 187–191

Lachniet, M. S., and Vazquez-Selem, L., 2005, Last Glacial Maximum equilibrium line altitudes in the circum-Caribbean (Mexico, Guatemala, Costa Rica, Colombia, and Venezuela): Quaternary International, v. 138–139, p. 129–144

Lal, D., 1991, Cosmic ray labeling of erosion surfaces: *in-situ* nuclide production rates and erosion models: Earth and Planetary Science Letters, v. 104, p. 424–439

Lavé, J., and Avouac, J. P., 2001, Fluvial incision and tectonic uplift across the Himalayas of central Nepal: Journal of Geophysical Research, v. 106, B11, p. 26,561–26,593,

Leeder, M. R., and Jackson, J. A., 1993, The interaction between normal faulting and drainage in active extensional basins, with examples from the western United States and central Greece: Basin Research, v. 5, n. 2, p. 79–102

Lodolo, E., Menichetti, M., Guzmán-Speziale, M., Giunta, G., and Zanolla, C., 2009, Deep crustal setting of the North American-Caribbean plate Boundary in Eastern Guatemala: Geofísica International, v. 48, n. 3, p. 263–277

Loke, M. H., and Barker, R. D., 1996, Rapid least-squares inversion of apparent resistivity pseudosections by a quasi-Newton method: Geophysical Prospecting, v. 44, n. 1, p. 131–152

Losson, B., and Quinif, Y., 2001, La capture de la Moselle. Nouvelles données chronologiques par datations U-Th sur spéléothèmes : Karstologia, v. 37, p. 29–40

Lugeon, M., 1901, Recherches sur l'origine des vallées des Alpes Occidentales : Annales de Géographie, 10, 52, p. 295–317, and 10, 54, p. 401–428

Lyon-Caen, H., Barrier, E., Lasserre, C., Franco, A., Arzu, I., Chiquín, L., Chiquín, M., Duquesnoy, T., Flores, O., Galicia, O., Luna, J., Molina, E., Porras, O., Requena, J., Robles, V., Romero, J., and Wolf, R., 2006, Kinematics of the North American-Caribbean-Cocos plates in Central America from new GPS measurements across the Polochic-Motagua fault system: Geophysical Research Letters, 33, L19309

McBirney, A. R., 1963, Geology of a part of the Central Guatemalan Cordillera: University of California Publications in Geological Sciences, v. 38, n. 4, p. 177–242

Maher, E., Harvey, A. M., and France, D., 2007, The impact of a major Quaternary river capture on the alluvial sediments of a beheaded river system, the Rio Alias, SE Spain: Geomorphology, v. 84, n. 3–4, p. 344–356

Mather, A. E., 2000, Adjustment of a drainage network to capture induced base-level change: an example from the Sorbas Basin, SE Spain: Geomorphology, 34, n. 3–4, p. 271–289

Miller, R. S., and Slingerland, R. L., 2006, Topographic advection on fault-bend folds: inheritance of valley positions and the formation of wind gaps: Geology, v. 34, n. 9, p. 769–772

Nishiizumi, K., Wintere, E. L., Kohl, C. P., Klein, J., Middleton, R., Lal, D., and Arnold, J. R., 1989, Cosmic ray production rates of ^{10}Be and ^{26}Al in quartz from glacially polished rocks: Journal of Geophysical Research, v. 94, B12, p. 17907–17915

Nguyen, F., Garambois, S., Jongmans, D., Pirard, E., and Locke, M., 2005, Image processing of 2D resistivity

data for imaging faults: Journal of Applied Geophysics, v. 57, n. 4, p. 260–277

Pederson, D. T., 2001, Stream piracy revisited: a groundwater sapping solution: GSA Today, v. 11, n. 9, p. 4–10

Pissard, A., Harmand, D., and Krook, L., 1997, L'évolution de la Meuse de Toul à Maastricht depuis le Miocène: Corrélations chronologiques et traces des captures de la Meuse lorraine d'après les minéraux denses: Géographie physique et Quaternaire, v. 51, n. 3, p. 267–284

Plug, L. J., Gosse, J. C., McIntosh, J. J., and Bigley, R., 2007, Attenuation of cosmic ray flux in temperate forest: Journal of Geophysical Research, v. 112, F02022

Ramsey, L. A., Hovius, N., Haines, J. A., and Hu, J. C., 2004, Entrenched, transverse rivers as geomorphic strain markers: insights from south-eastern Taïwan: EOS, Transactions American Geophysical Union, v. 85, no. 47, Fall Meeting Supplement, abstract T11D-1318.

Replumaz, A., Lacassin, R., Tapponnier, P., and Leloup, P. H., 2001, Long-term river offset and Plio-Quaternary slip-rate on the Red River fault (Yunnan, China): Journal of Geophysical Research, v. 106, n. B1, p. 819–836

Rizzo, E., Colella, A., Lapenna, V., and Piscitelli, S., 2004, High-resolution images of the fault-controlled High Agri Valley basin (Southern Italy) with deep and shallow electrical resistivity tomographies: Physics and Chemistry of the Earth, v. 29, n. 4–9, p. 321–327

Rohais, S., Eschard, R., Ford, M., Guillocheau, F., and Moretti, I., 2007, Stratigraphic architecture of the Plio-Pleistocene infill of the Corinth Rift: Implications for its structural evolution: Tectonophysics, v. 440, n. 1–4, p. 5–28

Rose, W. I., Newhall, C. G., Bornhorst, T. J., and Self, S., 1986, Quaternary silicic pyroclastic deposits of Atitlán Caldera, Guatemala, *in* Williams, S. N., and Carr, M. J., editors, Richard E. Stoiber 75th birthday volume: Journal of Volcanology and Geothermal Research, v. 33, p. 57–80

Rozanski, K., Araguas-Araguas, L., and Giofiantini, R., 1993, Isotopic patterns in modern global precipitation, *in* Swart, P. K., Lohman, K. C., McKenzie, J., and Savin, S., editors, Climate Change in Continental Isotopic Records: AGU, Washington, D. C., Geophysical Monograph Series, AGU, Washington, D. C. v. 78, p. 1–36

Rykwalder, P., 2008, Back-to-back adventures south of the border: National Speleological Society of America News, v. 66, n. 3, p. 9–19.

Samworth, E. A., Warburton, E. K., and Engelbertink, G. A. P., 1972, Beta decay of the ^{26}Al ground state: Physical Review C, v. 5, n. 1, p. 138–142

Schaller, M., von Blanckenburg, F., Hovius, N., and Kubik, P. W., 2001, Large scale erosion rate from in situ-produced cosmogenic nuclides in European river sediments: Earth and Planetary Science Letters, v. 188, n. 3–4, p. 441–458

Schlunegger, F., Slingerland, R., and Matter, A., 1998, Crustal thickening and crustal extension as controls on the evolution of the drainage network of the central Swiss Alps between 30 Ma and the present: constraints from the stratigraphy of the North Alpine Foreland basin and the structural evolution of the Alps: Basin Research, v. 10, n. 2, p. 197–212

Seeber, L., and Gornitz, V., 1983, River profiles along the Himalayan arc as indicators of active tectonics: Tectonophysics, v. 92, n. 4, p. 335–367

Seginer I., 1966, Gully development and sediment yield: Journal of Hydrology, v. 4, p. 236–253

Stein, R. S., and Barrientos, S. E., 1985, Planar high-angle faulting in the Basin and Range: Geodetic analysis of the 1983 Borah Peak, Idaho, earthquake: Journal of Geophysical Research, v. 90, n. B13, p. 11,355–11,366

Stock, G. M., Anderson, R. S., and Finkel, R. C., 2004, Pace of landscape evolution in the Sierra Nevada, California, revealed by cosmogenic dating of cave sediments: Geology, v. 32, n. 3, p. 193–196

Strahler, A. N., 1945, Hypotheses of stream development in the folded Appalachians of Pennsylvania: Geological Society of America Bulletin, v. 56, n. 1, p. 45–88

Suski, B., Brocard, G., Authemayou, C., Consenza Muralles, B., Teyssier, C., and Holliger, K., 2010, Localization and characterization of an active fault in an urbanized area in central Guatemala by means of geoelectrical imaging: Tectonophysics, v. 480, n. 1–4, p. 88–98

Süzen, M. L., Toprak, V., and Rojay, B., 2006, High altitude Plio-Quaternary fluvial deposits and their implication on the tilt of a horst, western Anatolia, Turkey: Geomorphology, v. 74, n. 1–4, p. 80–99

Swissboring Overseas, 2001, Estudio geotécnico sub-estación eléctrica Tactic, 30 p

Talling, P. J., Stewart, M. D., Stark, C. P., Gupta, S., and Vincent, S. J., 1997, Regular spacing of drainage outlets from linear fault blocks: Basin research, v. 9, n. 4, p. 275–302

Thouveny, N., Bourlès, D. L., Saracco, G., Carcaillet, J. T., and Bassinot, F., 2008, Paleoclimatic context of geomagnetic dipole lows and excursions in the Brunhes, clue for an orbital influence on the geodynamo?: Earth and Planetary Science Letters, v. 275, n. 3–4, p. 269–284

Tucker, G. E., and Whipple, K. X., 2002, Topographic outcomes predicted by stream erosion models: Sensitivity analysis and inter-model comparison: Journal of Geophysical Research, v. 107, n. B9, 2179

Van der Beek, P., Champel, B., and Mugnier, J.-L., 2002, Control of detachment dip on drainage development in regions of active fault-propagation folding: Geology, v. 30, n. 5, p. 471–474

Vanneste, K., Verbeeck, K., and Petermans, T., 2008, Pseudo-3D imaging of a low-slip-rate, active normal fault using shallow geophysical methods: The Geleen fault in the Belgian Maas River valley: Geophysics, v. 73, n. 1, p. B1-B9

Vogt, P. R., 1991, Estuarine stream piracy: Calvert County, U.S. Atlantic coastal plain: Geology, v. 19, n. 7, p. 754–757

Weissel, J. K., and Seidl, M. A., 1998, Inland propagation of erosional escarpments and river profile evolution across the southeast Australian passive continental margin, *in* Tinkler K., and Wohl E., editors, Rivers over rock: fluvial processes in bedrock channels: American Geophysical Union, Geophysical Monograph Series, v. 107, p. 189–206

Whipple, K. X., and Tucker, G. E., 2002, Implications of sediment-flux dependent river incision models for landscape evolution: Journal of Geophysical Research, v. 107, n. B2

Whittaker, A. C., Cowie, P. A., Attal, M., Tucker, G. E., and Roberts, G. P., 2007, Contrasting transient and steady-state rivers crossing active normal faults: new field observations from the Central Apennines, Italy: Basin Research, v. 19, n. 4, p. 529–556

Whittaker, A. C., Attal M., Cowie P. A., Tucker G. E., and Roberts G., 2008, Decoding temporal and spatial patterns of fault uplift using transient river long profiles: Geomorphology, v. 100, n. 3–4, p. 506–526

Zijderveld, J. D. A., 1967, The natural remanent magnetization of the Exeter Volcanic Traps (Permian, Europe): Tectonophysics, v. 4, n. 2, p. 121–153

Appendix 1. Aerial views of the Cahabón River valley

Figure A1. (A) Aerial view of the Santa Barbara canyon. View toward the northeast. Labeling of tributaries as used in the canyon growth simulation. The 'El Chupadero' waterfall is visible at the head of canyon branch (e). Note in the background the San Isidro tributary (SIT) valley, the site of the Santa Cruz avulsion (SCZ), and the relict upland surface. The incision of the Cahabón paleovalley into the upland surface is visible in the upper left corner. (B) Aerial view of the Cahabón paleovalley south of Purulhá. View toward the south. The head of the canyon of Purulhábranch (a) in the foreground corresponds to the 'Ram Tzul' waterfall. The U-shaped paleovalley of the perched Cahabón River is carved in serpentinized peridotes. La Union Barrios (UB) town is sited on the divide that separates the Purulhácanyon catchment from the Santa Barbara canyon catchment.

Appendix 2
Linear referencing of studied sites along the Cahabón River paleovalley

PT	X	Y	PT	X	Y	PT	X	Y	PT	X	Y
1	803948	1664450	12	791315	1690930	23	776965	1697870	34	779122	1710280
2	801858	1672070	13	790084	1691630	24	776172	1698760	35	778035	1710200
3	803284	1675210	14	789712	1692380	25	776641	1699390	36	777757	1711810
4	802863	1677350	15	788302	1692800	26	774989	1701200	37	779791	1713150
5	802393	1677730	16	788335	1693310	27	774978	1701230	38	781045	1711620
6	801680	1677730	17	787282	1694240	28	774997	1701190	39	782439	1711560
7	800385	1679520	18	787282	1694690	29	773353	1701330	40	783804	1713370
8	800790	1684880	19	787282	1694710	30	772935	1703560	41	790270	1713150
9	799219	1685460	20	787266	1695000	31	776391	1707020	42	792165	1713820
10	799186	1685440	21	776965	1697120	32	775889	1707690	43	793586	1713040
11	792530	1687920	22	776965	1697830	33	779345	1709750	44	796206	1713870

Table A2. Definition of the axis used for referencing outcrop and sample locations along the Cahabón River paleovalley Locations are given in kilometers along this axis from the Sierra de las Minas drainage divide down to the city of Cobán. Coordinates are in Universal Transverse Mercator zone 15, and the reference ellipsoid is WGS84. Axis is defined as a succession of straight segments, as defined by the mid-distance line between valley flanks. PT: point number; X and Y: longitude and latitude in meters, UTM 15 coordinates, projection WGS 1984.

Appendix 3
Grain-size analysis of the Cahabón River sediment

The sediment fill of the Cahabón paleovalley (fig. 6) is composed of a 40 m thick alternation of gravelly-cobbly channel belts 1 m to 3 m thick, alternating with meter-thick floodplain deposits (formation SB-RD2, see fig. 11 for outcrop-scale appearance). SB-RD2 is underlain by SB-DR1, a basal lag a few meters thick, rich in cobbles and boulders. The grain size distribution in SB-RD2 was obtained by sieving 10 to 190 kg of fresh material at 10 sites over the upper 10 km of the paleovalley. At each outcrop, sample size was adapted so that the weight of the largest clast amounts to less than 10 percent of the total sample weight. Samples were sieved and weighed in the field using 1, 2, 4, and 8 cm mesh sizes. Clasts larger than 8 cm were measured and weighted individually. Subsamples of the fraction smaller than 1 cm were taken and sieved in the laboratory using 0.25, 0.5, 1, 2, 4, and 8 mm mesh sizes. The grain size distribution in SB-RD1 was measured at PC5.5, near the waterfall "El Chupadero." Given the large abundance of boulders in SB-RD1, photographs of ~200 m^2 of the outcrop were taken to measure the boulder fraction (25.6 cm). Then 218 kg of the finer fraction was sieved using the same procedure as for SB-RD2. The grain size distribution was then processed using the gradistat macro for Microsoft Excel software developed by Blott and Pye (2001). The resulting D_{50} vs. D_{90} distribution is shown on figure A3.

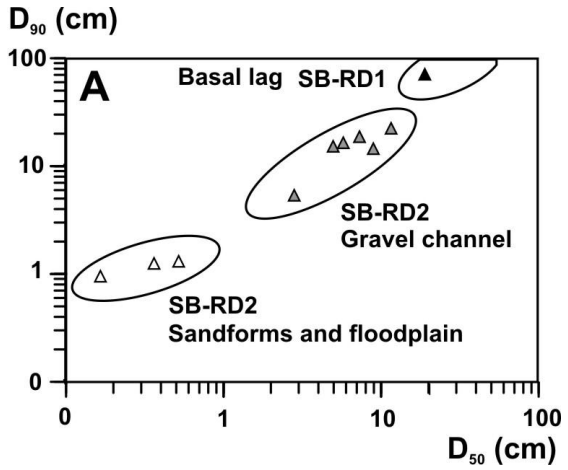

Figure A3. Grain size image of the Cahabón River quartzose-bearing gravel. *The channel belts SB-RD2 plot in the field of gravel and cobble-bedded rivers. Basal lag SB-RD1 was also deposited by a cobble-bedded river but is richer in boulders.*

Appendix 4
Sensitivity test of the ^{10}Be and ^{26}Al burial dating method to the burial history

Post-burial residual production of ^{10}Be and ^{26}Al will make apparent burial ages younger than true ages, if no post-burial production is assumed in age calculations. To evaluate this effect, we ran a series of numerical tests by varying a series of parameters that control the post-burial production. The following parameters are considered: EC, the catchment-wide erosion rate at the time of deposition; CP, the catchment-integrated production rate, which control the initial ^{10}Be and ^{26}Al concentrations before burial; SP, the surface annual production rate at the burial site; ID, the initial depth of burial; SR, the time-averaged sedimentation rate in the floodplain that controls the velocity of burial; MD, the maximum depth of burial; FD, the final depth of burial. For parameters EC, ID, and SR, we performed sensitivity tests by varying their value over a wide range around a reference central value. The corresponding variations on the amount of age correction are reported in table A4.

Site		SP	CP	MD m	FD m	BD ky	EC mm·y^{-1}	ID m	SR mm·y^{-1}	A corr. (%)
PC6.1	Reference	8.9	9.8	20	9.5	550	0.08	1.5	0.2	
	Range						0.01– 0.2	0 – 3	0.04 – 0.5	5
	A corr. %						0 – 10	4 – 5	5 – 5	
PC9.8	Reference	9.0	11.0	45	20	550	0.14	1.5	0.2	
	Range						0.01– 0.2	0 – 3	0.09 – 0.5	0.5
	A corr. %						0 – 2	1 – 0	2 – 1	
PC73.9	Reference	7.9	10.5	20	20	700	0.06	1.5	0.2	
	Range						0.01– 0.2	0 – 3	0.03 – 0.5	2
	A corr. %						0 – 5	2 – 1	4 – 2	
CLW62	Reference	11.2	12.8	10	10	200	0.01	1.5	0.2	
	Range						0.01– 0.2	0 – 3	0.06 – 0.5	0
	A corr. %						0 – 0	1 – 0	0 – 0	

Table A4. Effect of post-deposition ^{10}Be and ^{26}Al production on apparent burial ages
SP: ^{10}Be production at site considered (atom·g^{-1}·y^{-1}). CP − integrated ^{10}Be production in the contributing catchment (atom·g^{-1}·y^{-1}), EC − average erosion in the contributing catchment, ID − initial burial depth, SR − long-term sedimentation rate in the floodplain, MD − maximal burial depth, FD − final burial depth, BD − burial duration, A corr. − correction to apparent ages calculated for reference values, Reference − reference value, Range − tested range of values, A corr. % − correction to age and initiation erosion rate for the range of tested values, in %.

The values of SP and CP were calculated using a 10-m-precision DEM of the modern topography. The ArcGIS 9.2 solar radiation function was used to calculate topographic shielding on each cell of the DEM. Scaling factors for latitude and elevation following Dunai (2001), shielding factor of Heidbreder and others (1971) for topography, and shielding factor of Plug and others (2007) for forest cover where then applied at each cell. For the calculation of PC, cell corrections were summed over the upstream contributing catchment ach each dated site, for the part of the contributing catchment restricted to the quartzose feeding zone Z1+Z2. Calculated shielding was found to lower than the production rate by at most 4 -7 %.

The reference value for the catchment erosion rate EC at the time of deposition is the average of the erosion rates calculated for each sample following Schaller and others (2001). The initial burial depth ID is the depth burial of a sample within a few years or decades following its deposition. We maximized ID by collecting samples at the base of river channels. The preserved channel depth is a minimum of the initial burial depth. It is typically ~1.5 m and varies from 0 to 3 m. The reference value for sedimentation rate SR is discussed in the text.

Appendix 5. Magnetic polarity of river sediments

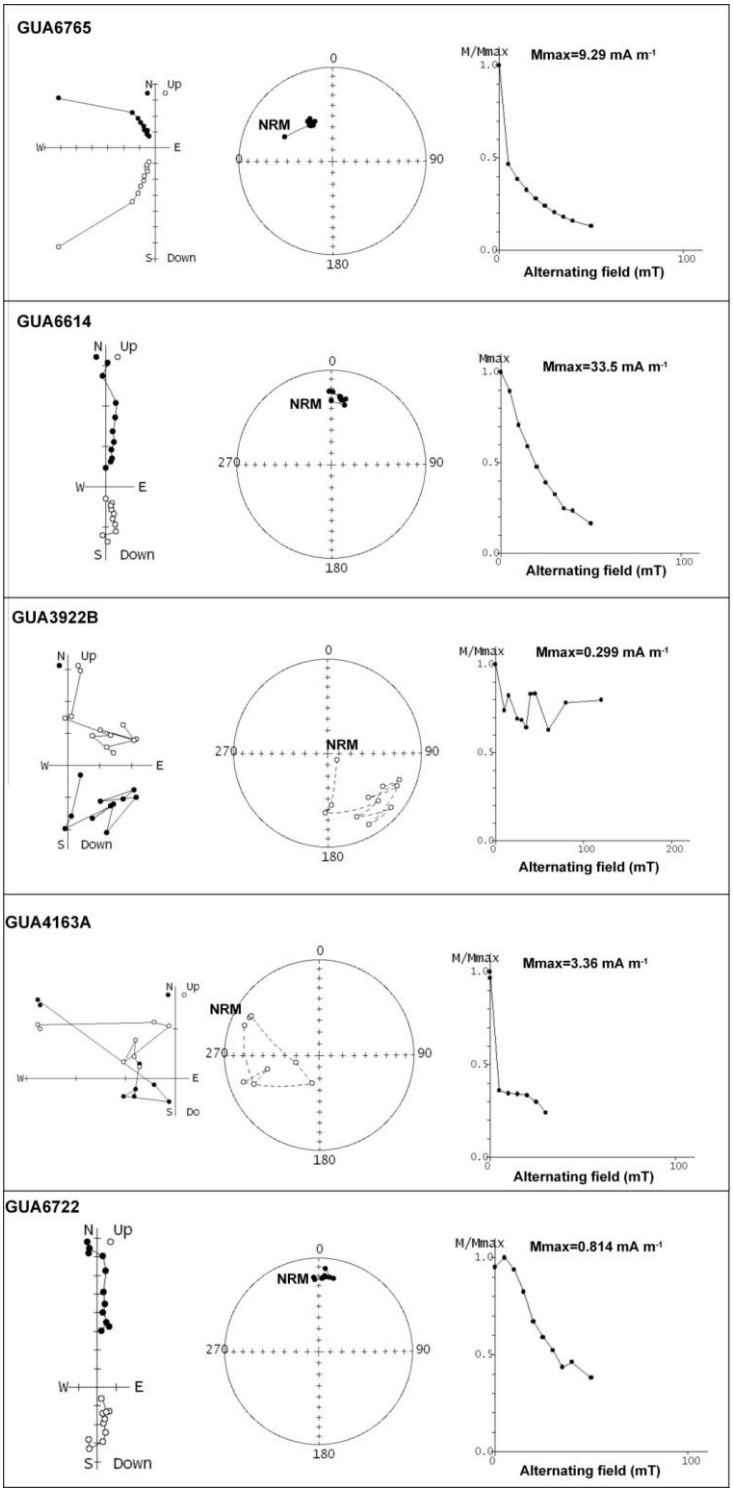

Figure A5. Orthogonal projection (Zijderveld, 1967) of the demagnetization of selected samples of the ancestral Cahabón River sediments.

Stereographic plots (Fisher, 1953) and demagnetization diagrams in figure A5 show the stepwise alternating field demagnetization of 5 selected samples: GUA6765 (site CLW 6.2), GUA6614 (site PC73.9), GUA3922B (site PC 2.5), GUA4163A (site PC 6.1), and GUA6722 (site PC 9.8). On the orthogonal projection plots, open and solid circles represent projections onto vertical and horizontal planes, respectively. On the stereographic plots, open, and solid circles represent reverse and normal inclinations, respectively. Graphs have been produced using PaleoMac software (Cogné, 2003).

Appendix 6
Notes on fault velocity calculations

Lack of rock exposure in the vicinity of the Niño Perdido Fault (NPF) prevents a precise measurement of the tectonic offset of geologic markers. We bracket the fault vertical slip rate using two end-member models of deformation. Where the Cahabón River intersects the fault, the relict upland surface displays ~220 m of vertical offset. This represents 40 % of the differential uplift along the upland surface from PC2 to PC15, the rest of the displacement being accommodated by distributed tilting south of the NPF (fig. 7). Ongoing tilting of the Chilascó River floodplain suggests that at least part of this distributed deformation is still underway. At the same time, the NPF has also been active recently, as indicated by a minimum offset of 50 m that affects the Cahabón River gravel across the NPF, measured from the base of the valley fill on the hanging wall of the NPF, down to the preserved surface of the valley fill on the footwall of the NPF. We therefore consider the following end-member models. In one end-member model, the observed finite 0.4/0.6 apportionment of faulting and tilting observed on the relict upland surface is considered to have been constant over the entire duration of deformation. A fault velocity of 0.10 ± 0.03 $mm \cdot y^{-1}$ (model 'a', table 3) is calculated using our proposed age of capture SB (540 ± 160 ky). In the end-member model, we consider that tilting has ceased and only the NPF accommodates the differential uplift since valley abandonment. This increases the slip rate to 0.24 ± 0.07 $mm.y^{-1}$ (model 'b', fig. 7 and table 3). If the fault velocity has been constant since the beginning of the fault activity, then the NPF would start at 920 ± 270 ky in model 'b' and 2.2 ± 0.6 My in model 'a'. If the slip rate may have increased after fault inception, then activity would start earlier in the late Pliocene-Early Quaternary, a view consistent with the regional geodynamics (Authemayou and others, 2011).

Further downstream, the ancestral Cahabón River crosses the southern fault of the Purulhá trough (PT-SF) between PC21 and PC23. The wide quartzose-gravel-covered valley floor of the paleovalley is uplifted south of the fault by some 50 m (fig. 7). The axial drainage of the valley is now confined into a narrow gorge incised at the center of the valley floor. The gorge connects downstream to the PL canyon. The gorge may result from the propagation of the PL southwards (branch 'a', fig. 8), in which case it postdates capture PL, or it results from a reduction in the stream power of the Cahabón River consecutive to the river beheading in SB. These events set lower and upper boundaries on the time at which the offset started. Capture SB is dated at 540 ± 160 ky. Quartzose gravel disappearance occurred soon after or coevally to the abandonment of the San Isidro alluvial fan in PC9.8, at 400 ± 230 ky. This is the lower temporal limit for slip rate calculation (model 'c' in table 3). The age of the PL capture is not known, but younger than terrace T2 in the Depression of Cobán, itself younger than the last major geomagnetic reversal (730 ky). This sets the upper limit of our slip rate calculation (model 'd' in table 3).

The total vertical throw of the upland relict surface across the NPF increases eastwards from 150 m on the western interfluve of the Cahabón valley up to 250 m over its eastern interfluve. The apparent throw across the PT-SF increases westward. At the longitude of the ERT surveys, the bedrock is deeper than the valley fill imaged by ERT (~80m), but it crops out on the lip of the branch 'b' in the PL canyon. This implies that the bedrock floor deepens longitudinally by at least 80 m over 6 km along the PT-SF. Because the floor of the tectonic trough widens coevally, we use trough width as a proxy for trough depth. If this approximation is correct, then the deepest part of the trough is located two kilometers further west (fig. 8). Unless the trough is tilted westward by some far-field regional deformation, deepening of the trough westward is attributable to larger slip on the PT-SF. Deepening will be compensated by uplift of the footwall and the ratio of subsidence to uplift can vary in proportion from 1:6 (Stein and Barrientos, 1985, model 'e') to 1:1 (Jackson and Leeder, 1994, model 'f'). In the area of the ERT profiles, the height of PT-SF footwall is limited by a straight, regular crest line that corresponds to the beveled floor of a Miocene paleovalley. This paleovalley postdates the relict upland surface but predates the inception of transtension (Brocard and others, 2011). It is used here as a marker for the finite

throw of the PT-SF. Dividing the total measurable offset of the PT-SF, from the crest line down to the minimum basement depth in the trough, by our calculated fault rate provides a minimum age on the inception of faulting. Fault inception is thus found to start between 0.9 and 3.5 My for a constant fault slip rate.

Commercial boreholes for the construction of a power plant have been drilled in an alluvial fan, 2 km downstream of the ERT profiles PC30.8 and PC33.0 (fig. 8). The presence of the power plant impeded the use of ERT in this fan. The boreholes reached a depth of ~25 m and encountered an alternation of layers that closely mimics the layering imaged on the ERT sections (data courtesy of Rodolfo Alvarado, Swissboring Overseas Inc.). In the boreholes, two layers of massive gray to reddish silty clay (L1, 4.5m thick, and L3, >11 m thick) are separated by an intervening 9.5 m thick silty sand layer (L2). Small quarries near Purulhá, together with a <5 m long drill core at PC23.3 also expose the massive silty clay (L1). It contains a few seams of compact, strongly weathered gray volcanic ash rich in kaolinite, halloysite, bentonite, and volcanic quartz. We correlate this silty clay to the units that exhibit electrical resistivities < 20 Ohm·m in the ERT sections (L1 and L3, figs. 8A and 8B). Unit L1 is 6 to 12 m thick, and L3 is 30 to 40 m thick along the ERT sections. The intervening 10 to 22-m-thick layer L2 with a resistivity of 20 to 150 Ohm·m is correlated to the intervening silty sand encountered in the boreholes. The silty sand was slightly over-pressured when it was drilled at the end of the rainy season.

The layering results from changing properties in the sediment column (material and/or grain size) and thus reflects temporal changes in erosion in the feeding catchments. Layering is remarkably similar from fan to fan thus indicating that it was determined by climate-driven changes and records the effects of climatic oscillations on the sedimentary material brought to the fans (for example Allen and Densmore, 2000). Atmospheric moisture strongly decreased during the last glaciation in Guatemala (for example Hillesheim and others, 2005), while the glacier ELA was lowered by 1300 to 1500 m (Lachniet and Vazquez-Selem, 2005). The observed layering could well reflect the alternation of cold and dry glacial periods and warm and wet interglacial periods. Carbonates underlie 25 to 45 % of the feeder catchments. During dryer periods and under reduced vegetation cover, coarser, limestone rich material could be delivered to the fans, while wet periods are expected to promote the export of weathering-derived clay. Numerical simulations suggest that such ~10 to 100-km^2-large catchments on the hanging wall of normal faults respond and adjust to climate fluctuations over timescales of 10^5 years (Ellis and others, 1999; Allen and Densmore, 2000). Fan sedimentation in the trough of Purulhá is therefore expected to resonate to the typical 10^5 y duration of the Upper Pleistocene glacial-interglacial oscillations, while shorter time fluctuations could be filtered out or could produce layering that is too thin to be imaged by ERT. If layer L1 corresponds to the current interglacial (marine isotope stage MIS1 with duration 18 ky), L2 to the last glaciation (MIS 2-4, duration 60 ky), and L3 to the previous interglacial s.l. (MIS 5, duration 50 ky), then, the sedimentation rate fluctuates between 0.6 to 0.9 mm·y^{-1} (PC 29.5–30.8) and 0.3 mm·y^{-1} (PC 33.0) during the interglacial periods, and between 0.4 mm·y^{-1} (PC 29.5–30.8), and 0.2 mm·y^{-1} (PC 33.0) during the glaciation. Subsidence at site PC 33.0 is less than at sites PC30.8 and 29.5 because the drilled fan is located farther from the fault. Sedimentation values in the fan closest to the PT-SF are consistent with our independent estimate using the vertical offset of quartzose-bearing alluvium (0.7 ± 0.4 mm·y^{-1}).

From the trough of Purulhá down to the trough of Tactic, the Cahabón River flows across the rotating block delimited to the south by the PS-TF and to the north by the Polochic fault. Downstream of PC35.2 (fig. 1), subsidence reverts to uplift and increases steadily down until the Cahabón River enters the tectonic trough of Tactic. Assuming rigid block rotation of horizontal E-W axis with a hinge at PC35.2 (Pasmolón), then vertical uplift is predicted to reach a maximum of 0.2 to 0.7 mm·y^{-1} near the trough of Tactic.

Appendix 7
Models of post-capture canyon development

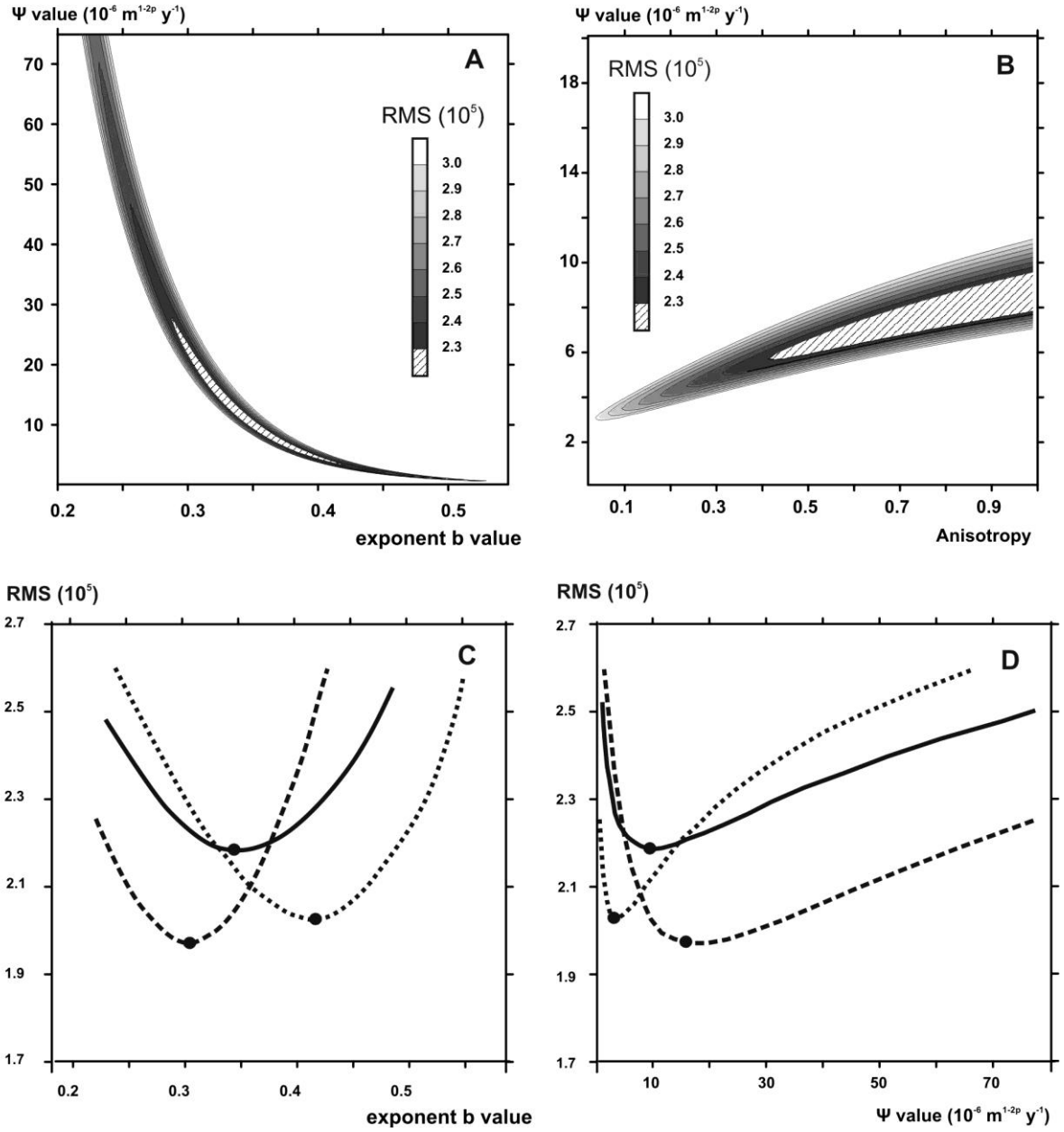

Figure A7. Best-fitting values for the parameters ψ and b from equation (1) in the canyon of Santa Barbara (SB) RMS refers to the square root of the sum of squared misfits in the timing of arrival of headward erosion at its present location along streams '*a*' to '*f*' in canyon SB.

Panel A: combinations of the parameters ψ and b in the case of the increasing area model (SB_{Aint}), and resulting RMS map.
Panel B: effect of bedrock E-W anisotropy. Anisotropy is the ratio of N-S-value of ψ over E-W-value of ψ; the value is 1 when the medium is isotropic. RMS map for a range of ψ and anisotropy values. Anisotropy does not improve the fit compared to the simple isotropic model.
Panel C: projection of the best-fitting values of panel A on the b-exponent axis, showing the best-fit value of the b-exponent (dots) for three models: evolving area (SB_{Aint}, solid line), minimum area (SB_{Amin}, dashed line , and maximum area (SB_{Amax}, doted line).
Panel D: projection of the best-fitting values of panel A on the ψ-axis, showing best-fit values (dots), for the same three models.

Stream	L (Km)	A (Km^2)	J. L (Km)	A_{SBmin} (Km^2)	A_{SBmax} (Km^2)	A_{main} (Km^2)
SBa	1.25	1.6	0.00	85.4	148	-
SBb	2.32	8.5	0.45	76.6	137	-
SBc	1.08	2.3	2.41	71.4	132	-
SBd	1.15	2.9	2.79	30.0	129	-
SBe	1.75	17.0	3.20	11.7	112	-
SBf_k	1.16*	-	4.36	11.1	111	-
	-	-	0.00	-	-	19.0
SCZa	0.46	9.6	0.51	-	-	18.7
$SCZb_k$	0.38*	-	0.89	-	-	7.8
	-	-	0.00	-	-	71
PLa	1.70	25	1.45	-	-	45
PLb_k	1.26*	-	2.71	-	-	38

Table A7. Length and drainage area in streams draining into the canyons of capture

L – length of stream affected by headward erosion, upstream of junction with trunk stream (*-along main stream, upstream from last junction), A – drainage area at junction with trunk stream, JL – distance of the junction to the capture site. A_{SBmin}, $A_{SBmax,}$ A_{SBint} – drainage area of stem stream SBf at junction with tributary, for the minimum, maximum and intermediate model, respectively (see text).

Appendix 8

Isotopic compositions of the Lake Chichój, the Cahabón River and springs along the Polochic fault

Site	*Longitude*	*Latitude*	*Depth (m)*	*$\delta^{18}O$ SMOW*		*δD SMOW*	
Laguna Chichoj	770,607	1,699,699	0	-5.98	± 0.08	-39.11	± 0.56
Laguna Chichoj	770,607	1,699,699	5	-5.95	± 0.03	-39.43	± 0.52
Laguna Chichoj	770,607	1,699,699	10	-5.60	± 0.02	-36.49	± 0.14
Laguna Chichoj	770,607	1,699,699	15	-5.69	± 0.04	-36.89	± 0.11
Laguna Chichoj	770,607	1,699,699	20	-5.62	± 0.04	-36.85	± 0.28
Laguna Chichoj	770,607	1,699,699	25	-5.67	± 0.06	-37.12	± 0.28
Cahabón River	777,880	1,712,530	-	-7.15	± 0.08	-42.57	± 0.20
Spring Polochic F.	771,391	1,696,924	-	-7.12	± 0.06	-44.63	± 0.33
Spring Polochic F.	770,227	1,697,073	-	-7.09	± 0.05	-44.97	± 0.32
Spring Polochic F.	768,351	1,697,085	-	-7.16	± 0.02	-44.93	± 0.31

Table A8. Longitude and latitude are in UTM coordinates zone 15 N, reference ellipsoid WGS 1984.